UNIVERSIDADE ESTADUAL DE CAMPINAS
FACULDADE DE ENGENHARIA MECÂNICA
E INSTITUTO DE GEOCIÊNCIAS

FUAT CAMPOS PEREIRA

ANALYSIS OF CROSS-LINKED POLYMER GEL FOR LOST CIRCULATION CONTROL

ANÁLISE DE GEL POLIMÉRICO RETICULADO PARA CONTROLE DE PERDA DE CIRCULAÇÃO

CAMPINAS
2020

FUAT CAMPOS PEREIRA

ANALYSIS OF CROSS-LINKED POLYMER GEL FOR LOST CIRCULATION CONTROL

ANÁLISE DE GEL POLIMÉRICO RETICULADO PARA CONTROLE DE PERDA DE CIRCULAÇÃO

Dissertation presented to the School of Mechanical Engineering and Institute of Geosciences of the University of Campinas in partial fulfillment of the requirements for the degree of Master in Petroleum Sciences and Engineering in the area of Reservoirs and Management.

Dissertação apresentada à Faculdade de Engenharia Mecânica e Instituto de Geociências da Universidade Estadual de Campinas como parte dos requisitos exigidos para a obtenção do título de Mestre em Ciências e Engenharia de Petróleo na área de Reservatórios e Gestão.

Orientadora: Profa. Dra. Rosangela Barros Zanoni Lopes Moreno

Este exemplar corresponde à versão final da tese defendida pelo aluno Fuat Campos Pereira e orientada pela Profa. Dra. Rosangela Barros Zanoni Lopes Moreno.

CAMPINAS
2020

Ficha catalográfica
Universidade Estadual de Campinas
Biblioteca da Área de Engenharia e Arquitetura
Rose Meire da Silva - CRB 8/5974

Pereira, Fuat Campos, 1994-
P414a Analysis of cross-linked polymer gel for lost circulation control / Fuat Campos Pereira. – Campinas, SP : [s.n.], 2020.

Orientador: Rosângela Barros Zanoni Lopes Moreno.
Dissertação (mestrado) – Universidade Estadual de Campinas, Faculdade de Engenharia Mecânica.

1. Engenharia do petróleo. 2. Poços de petróleo. 3. Polímeros. 4. Reticulação. 5. Reservatórios - Fratura. I. Moreno, Rosângela Barros Zanoni Lopes, 1966-. II. Universidade Estadual de Campinas. Faculdade de Engenharia Mecânica. III. Título.

Informações para Biblioteca Digital

Título em outro idioma: Análise de gel polimérico reticulado para controle de perda de circulação
Palavras-chave em inglês:
Petroleum engineering
Oil wells
Polymers Cross-
linking Reservoirs -
Fratures
Área de concentração: Reservatórios e Gestão
Titulação: Mestre em Ciências e Engenharia de Petróleo
Banca examinadora:
Rosângela Barros Zanoni Lopes Moreno [Orientador]
Paulo Roberto Ribeiro
Paulo de Tarso Vieira e Rosa
Data de defesa: 30-11-2020
Programa de Pós-Graduação: Ciências e Engenharia de Petróleo

Identificação e informações acadêmicas do(a) aluno(a)
- ORCID do autor: https://orcid.org/0000-0002-7131-3237
- Currículo Lattes do autor: http://lattes.cnpq.br/3536660867190682

UNIVERSIDADE ESTADUAL DE CAMPINAS
FACULDADE DE ENGENHARIA MECÂNICA
E INSTITUTO DE GEOCIÊNCIAS

DISSERTAÇÃO DE MESTRADO ACADÊMICO

ANALYSIS OF CROSS-LINKED POLYMER GELS FOR CIRCULATION LOSS CONTROL

ANÁLISE DE GEL POLIMÉRICO RETICULADO PARA CONTROLE DE PERDA DE CIRCULAÇÃO

Autor: Fuat Campos Pereira

Orientadora: Profa. Dra. Rosangela Barros Zanoni Lopes Moreno

A Banca Examinadora composta pelos membros abaixo aprovou esta Dissertação:

Profa. Dra. Rosangela Barros Zanoni Lopes Moreno
Departamento de Energia / Faculdade de Engenharia Mecânica / Universidade Estadual de Campinas

Prof. Dr. Paulo Roberto Ribeiro
Departamento de Energia / Faculdade de Engenharia Mecânica / Universidade Estadual de Campinas

Prof. Dr. Paulo de Tarso Vieira e Rosa
Departamento de Físico-Química / Instituto de Química / Universidade Estadual de Campinas

A Ata de Defesa com as respectivas assinaturas dos membros encontra-se no SIGA/Sistema de Fluxo de Dissertação/Tese e na Secretaria do Programa da Unidade.

Campinas, 30 de Novembro de 2020

DEDICATION

This master's dissertation is dedicated, first of all, to God, to my dear parents Marco and Daniela, to my dear girlfriend Aracely, to my family, friends and my dear professor Rosângela.

ACKNOWLEDGEMENTS

I thank God for the guidance and being my emotional and spiritual support, allowing me to achieve all my goals and dreams.

I express my gratitude to Profa.Dra. Rosângela Barros Zanoni Lopes Moreno, for the trust and opportunity provided, for sharing her knowledge and advice with me.

To my parents, sisters and my family, for giving me inspiration and emotional support.

To my beloved girlfriend, who was my support in difficult days, always giving me inspiration and love.

To my dear friend and colleague Karl Jan Clinckspoor, for his support and knowledge provided

To all my dear friends and colleagues from LABORE and FEM at UNICAMP, for their friendship and help in the details of this dissertation.

A special note of gratitud to my friend and professor Pedro Marcelo Adrian Herbas, for the friendship and trust provided.

This study was financed in part by the Coordenação de Aperfeiçoamento de Pessoal de Nível Superior – Brasil (CAPES) – Finance Code 001" and in part by the on going R&D Project intituled "Projeto Reológico de soluções de Combate à Perda de circulação em Carbonatos Fraturados" (Universidade de Campinas (Unicamp)/PETROBRAS/ANP) – Rheological Fluid Design for Circulation Loss Control in Fractured Carbonate, sponsored by PETROBRAS - Petróleo Brasileiro S/A under the ANP R&D levy as "Compromisso de Investimentos com Pesquisa e Desenvolvimento".

RESUMO

Palavras Chave: Perda de Circulação, Polímeros Reticulados, Reologia, RMN.

A perda de circulação é um dos maiores problemas apresentados durante a perfuração de poços. A perda de circulação tem sido um dos fatores que geram altos custos e maior tempo de operações não produtivas offshore e onshore. Diversos estudos são desenvolvidos para resolver este problema da melhor maneira possível, pois requer a preparação e a circulação de pílulas de fluidos de tratamento com diferentes componentes através dos sistemas de perfuração. Um método para combater a perda de circulação inclui o uso de sistemas de polímeros reticulados formadores de gel, que podem conter ou não sólidos, e que gelificam e selam as zonas de perda.

Este estudo apresenta uma metodologia de trabalho experimental para o projeto de um gel de polímero reticulado para o combate de perda de circulação. Dois tipos de géis apresentados na literatura foram escolhidos para avaliação, o primeiro, um gel simples consistindo apenas da mistura entre um agente gelificante e um agente reticulante com a salmoura, e o segundo, tendo como base a mesma formulação do primeiro, mas com a formação de uma polimerização in-situ pela adição de ácido acrílico e de persulfato de amônio. Este segundo sistema levou a um incremento das redes reticuladas, mostrando assim ser a melhor opção por ter um melhor desempenho nas avaliações de cinética de reação e de estabilidade. Estas avaliações tiveram como base estudos reológicos, de ressonância nuclear magnética e testes de garrafa de Sydansk. A capacidade de filtração dos géis foi analisada por meio de testes de filtração estática em discos de alta permeabilidade.

Com os resultados obtidos dos testes, foi possível definir um gel com as melhores caraterísticas para o combate de perda de circulação. Este foi submetido a um processo de otimização através de um planejamento experimental a uma temperatura de 70°C, chegando assim a formulações ótimas, avaliadas por meio das superfícies de resposta dos diferentes resultados reológicos e de ressonância nuclear magnética. Foram obtidas três formulações do gel com boa estabilidade, boa cinética e diferentes valores do Módulo de platô G'_p. Estas formulações foram avaliadas em testes de filtração estática adaptado, sendo constatado que os géis com altos valores de Módulo de platô G' conseguem resistir valores de pressão maiores.

Concluindo, o planejamento experimental permitiu determinar a influencia de cada uma das variáveis analisadas nos resultados, facilitando a escolha das formulações promissoras e que atendem aos objetivos desejados para aplicação em um campo alvo.

ABSTRACT

Key Words: Lost Circulation, Cross-linked Polymers, Rheology, NMR.

Lost circulation is one of the biggest problems presented during wellbore drilling. Lost circulation has been one factor that generates high costs and longer non-productive time of offshore and onshore operations. Several studies have attempted to solve the lost circulation in the best possible way since it requires the preparation and circulation of a new pill with different components through the system. One method to combat this problem includes the use of cross-linked gel-forming polymer systems, which may or may not contain solids, which would gel and seal unwanted areas and prevent losses.

This experimental study presents a working methodology for designing a cross-linked polymer gel to combat lost circulation. Two types of gels were chosen from the literature to be evaluated. The first one is a simple gel, which is only a mixture between a gelling agent and a cross-linking agent with brine. The second one is based on the same formulation as the first system, but it includes an in-situ polymerization due to adding acrylic acid and ammonium persulfate, which led to an increase in the reticulated networks. The study pointed out the second gel as the best option since it had a more robust formulation on reaction and stability kinetics obtained by rheological studies, NMR, and Sydansk bottle testing. The filtration capacity of the gels was analyzed through static filtration tests on high permeability disks.

With the results obtained from the tests, it was possible to define a gel with the best characteristics for combating lost circulation. That was subjected to an optimization process through an experimental design at a temperature of 70 °C, thus reaching optimal formulations evaluated through response surfaces of the different rheological and NMR results. Three gel formulations were obtained with good stability, good kinetics, and different values of the Plateau Module G'_p to be evaluated in an adapted static filtration test. Therefore, it was ratified that gels with high values of Plateau Module G'_p can resist higher pressure values.

In conclusion, the design of experiments allowed us to determine the influence of each of the analyzed variables on the results, facilitating the choice of promising formulations that fulfill the desired characteristics for a target field application.

LIST OF FIGURES

LIST OF TABLES

LIST OF NOMENCLATURES

Latin characters and expressions

A	-	Area	-	$L^2M^0T^0\Theta^0N^0$
B_0		Static magnetic field strength		
B_1		Amplitude of the oscillating field pulse		
c	-	Concentration	-	$L^{-3}M^1T^0\Theta^0N^{0\dagger}$
c^*	-	Concentration characteristic of the transition between dilute and semidilute concentration regimes	-	$L^{-3}M^1T^0\Theta^0N^{0\dagger}$
c^{**}	-	Concentration characteristic of the transition between semidilute and concentrated concentration regimes	-	$L^{-3}M^1T^0\Theta^0N^{0\dagger}$
F		Fisher-Snedesor distribution		
G'	-	Elastic Modulus	-	$L^{-1}M^1T^{-2}\Theta^0N^{0}$-
G''	-	Viscous Modulus	-	$L^{-1}M^1T^{-2}\Theta^0N^{0}$-
G'_p	-	Plateau Modulus	-	$L^{-1}M^1T^{-2}\Theta^0N^{0}$-
k	-	Constant of hill equation	-	
K	-	Consistency index	-	
m	-	Mass	-	$L^0M^1T^0\Theta^0N^0$
M_A		Amplitude of the torque		
M_w	-	Molar mass	-	$L^0M^1T^0\Theta^0N^0$
MS		Mean squares		
n		Behavior Index		
P	-	Pressure	-	$L^{-1}M^1T^{-2}\Theta^0N^0$
q	-	Volumetric flow rate	-	$L^3M^0T^{-1}\Theta^0N^0$
R^2	-	Coefficient of determination	-	
SS	-	Sum of squares	-	-
t	-	Time	-	$L^0M^0T^1\Theta^0N^0$
$_t$		Spin-echo time		$L^0M^0T^1\Theta^0N^0$
T		Transverse relaxation time		$L^0M^0T^1\Theta^0N^0$
TE		Dephasing time		$L^0M^0T^1\Theta^0N^0$
w_H	-	Hydraulic aperture	-	$L^0M^0T^0\Theta^0N^0$
X	-	Matrix	-	-
$\hat{y}$		Column vector		

Greek characters

α		Phase angle in spin-echo detection		
β	-	Column vector containing the model coefficients	-	-
δ		Phase shift angle		
$\dot{\gamma}$	-	Shear rate	-	$L^0M^0T^{-1}\Theta^0N^0$
$\dot{\gamma}_0$	-	Maximum shear rate for the low shear rate Newtonian plateau	-	$L^0M^0T^{-1}\Theta^0N^0$
$\dot{\gamma}_\infty$	-	Minimum shear rate for the high shear rate Newtonian plateau	-	$L^0M^0T^{-1}\Theta^0N^0$
Δ	-	Differential	-	-
η	-	Apparent viscosity	-	$L^{-1}M^1T^{-1}\Theta^0N^0$
η_0	-	Viscosity characteristic of the low shear rate Newtonian plateau	-	$L^{-1}M^1T^{-1}\Theta^0N^0$
η_∞	-	Viscosity characteristic of the high shear rate Newtonian plateau	-	$L^{-1}M^1T^{-1}\Theta^0N^0$
θ	-	Angle	-	$L^0M^0T^0\Theta^0N^0$
σ^2		Populational Variance		
μ	-	Viscosity	-	$L^{-1}M^1T^{-1}\Theta^0N^0$
τ	-	Shear stress	-	$L^{-1}M^1T^{-2}\Theta^0N^0$
τ_y	-	Yield stress	-	$L^{-1}M^1T^{-2}\Theta^0N^0$
τ_f	-	Flow limit	-	$L^{-1}M^1T^{-2}\Theta^0N^0$

τ_0	-	Shear stress above which there is flow	-	$L^{-1}M^1T^{-2}\Theta^0N^0$
ϕ_A		Amplitude of the deflection angle		

Superscripts

-1	-	Inverse of Matrix
T	-	Transpose of Matrix
k	-	Power
max	-	Maximum

Subscripts

R	-	Regression
r	-	Residuals
pe	-	Pure error
LOF	-	Lack of fit
min	-	Minimum
T		Total

Acronyms

AA		Acrylic Acid
API	-	American petroleum institute
APS		Ammonium Persulfate
CMC	-	Carboxymethylcellulose
COO^{-}.		Polymer Carboxylate Group
CPMG	-	Carr, Purcell, Meiboom, and Gill method
Cr	-	Chromium
DOE	-	Desing of experiments
DMN		Dynamic mechanical analysis
DS	-	Degree of substitution
ECD	-	Equivalent circulation density
Fe	-	Iron
FG		Fracture Gradient
HEC	-	Hydroxyethylcellulose
HPAM	-	Partially hydrolyzed polyacrylamide
HPHT		High pressure – High temperature
LCM		Lost circulation material
LRNMR		Low resolution nuclear magnetic resonance
LVE	-	Linear viscoelasticity
I	-	Identity
n	-	Number of observations
NE	-	Number of experiments
NL		Number of levels
NMR		Nuclear magnetic resonance
NR		Number of replicates
NV		Number of variables
m		Number of distinct levels
p		Number of parameters
PAA		Poly (acrylic acid)
PAC	-	Polyanionic cellulose
PAM	-	Polyacrylamide

R_o	-	Radius of drop curvature
SCL	-	Scleroglucan
SPG	-	Schizophyllan
U	-	Interstitial velocity
TDS	-	Total dissolved solids
XG	-	Xanthan gum

SUMMARY

1 INTRODUCTION

The upstream activities of the oil and gas industry refer to all stages involved, from exploration to field abandonment. Those activities include exploration, appraisal, development planning, production, decommissioning phases, and economic, legal, and technical aspects (Jahn et al., 2008; David et al., 2017; Bleackley and Strathman, 2011).

Seismic and geological studies and the drilling of exploratory wells allow us to verify areas of potential interest. During drilling, formation and fluids information is collected by electrical logs to determine the depth and the amount of oil and/or gas available in the exploration area. Once the exploration stage success has been proved, the appraisal stage is carried out in which reservoir features are improved, helping to reduce economic and reservoir uncertainties for its subsequent development. An adequate production/injection strategy must be designed during the field development phase, establishing the wellbore unit arrangements and production installations. The production phase starts with the first commercial hydrocarbon is produced. After oil and gas extraction and separation, they are transported to be processed and distributed (downstream activities). The reservoir production time is limited to its economic profitability. Hence, the wells will be plugged and abandoned. The useful life of oil and gas fields varies between 15 and 30 years and up to 50 years for large reservoirs (Paulauskiene, 2018; Speight, 2015).

Drilling engineers are in charge of designing and implementing drilling programs to drill and casing the well in the fastest, cheapest, and safest way possible, taking all environmental considerations into account (Bourgoyne et al., 1986). Once the drilling stage is completed, the production or completion engineers assume responsibilities (Caenn et al., 2011).

According to Islam and Hossain (2020), drilling operation is the most expensive stage of the oil industry and can represent almost a quarter of the total field cost. Therefore, significant operational, technical, and financial efficiencies are required. The drilling phase needs to be well designed and operated to guarantee maximum safety for engineers and operational workers, looking for minimal formation damage and applying the lowest costs in the shortest time possible. The most common drilling problems are, in no particular order, pipe sticking, lost circulation, hole deviation, drilling failures, borehole instability, mud contamination, hole cleaning, drilling-induced formation damage, and hydrogen sulfide-bearing zones (Hassan, 2018).

Lost circulation can occur while drilling, running casing/liner, completing, or cementing the well. Correcting this problem requires a high non-productive time, besides the amount of the drilling fluid lost into the formation. From the historical point of view, lost circulation is one of the most contributing factors to the high completion and drilling operations costs. Solving the problem takes a long time since it requires preparing a new pill with different

components and circulating that pill through the system, resulting in a non-productive time (Feng and Gray, 2018). According to Elkatatny et al.(2020), lost circulation interventions require up to 3 days to control onshore well, whereas the duration increases to 7 days in offshore wells. Those costs can reach approximately one billion dollars per year, including drilling mud loss, time loss, and treatment costs. Just treatment fluids to mitigate loss can cost around 200 million dollars annually. Lost circulation in onshore drilling operation costs near 65,000 dollars per day, whereas it is about 120,000 dollars per day in the offshore drilling operation. The annual mud loss into rock formations is about 1.8 million bbl.

The knowledge of different types of formations in which the lost circulation can occur helps prevent and manage this problem. Selection of an appropriate LCM or strengthening fluids and different downhole conditions must be considered. Fluid loss can be classified into different types, seepage loss occurs when drilling fluid flows through large porous or highly permeable formation, such as loose sand and gravels; partial loss refers to circulation loss through unconsolidated or fractured formations; and, finally, severe loss and no fluid return can happen due to the presence of cavernous, faults or fractures. Some of the standard and recommended practices of preventive and restorative measures are summarized in a decision-making flow chart shown in ANNEX A (Magzoub et al., 2020).

Many authors have shown the efficiency of cross-linking polymers in several laboratory and field studies focusing on lost circulation (Cole et al., 1995; Chang et al., 1998; Al-Muntasheri et al., 2008; Gibson et al., 2011; Gamage et al., 2014; Jiang et al., 2019). Cross-linked polymer gels are high-strength materials resulting from physical or chemical cross-linking bonds between polymer chains (Luzardo et al., 2015).

The evolution in cross-linking polymers research has been acquiring great importance due to the versatility of its mechanical properties and uses in areas such as health, food, engineering, among others (Ahmad, 2001; Russell et al., 2019). One of those research was developed by Hussain et al. (2018) and consists of a method to prepare a novel hydroxyethyl cellulose based on self-healing HEC/PAA-Fe^{3+} cross-linking polymer gel with robust mechanical properties. The incorporation of dynamic metal-ligand interactions in a physically (H-bonded) cross-linked network enhanced the gel mechanical properties and self-healing efficiency without external intervention, thus showing properties of interest for the gel application as lost circulation control agent.

1.1. Motivation

Besides the additional cost and non-productive time, lost circulation can also damage hydrocarbon-bearing zones. Formation damage can happen any time during the lifecycle of a wellbore (drilling, completion, production, or work-over operations) and includes permeability plugging by solids invasion, wettability alteration, phase trapping, interaction resultant of the incompatibility between fluids and rocks. Solids invasion is a common type of LCM treatment-induced formation damage and occurs when LCM containing solids moves into

the formation and occupies the matrix pore space. Its severity is very high in open hole completions (Patel and Singh, 2016). Besides, LCM treatments are not suitable in severe loss cases (Lavrov, 2016).

Various laboratory-scale studies have demonstrated the potential of cross-linked polymer gels in controlling the severe lost circulation (Himes et al. 1994; Cole et al., 1995; Chang et al., 1998; Al-Muntasheri et al., 2008; Gibson et al., 2011; Songire and Uppuluri, 2014; Gamage et al., 2014; Jiang et al., 2019). However, these fluids are complex, requiring knowledge improvement and problems overcoming, such as large-scale production, costs, and logistics. It is crucial to integrate cross-linked polymer gels characterization, kinetic evaluation, and laboratory-scale stability with field operations scales.

According to Songire and Uppuluri, 2014, or Himes et al. 1994, treatment procedures using cellulose derivative cross-link polymers are reversible using different breakers or internal breakers, making this method more favorable to be less or non-harmful to the formations.

1.2. Objectives

The present work aims to design a solid-free cross-linking polymer to remediate lost fluid circulation in cavernous, fault, or fractured formations.

The results of this project are expected to reach the following objectives:

- Characterize and evaluate cross-linked polymer gel systems by rheology, NMR, and bottle testing.
- Study the behavior of the cross-linked polymer gel system to be selected employing a design of experiments. That will be achieved by analyzing response surfaces obtained through rheology and NMR results.
- Evaluate the performance of the cross-linked polymer gel system through static filtration tests on high permeability discs.

1.3. Dissertation Structure

This work is composed of six chapters.

Chapter 1 presents the introduction, the knowledge gap that motivated this work, and the objectives to contribute to different topics of existing knowledge.

Chapter 2 covers the basic concepts and theories for rheology, NMR, lost circulation problems, and cross-linking polymer gel systems. This chapter also includes characterization procedures applied to cross-linking polymers, influencing parameters on their rheological behavior, and stability and kinetics evaluation methods.

Chapter 3 introduces all the materials, devices, and equipment used and a detailed explanation of the experimental methods applied to develop this research.

Chapter 4 shows the results obtained and the discussions regarding the methodology applied to achieve those results.

Finally, Chapter 5 exhibits the main conclusions obtained throughout this research.

2. LITERATURE REVIEW

This chapter presents a literature review of lost circulation and concepts related to cross-linked polymers.

2.1. Lost Circulation and Mechanisms

Lost circulation refers to the inflow of drilling fluid into formation instead of returning to the surface. That occurs due to a differential pressure between the wellbore hole and the formation pore pressure. It is usually classified by literature as one of the most common problems during drilling operations, causing considerable economic losses for the oil and gas industry (Lavrov, 2016; Chen et al., 2017; Feng and Gray, 2018).

The drilled formation information allows minimizing the lost circulation problem by controlling the fluid properties, the penetration rate, weight on the bit, revolutions per minute (RPM), and strokes per minute (SPM). The information obtained requires specific data, which are generally limited. Therefore different methods to prevent and mitigate lost circulation events are developed (Al-Hameedi et al., 2017).

The lost circulation can be detected by controlling the mud tank levels. A decrease in it means that volume is being lost towards the formation, leading to severe problems in drilling processes. When the annular section is not filled with fluid, the hydrostatic pressure decreases until the differential pressure between the mud column and the formation is not enough to prevent the inflow of formation fluids into the well, with the potential to result in a kick, an explosion, or an underground blowout. Lost circulation can also lead to the drill string sticking (DeGeare, 2003; Ezeakacha et al., 2018). According to DeGeare (2003), that happens when the drilling fluid hydrostatic pressure fractures the unconsolidated or high permeable formations, and the drilling fluid flows into the fractures causing washouts (see **Fig. 2.1**).

When the hydrostatic pressure exceeds the fracture gradient of an intact formation and/or pore pressure of formations with open fractures, lost circulation can occur. Aadnøy and Looyeh (2019) list the most common consequences of excessive hydrostatic pressure as follows:

- Excessive overbalanced mud weight
- Rock cuttings remaining in the annulus due to low hole cleaning
- Elevated viscosity and rheological properties
- Restricted annular space
- Excessive surge pressure while running the drill string or casing in the hole
- Combination of the above factors

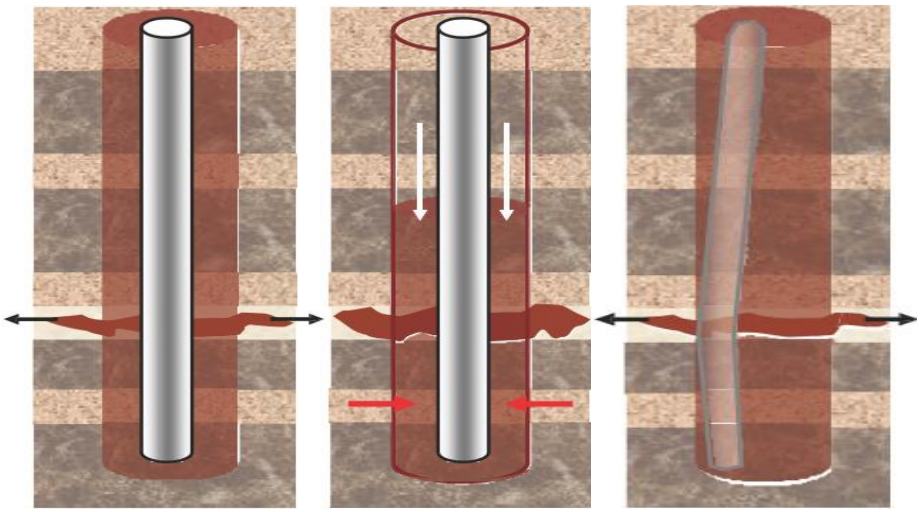

Fig. 2.1 Lost Circulation / Kick Scenario / Differential Sticking At or Near Loss Zone (adapted from DeGeare, 2003)

Drilling engineers aim to maintain equivalent circulation density (ECD) within the mud density window to avoid lost circulation or wellbore instability events. The failure causes a discontinuity on the possible stability profiles, ranging from fluid formation influx to severe or total drilling fluid loss and wellbore collapse (Cook et al., 2011), see ¡Error! No se encuentra el origen de la referencia..

At point A, the ECD window (purple section) lies between the pore pressure (blue line) and the fracture gradient (red line). In the depleted zone (B), the pore pressure and the fracture gradient shift to lower pressure levels. The production in the interval causes the ECD window to become narrower. At point C, there is a formation with poor mechanical properties, where the lower limit of the ECD window is defined by the wellbore collapse pressure and not by the pore pressure (green line). At point D, the pore pressure is high, and the fracture gradient is low, being a challenge to maintain the hydrostatic pressure into the ECD window (Cook et al., 2011).

Table 2.1 shows the classification of lost circulation based on the severity of the loss.

Table 2.1 Types of lost circulation (adapted from Elkatatny et al., 2020)

Classification	Typical loss rate (bbl/h)
Seepage	<25
Partial	25-100
Severe	>100
Total	No returns

Fig. 2.3 shows potential zones for lost circulation. In that figure, A refers to unconsolidated and depleted zones; B shows the induced fractures by excessive pressure; C is cavernous or fissures in carbonates formation; D is high permeability and high porosity formation, and E represents natural fractures, geological faults, and transition zones between carbonates and hard shale (API, 2001).

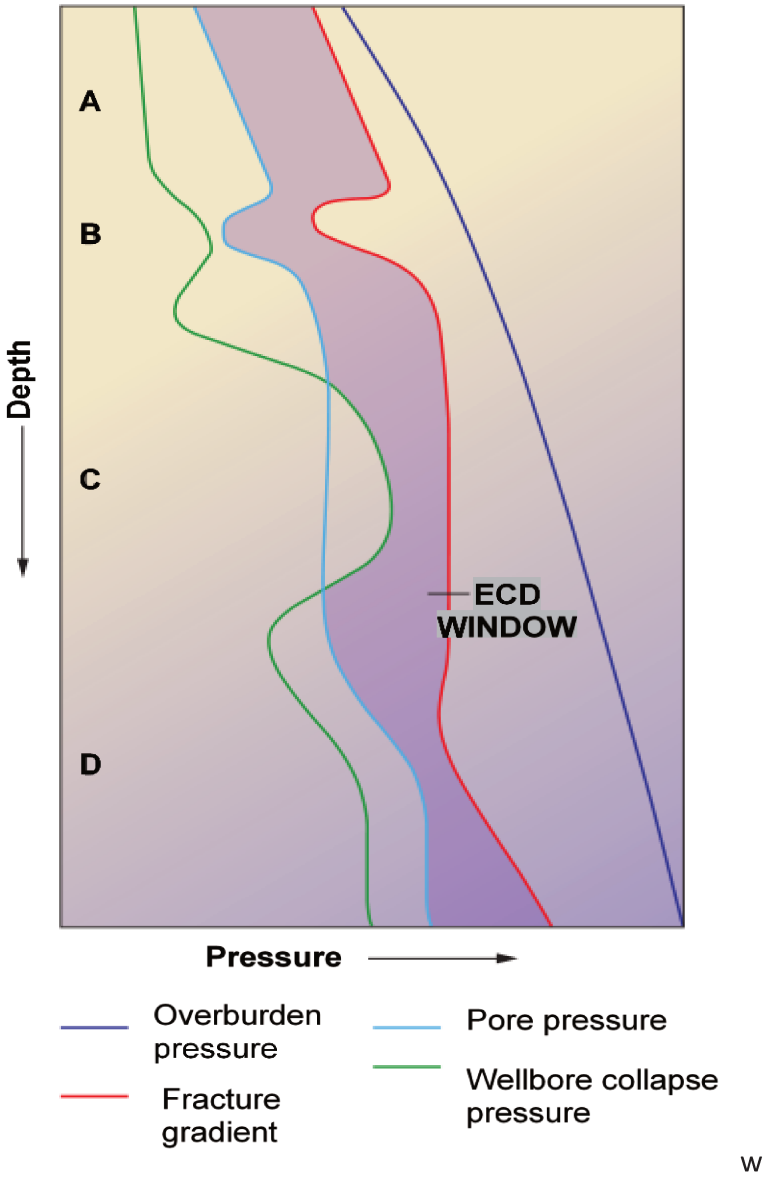

w

Fig. 2.2 Pressure gradient regimes in a wellbore (adapted from Cook et al. 2011)

In many cases, lost circulation can not be avoided, such as in cavernous, fissured, fractured, or low-pressure unconsolidated formations (usually sands) (API, 2001).

Highly permeable formations with high intergranular porosity are generally found at shallow depths. Due to the large pore sizes in this kind of zone, the formation of a filter cake on the wellbore face is not always effective; consequently, when this formation type is drilled, and the hydrostatic pressure exceeds the formation pore pressure, the mud leaks into the rock resulting in lost circulation. The loss generally begins with a gradual well level reduction and, if corrective actions are not taken, the loss can exceed the platform pumping capacity. This type of sludge leakage can range from seepage to severe leakage, and often it leads to a differential stuck pipe (Ghalambor et al., 2014; Magzoub et al., 2020).

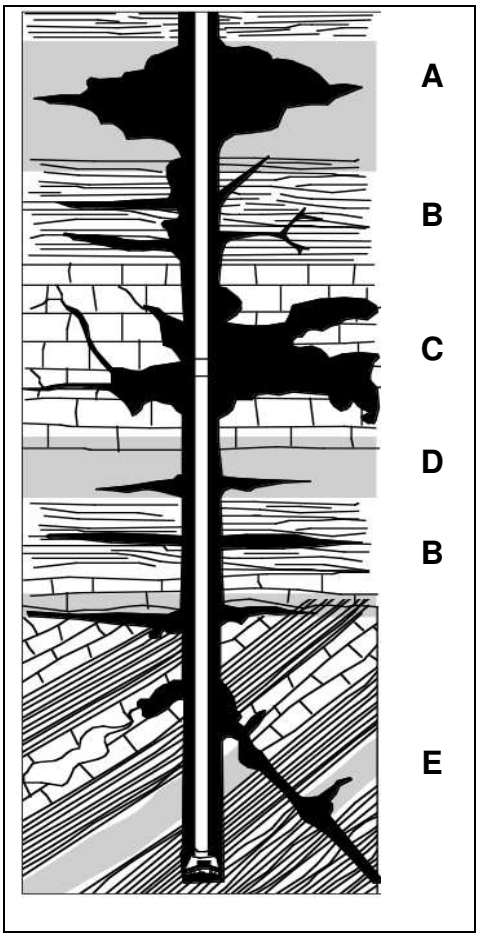

Fig. 2.3 Lost circulation sections (adapted from American Petroleum Institute API-, 2001)

A low overbalance in formations with fissures or naturally fractured can be enough to generate lost circulation. These formations are generated by geological movements that occur after sedimentation and compaction, and their highest frequency of occurrence is near faults and areas affected by tectonic forces and stresses. The initial loss rate can be low (leakage); however, it can quickly become severe if drilling continues. These areas have caused some of the most recorded troublesome lost circulation incidents (Kumar et al., 2011; Chellappah et al., 2018).

Cavernous and vugular openings are usually found in carbonate and limestone formations. In those cases, losses during drilling often are characterized by sudden and complete losses, with the bit often dropping several feet. Frequently the loss rates exceed rig pumping capabilities. The caverns result from water percolation through the formations over geological periods creating channels. Caverns can be part of a more extensive system where the voids may range from pinholes to tunnels. The pore pressure in these formations usually is sub-normal, meaning they are below the freshwater gradient (0.433 psi/ft). Caverns are the most challenging lost circulation zones to re-establish circulation (Beda and Carugo, 2001).

According to the ECD window, lost circulation in depleted formations can occur because these areas present reduced pore and fracture pressures and, as a consequence, a lower capacity of overburden pressure. The mud weight used to maintain overbalanced drilling in upper formations can be too high for the depleted formation, forcing the mud to invade the depleted low-pressure formation. When this situation can occur, plans to prevent lost circulation and avoid pipe sticking in the depleted zone should be formulated. Bridging agents and special fillers should be used to form a suitable seal and a good plaster in the depleted area (Feng and Gray, 2017).

Loss in induced fracture occurs when the ECD is greater than the fracture gradient, causing a fracture to open. Once a fracture has been created or opened by pressure, it is not easy to seal it, and the original integrity of the formation may not be restored. The lost circulation can persist, although the pressure is later reduced. That is one reason why treatment should be applied to prevent the seal from reopening or a fracture of propagating (Feng et al., 2016; Ghalambor et al., 2014; Beda and Carugo, 2001).

2.2. Lost Circulation Control Systems

Cook et al. (2011) present the prevention processes and lost circulation remediation in four levels, as shown in **Fig. 2.4**. The first level refers to best drilling practices, applying geomechanical models to calculate the risk of wellbore collapse or having lost circulation. Other methods as expandable casings, controlled pressure drilling, or casing techniques can be used during drilling. The second level focuses on selecting the drilling fluid, where the best rheological properties must be studied and selected to minimize or cure the lost circulation. The third level shows the wellbore strengthening materials, which consist of particulate materials with the appropriate formula and dimension to place into a fracture, avoiding the fracture propagation. The lost circulation remediation is shown in the fourth level, where different pills are used to stop or cure the loss.

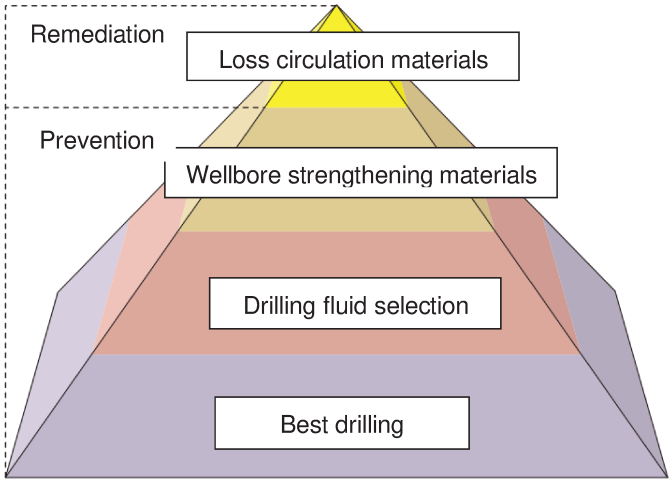

Fig. 2.4 Comprehensive lost circulation management program (adapted from Cook et al. 2011)

Numerous treatments have been proposed for curing lost circulation. However, there is no universal treatment suitable for all types of loss. The selection of LCMs or settable plugs are highly dependent on the formation types, fluid loss mechanisms (e.g., loss into pores, natural fractures, induced fractures, and vugs), and loss severity. The systems currently used to treat lost circulation problems are divided into several groups, as shown in **Fig. 2.5** (Bruton et al., 2001).

The properties required by lost circulation treatment systems are summarized below (Lavrov, 2016):

- The treatment system must be easily pumpable down the hole.
- The treatment system must be compatible with the fluids existing in the well.
- The system must be able to create an effective seal over the loss zone.
- The seal made must have the ability to withstand different pressure variations without any displacement occurring.

  The treatment system must be easily removable for future production in the area, by acid treatment or autodegradation.

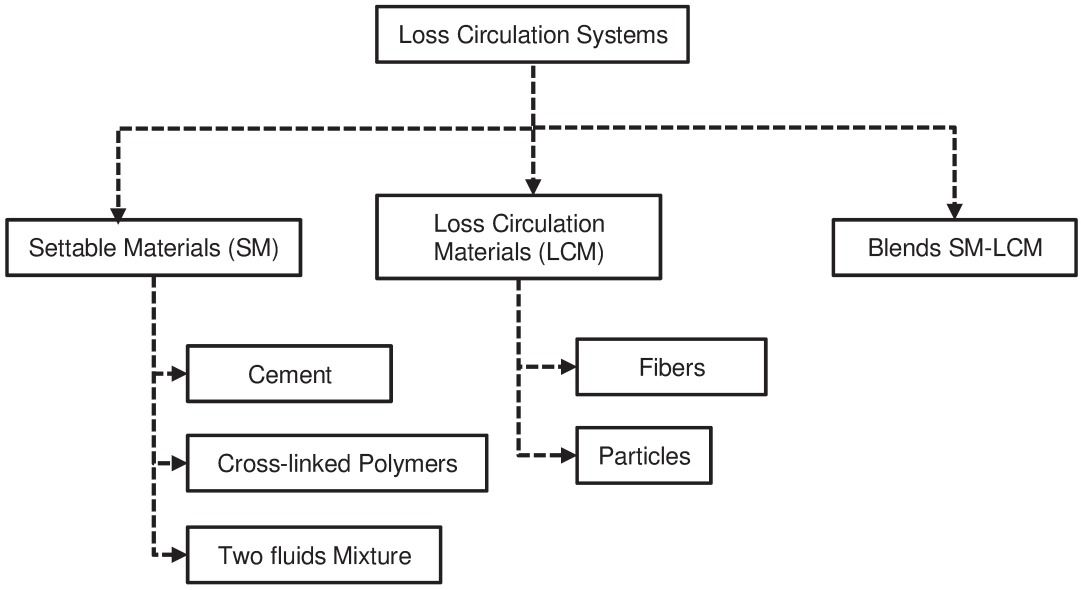

Fig. 2.5. Classification of lost circulation treatments (adapted from Lavrov 2016)

Settable material is pumped in its liquid state and acquires properties of a solid at the bottom of the well over time, thus sealing the area where the loss occurs. The settable material requires a low apparent viscosity during its liquid state to be displaced to the bottom hole, but it must be more viscous than the drilling fluid to displace it and completely replace it in fracture zones

The elastic limit is a characteristic of settable material, determining the system sealing ability to withstand under the applied differential pressure. The maximum pressure gradient that a seal can sustain at the fracture in the well during a pressure increase is simulated by two plates that consider a Bingham fluid flow. That procedure helps to determine the shear stress in the fracture walls (see **Eq. 2.1**). Therefore, to ensure efficient plugging, the shear stress at the wall must not exceed the settable material yield stress (Lavrov, 2016; Lecolier et al., 2005).

$$|\nabla P|_{max} = \frac{2\tau_y}{w_h} \qquad \textbf{Eq. 2.1}$$

where w_h is the hydraulic width of the fracture and τ_y is the yield stress of the settable material.

Cement sealing treatment is an effective system in vugular formations because cement compressive strength is higher than other settable systems (Lavrov, 2016).

The use of granular particles and flakes is effective against seepage or partial losses, but not for severe and total losses. Particles used as lost circulation materials (LCM) are known to decrease in size and change shape as they circulate. That is caused by different effects, such as particles impact among themselves or the bottom hole. Therefore, laboratory studies are required to estimate the degree of particle mechanical degradation (Lavrov, 2016). Many combinations or blends of settable material and LCM were evaluated in laboratory tests to determine their efficiency to treat all kinds of lost circulation. Different scenarios were evaluated to optimize the formulations. Alsaba and Nygaard (2014) observed that LCM's blends require a good particle distribution to guarantee their ability to seal a wide range type of fractures.

Cross-linked polymers are viscoelastic material composed of one or more polymers and cross-linking agents, typically metal ions or bifunctional organic molecules. The cross-linking process, or reticulation, involves the chemical or physical bonding of polymer chains, creating a three-dimensional network. The cross-linking bonds provide anchor points and allow for elastic energy storage, thus providing elastic properties for the gel. Despite the small amount of polymer relative to solvent, polymer gels can have high strengths. The elasticity of the polymer gel depends on the solvent amount and the flexibility of polymer chains. The gel strength reflects, among other aspects, the solvent thermodynamic quality. In some cases, a fragile gel is formed when the solvent has a low thermodynamic quality compared to the polymers (Feng and Gray, 2018)(Moradi-Araghi, 2000).

The two-liquid pill systems consist, as their name says, of two liquids that are separately pumped until they reach the loss zone and come into contact with each other forming a seal at the bottom hole. Spacers are shifted to avoid a possible mixing between these fluids before the interest zone. These two fluids can be pumped through different methods (Lavrov, 2016).

Cross-linked polymer systems are different from cement because cement plug technology is typically applied to non-production zones and is an irreversible process. That is the main reason cross-linked polymers appear as an alternative for lost circulation control. This system has high gel strength, a relatively low cost, and it can be removed before reservoir production beginning (Luzardo et al., 2015). Songire and Uppuluri (2014) demonstrated various breakers performance (oxidizers or delayed-release acids) and self-degrading cross-linked hydroxyethyl cellulose systems.

2.3. Cross-linked Systems

The main objective of cross-linking systems is to avoid undefined deformations under an applied overload, therefore restricting the movement of the chain. However, the segments of molecular cross-linked polymers remain flexible, under suitable temperature conditions, the polymer mass becomes rubbery or rigid, and the system can only flow if there is a rupture of the covalent bonds (Brydson, 2017).

On the other hand, if the cross-linking degree increases, also called cross-link density, the distance between cross-links segments decreases, and a tighter and less flexible network forms, and the segment motion becomes more restricted. Only the rigid (glass-like) state will exist in polymers with a high cross-link density. That state is commonly encountered when using thermosetting plastics such as phenolic, aminoplastic, and epoxide resins (Brydson, 2017).

Cross-linked polymers can be classified into physical and chemical hydrogels based on their cross-linking mechanism, as in **Fig. 2.6**.

Physically cross-linked hydrogels or reversible gels have gained significance due to their relative easiness of production and the advantage of not using cross-linking agents during their synthesis protocol. Physical interactions between different polymer chains prevent the dissolution of physically cross-linked gels. The selection of hydrocolloid type varies according to the concentration and polymer pH, which leads to the formation of a wide variety of gel textures. This investigation area has currently received considerable attention in food, pharmaceutical, and biomedical applications (Varaprasad et al., 2017).

The covalent bonding of polymers forms chemical or permanent cross-links through the polymerization of end-functionalized macromonomers. The hydrogel structure absorbs large amounts of water thanks to hydrogen bonds, swelling properties, and elastic modulus. The kind and degree of cross-linking affect the molecule transport and the network properties. Chemical cross-linked hydrogels can be obtained from natural, synthetic, or synthetic/natural polymers (Maitra and Shukla, 2014).

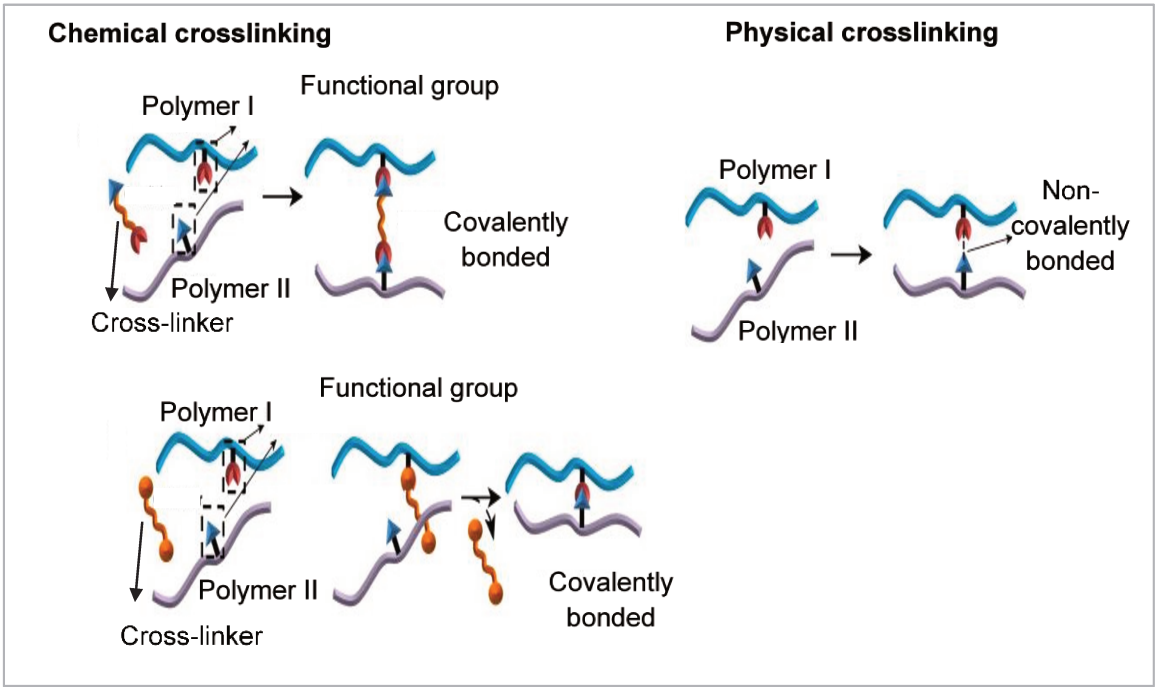

Fig. 2.6 Schematic of methods of cross-linking (adapted from Reddy et al., 2015)

Cross-linked polymer systems are used extensively in various phases of the oil industry, as an agent in conformance enhanced oil recovery process, as a proppant in fracture fluid, or as a lost circulation control agent in our case.

Many authors have developed cross-linked systems to combat lost circulation, and a compilation is shown in **Table 2.2.**

Table 2.2 Compilation of research about cross-linking gels as lost circulation control agent

System	Overview	Reference
Hydroxyethylcellulose cross-linked system	The study carried out is based on the application of a gel with an internet breaker for its degradation at a well-scale after the excellent filtrations shown in a core test apparatus for formation damage in high permeability rocks.	(Blauch et al., 1989)
Reversible hydroxyethylcellulose cross-linked system (XLHEC)	The authors demonstrated the efficiency of a cross-linking system to treat the lost circulation in high-permeability cores using static fluid loss tests and recovered permeability tests by applying gel breaking mechanisms.	(Himes et al., 1994)
Double derivatized hydroxyethylcellulose cross-linked system (DDHEC)	This work evaluated cross-linking HEC systems in different brine types to control the lost circulation in the laboratory through tests in horizontal core permeameter and vertical hassler sleeve. Gel degradation tests were carried out by adding external and internal breakers, evaluating their effectiveness in the recovered permeability test.	(Cole et al., 1995)
Hydroxyethylcellulose dissolvable particulate system	This article shows the study of a reticulated system for the control of the lost circulation, evaluating all its physicochemical properties and its efficiency in dynamic and static fluid loss tests under wide conditions of temperature and pressure. In addition to studying gel breakers through the recovered permeability test	(Nguyen et al., 1996)

Cross-linked-HEC Fluid	The study shows a procedural study of the use of an HEC and zirconium cross-linking system, showing its compatibility with different brines and breakers, performing kinetic and stability tests at different temperatures and pH, forming a gel capable of stopping the loss of fluids in 2 Darcies formations and temperatures up to 290 ° F.	(Chang et al., 1998)
Activated cross-linked pills	The authors describe the development and application of chemically activated cross-linked pills of different generations capable of sealing fluid loss areas and showing a procedural and compatibility study with different types of accelerators, retarders and spacers.	(Bruton et al., 2001)
Chemically Activated Cross-linking Pill	This paper shows the design and planning of chemically activated cross-linking pills applied to avoid lost circulation in the sub-salt loss zone of the Hassi Messaoud field, showing reductions in non-productive time	(Ferras et al., 2002)
Carboxymethylhydroxyethyl cellulose pill (CMHEC)	This paper evaluates the effects of permeability and pH in a zirconium-based cross-linked fluid loss pill, showing that the system efficiency is highly dependent on the differential pressure applied.	(Vollmer and Lejeune, 2005)
Colloidal Dispersion Gel (CDG)	The authors evaluate the technical procedure and economic analysis of a colloidal dispersion gel application in the Daqing Oilfield. They showed the effect of temperature, pH, and biodegradation on these systems.	(Chang et al., 2006)
Pre-Cross-linked Pills	This study characterizes pre-cross-linked solids-free pills and their capability to inhibit fluid loss under various conditions of temperature and flow rates in high temperature-high pressure cells and alkoxide disks representing a perforated formation.	(Gibson et al., 2011)
Fluid-Loss-Pill Formulation	This paper studies a solids-free fluid-loss pill based on a synthetic water-soluble polymer and a metal-based cross-linker, evaluating the gel-stability by static aging test, kinetics at different pH and temperature, fluid-loss control in HP/HT filter press, and gel break experiments.	(Gamage et al., 2014)
Cross-linked hydroxyethyl cellulose (CLHEC) system	This article studies the ability to control the loss of solid-free pills based on a cross-linked gel in an HP/HT fluid loss cell. It also shows the compatibility and kinetic reaction with different types of breakers applying a pressure differential of 100 psi and 260 °F.	(Songire and Uppuluri, 2014)
HPAM/PEI cross-linked gel	The authors analyzed the rheological behavior, differential scanning calorimetry, and effectiveness of the HPAM and PEI gel system as LCM in a synthetic core at a particular pressure using a 300 Darcies value of permeability at room temperature.	(Hashmat et al., 2016)
Polyacrylamide cross-linked system	The authors evaluated the lost circulation control capacity of HPAM and phenol-formaldehyde in a synthetic core composed of a transparent plexiglass cylinder and packed with glass beads, varying the permeability between 300 and 2960 Darcies.	(Hashmat et al., 2017)
Cross-linked partial hydrolysis polyacrylamide gel	The authors evaluated the capacity of PHPA gels to remediate lost circulation under high-temperature conditions and different pH ranges. They evaluated the viscoelastic gel property and gel compressive strength. The fluid loss control capacity was measured by a gel plugging agent material test apparatus using a removable cylindrical iron with different width slots.	(Jiang et al., 2019)

The use of cross-linked polymeric gels is very extensive in many industries. There are infinite combinations between cross-linking agents and polymers. Many of them can serve as an excellent solution to lost circulation problems, and the formulation proposed by Hussain et al. (2018) can be one of those. That consists of a synthesis of iron (III) containing hydroxyethylcellulose, HEC, based hydrogel with a mixture of in situ polymerized poly acid acrylic, PAA, that develops high mechanical properties. The reaction process is represented in **Fig. 2.7**.

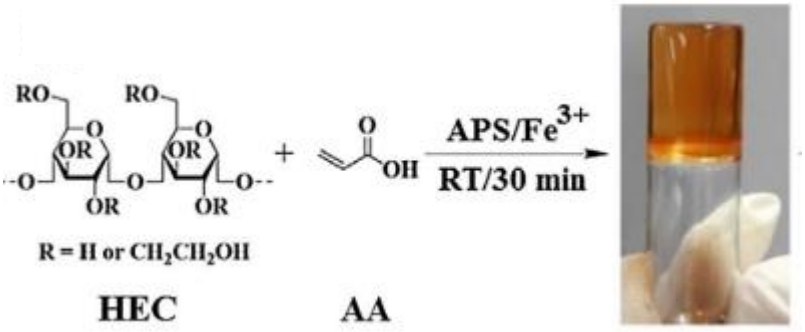

Fig. 2.7 Schematic diagram for the synthesis of HEC/PAA-Fe^{3+} hydrogel (adapted from Hussain et al. 2018)

2.4. Rheology

Different types of rheometers allow obtaining stress or strain responses applied to complex materials. Historically, rheometers were categorized as stress-controlled (a force is applied and the resulting deformation is measured) or strain-controlled (a deformation is applied, and the resulting force is measured). A new range of versatile rheometers allows performing both types of tests. Although strain-controlled instruments are more expensive than stress-controlled ones, they allow higher oscillation frequencies to be accurately probed and do not require frequent inertial calibration (Grillet et al., 2012).

2.4.1. Rotational Test

The relationship between stress and shear rate somewhat defines the rheological behavior of fluids. For Newtonian fluids, there is a proportionality constant between these parameters, defined as dynamic viscosity. However, for non-Newtonian fluids, the relationship between stress and shear rate has a non-linear behavior. In this case, the term apparent viscosity is preferable, meaning the viscosity the fluid would have in that flow condition if it were Newtonian. Mathematically, the stress-shear ratio is known as the flow equation, and its graphical representation is called the flow curve (Machado, 2002). **Fig. 2.8** shows flow curves for some fluids according to the shear stress behavior, and **Table 2.3** shows the equation for each kind of fluid.

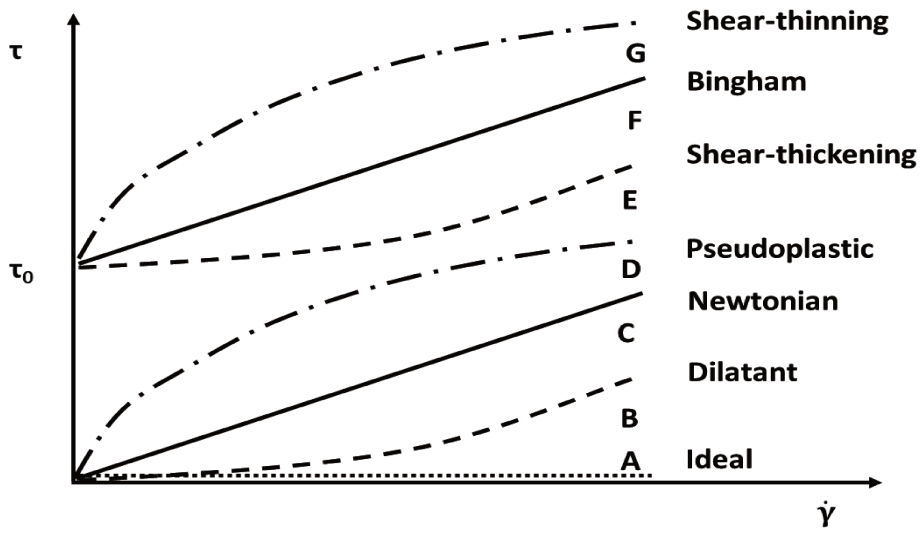

Fig. 2.8 Behavior of flow curves for some kinds of fluids (adapted from Machado 2002)

Curve A represents the behavior of an ideal fluid. There is no viscosity in this fluid type, and, therefore, the shear stress is zero for any shear rate. Curve B illustrates a dilatant fluid, where apparent viscosity increases with increasing shear rate. Curve C illustrates the behavior of a Newtonian fluid where the stress is proportional to the shear rate. Fluid D represents a pseudo-plastic fluid. Unlike the dilating fluid, the apparent viscosity decreases with increasing shear rate in this type of fluid. Fluid E, also known as shear-thickening fluid, is similar to the dilating fluid; however, this fluid only moves after limited flow stress (τ_0), or critical stress is applied. Fluid F, or Bingham, is seen as a fluid similar to a Newtonian one, but it also requires minimum stress to start the flow. Finally, the G curve represents a shear-thinning fluid. This fluid has a behavior similar to a pseudoplastic type fluid but requiring critical stress for the flow.

Table 2.3 Flow equation for each kind of fluid adapted from Machado (2002)

Fluid	Model Equation	Behavior Index
Ideal	$\tau = 0$	
Dilatant	$\tau = k\,(\dot{\gamma})^n$	n>1
Newtonian	$\tau = \eta\dot{\gamma}$	
Pseudoplastic	$\tau = k\,(\dot{\gamma})^n$	n<1
Plastic	$\tau = \tau_0 + k\,(\dot{\gamma})^n$	n>1
Bingham	$\tau = \tau_0 + \eta_p\,\dot{\gamma}$	
Herschell-Buckley	$\tau = \tau_0 + k\,(\dot{\gamma})^n$	n<1

Some empirical models have been proposed to describe these fluids behavior in one or more of these regions. The model proposed by Ostwald and Waele, also known as power-law, is the model that describes the pseudoplastic behavior of the polymeric solutions (Bird et al., 1960). However, this model does not present satisfactory parameters in the Newtonian regions, both in the upper plateau and lower plateau. A model capable of describing the behavior of polymeric solutions in the three regions was given by Carreau (1972).

The flow equations of the power-law and Carreau rheological models are shown in **Table 2.4,** where η is the apparent viscosity, and Λ is the longest relaxation time. The graphical comparison between these models is shown in **Fig. 2.8**.

Table 2.4 Rheological models and flow equations adapted from Machado (2002)

Rheological Model	Flow Equation	
Power law	$\eta = K(\dot{\gamma})^{n-1}$	**Eq. 2.2**
Carreau	$\eta = \eta_\infty + (\eta_0 - \eta_\infty)[1 + (\Lambda\dot{\gamma})^2]^{(n-1)/2}$	**Eq. 2.3**

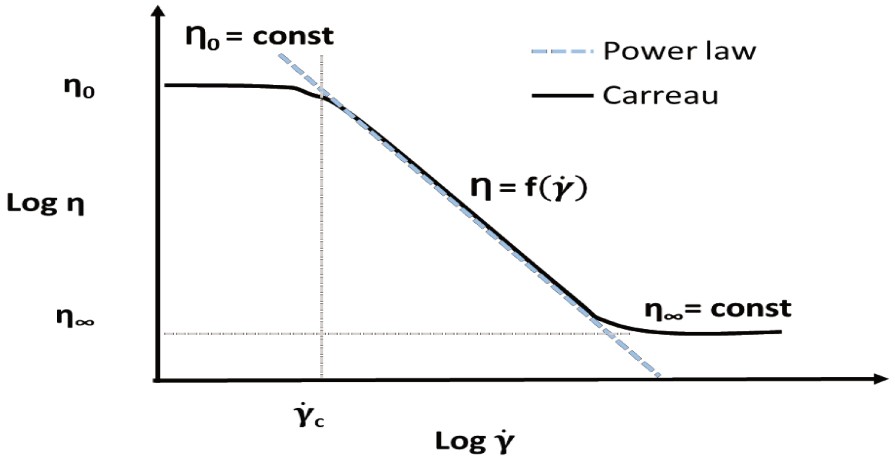

Fig. 2.9 Graphical comparison between the power law and Carreau rheological models

According to Szopinski et al. (2015), there are five distinct solution states in a thermodynamically suitable solvent: ideally diluted particle solution, semi-diluted particle solution, semi-diluted network solution, concentrated particle solution, and concentrated network solutions, as is showed in **Fig. 2.10,** where M_w is the polymer molar mass, $(c \cdot [\eta])^*$ is called the critical overlap concentration, or c*, c** delimitates two different states of the polymer solution, semi-diluted network solution, and concentrated network solution.

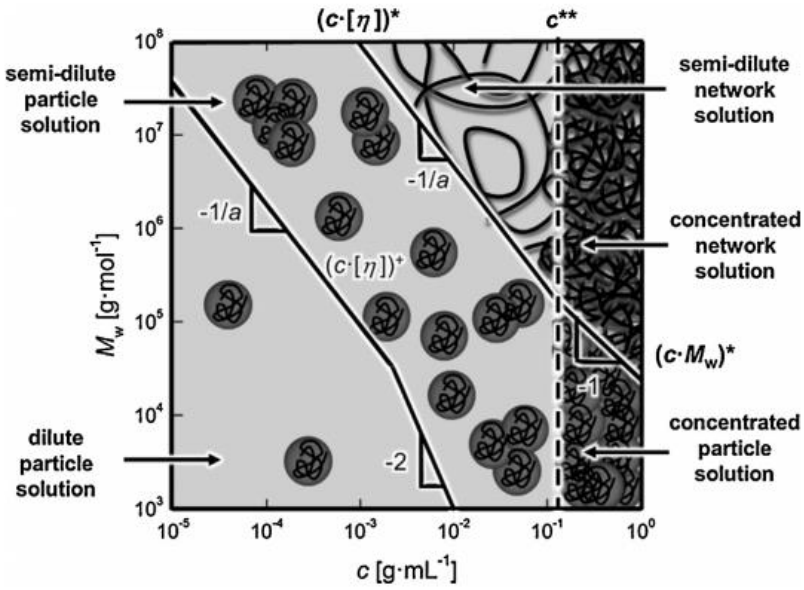

Fig. 2.10 Outline of the five states of polymer solutions (adapted from Szopinski et al., 2015)

The determination of the possible concentration regimes in polymer solutions ranges from the diluted regime to the semi-dilute one until the concentrated regime is reached. That makes it possible to understand the behavior of the polymer chains in the solution. The Brownian motion causes the polymer chains to fluctuate in solution. When concentrations are low, these individual polymer chains adopt a random spiral conformation, separating from each other and moving independently. When the individual chains initiate a physical interaction with each other, the overlapping concentration, c*, occurs. Under a dilute regime, c < c*, the translational diffusion of molecules in solution is not affected by intermolecular overlap. The molecules pack together, occupying a hydrodynamic volume. When the concentration increases, the semi-dilute regime is reached, resulting in an entanglement of the chains in the solution. The transition from the semi-dilute to the concentrated one occurs at the critical concentration of aggregation (c**), where the appearance of the aggregates can be observed, and the molecules can no longer contract (Oliveira et al., 2013).

Currently, there is a wide selection of polymers. One of them is cellulosic derivatives, such as hydroxyethylcellulose (HEC) and carboxymethylcellulose (CMC). HEC is a linear polysaccharide non-ionic polymer based on a modified cellulose structure with hydroxyethyl side chains (see **Fig. 2.11**). It is used as bulk thickeners for high-density brine fluids, such as clear completion fluids, gravel packs, and fracturing fluids, but it is not typically used in drilling fluids because it has no solids suspension ability (Caenn et al., 2011).

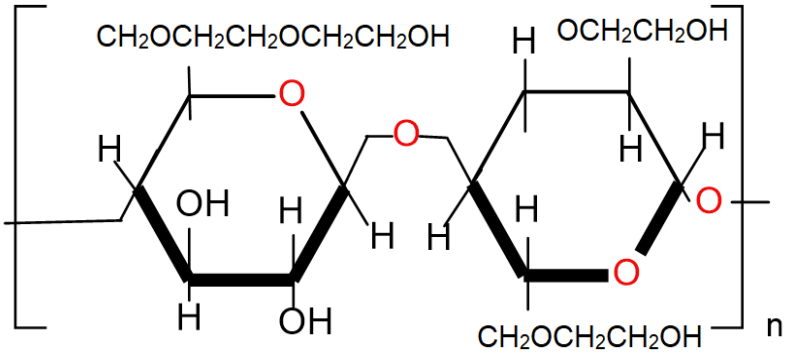

Fig. 2.11 Molecular structure of the hydroxyethylcellulose (HEC)

CMC is similar to HEC but is a linear polysaccharide anionic polymer modified with carboxymethyl (CM) (see **Fig. 2.12**). Its functionality depends on the degree of substitution (DS), the number of CM side chains, and molar mass (MW). Its uses are as fluid loss control in drilling operations; high MW is a bulk thickeners with minimal low shear-rate viscosity and minimal suspending ability (Caenn et al., 2011)(Fink, 2015).

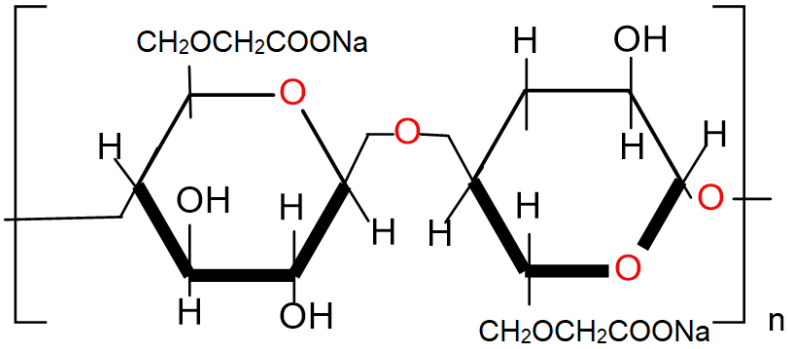

Fig. 2.12 Molecular structure of the carboxymethyl cellulose (CMC)

Castelain et al. (1987) determined the transition regimes of cellulose derivatives in aqueous solutions by plotting the apparent viscosity at a specific shear rate versus polymer concentration in the logarithmic scale, see **Fig. 2.13**.

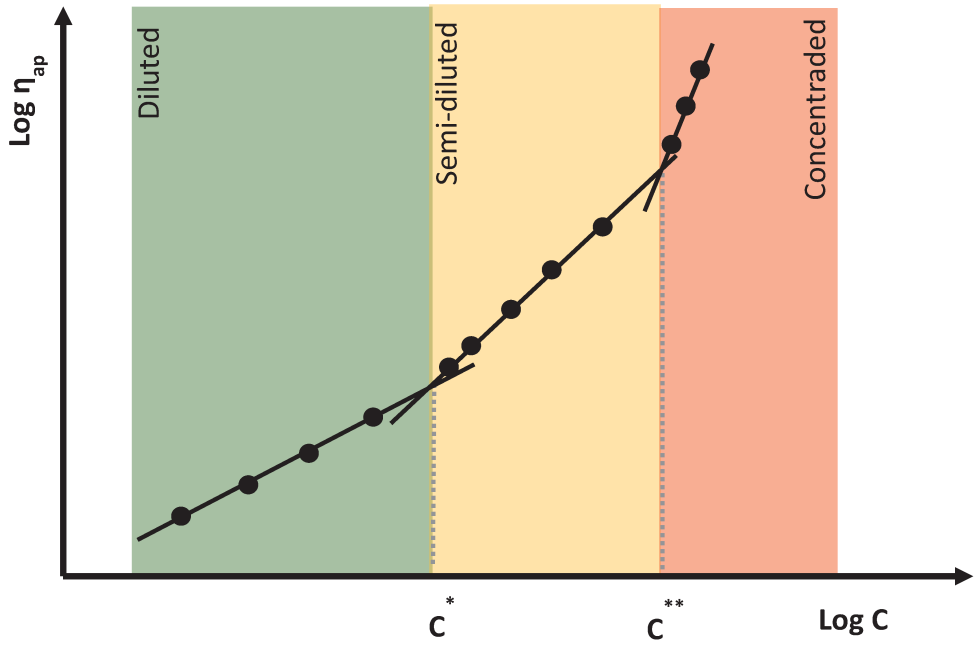

Fig. 2.13 Transition regimes of cellulose derivatives (adapted from Benchabane and Bekkour, 2008)

According to Nguyen et al. (1996) and Ouaer and Gareche (2018), the semi-diluted regime determination helps operators assess the levels of friction pressure pumping and the polymer concentration for a sufficient viscosity to transport and suspend cuttings.

2.4.2. Oscillatory tests

Oscillatory tests or mechanical analyses are used to evaluate different viscoelastic materials behavior, such as polymer solutions, emulsions, pastes, cross-linked polymers, in addition to some types of solids (Mezger, 2014).

The two-plate model is used to explain oscillatory tests (see **Fig. 2.14**). Stress relaxation and creep or stress retardation tests are convenient to study material responses to long-term loads (from minutes to days). However, these tests are less accurate for short-term loads. Oscillatory tests, in which the stress resulting from a sinusoidal strain is measured or vice versa, are better tools to investigate the polymer response at a short time range. The most common test is in oscillation, which will be described in more detail here. If the specimen under testing in a sinusoidal oscillatory behaves like an ideal elastic, the input strain, γ_{xy}, and stress response, τ_{xy}, would be as follows in **Eq. 2.4** and **Eq. 2.5** (Mezger, 2014):

$$\gamma_{xy}(t) = \gamma_0 \sin \omega t \qquad \textbf{Eq. 2.4}$$

$$\tau_{xy}(t) = \tau_0 \sin \omega t \qquad \textbf{Eq. 2.5}$$

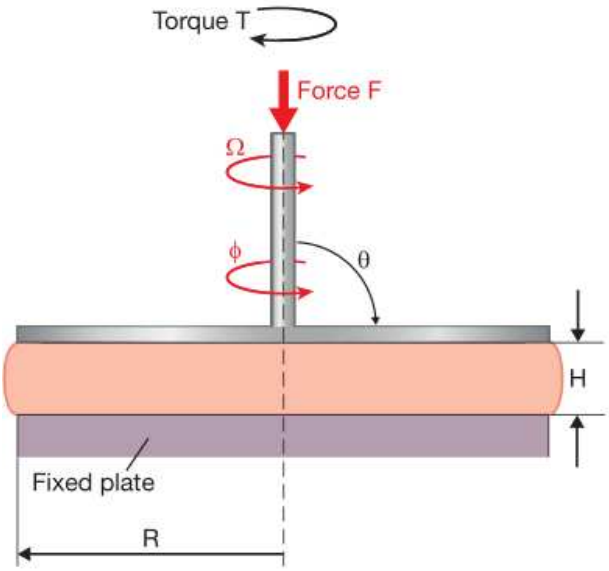

Fig. 2.14 Schematic diagram of a parallel-plate rheometer (adapted from Osswald and Rudolph, 2002)

When presetting the strain γ, the τ-curve behaves as a phase-shifted sine function due to a viscoelastic component, with a phase shift angle δ between the preset and the resulting curve (see **Eq. 2.6**). The shifting angle is usually specified in degrees [°], or in some cases, in rad. Sometimes, δ is referred to as the loss angle, as showed in **Fig. 2.15**.

$$\tau_{xy}(t) = \tau_0 \sin(\omega t + \delta) \qquad \textbf{Eq. 2.6}$$

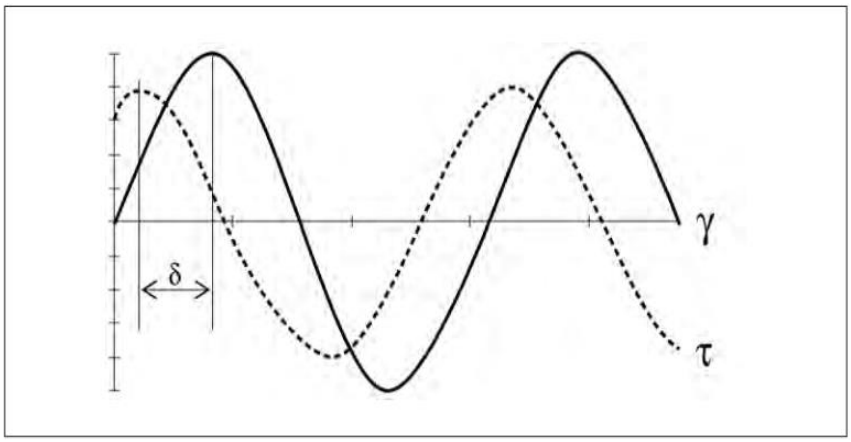

Fig. 2.15 Stress and strain time-dependent function test (adapted from Mezger, 2014)

Due to the phase shift, the overall behavior of a viscoelastic material can be subdivided into two parts, one that considers only the purely elastic part (δ = 0°), and one that considers only the purely viscous part (δ = 90°). That is expressed by **Eq. 2.8**.

$$G = G' + G'' \qquad \textbf{Eq. 2.7}$$

where G' is the storage or elastic modulus, and it is a measure of the deformation energy stored by the sample during the shear process. After the load removal, that energy is entirely available, and it acts as the driving force for the deformation process, compensating partially or entirely the previous deformation of the structure. Materials storing the total applied deformation energy shows completely reversible deformation behavior since, after a load cycle, they occur with an unchanged shape (Mezger, 2014). G'' is the loss or viscous modulus, and it is a measure of the deformation energy used by the sample during the shear process. **Table 2.5** summarizes the responses of the phase-shift angle. The energy spent during the flow is used to heat the sample and the surrounding environment (Mezger, 2014).

Table 2.5 Responses of the phase shift angle, viscous and loss modulus

Completely viscous behavior	Viscoelastic behavior of a liquid	The behavior of a half elastic half viscous material	Viscoelastic gel behavior	Completely elastic behavior
δ = 90°	90° > δ > 45°	δ = 45°	45° > δ > 0°	δ = 0°
tanδ → ∞	tanδ > 1	tanδ = 1	tanδ < 1	tanδ →0
(G' → 0)	G" > G'	G' = G''	G' > G''	(G'' → 0)

The kinetic tests are used to evaluate the behavior of the material with properties of setting, chemical curing, or particular evolution over time. It can be performed under both shear conditions, measuring the established temperature, i.e., these tests are carried out under isothermal conditions and constant low shear conditions, to keep the test in the linear viscoelasticity range (LVE) to avoid disturbances in the reaction kinetics and guarantee a cross-linking process (Mezger, 2014). **Fig. 2.16** shows the critical time (t_{CR}) or the time referring to the point where the curves of G', G'' start to sloping up with time, and t_{SG}, representing the gelling onset or the point where $\tan \delta = 1$.

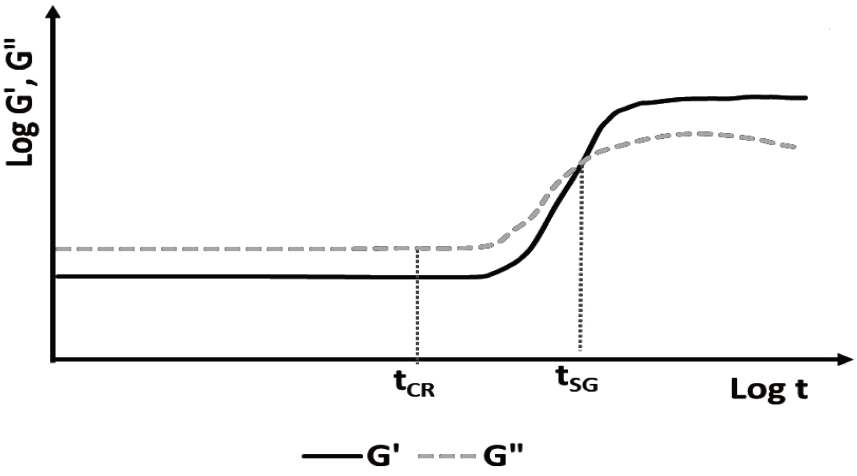

Fig. 2.16 Kinetic Evolution of cross-linking polymer (adapted from Mezger, 2014)

Many authors have been studying gel characteristics. Romero-Zeron et al., 2008 and Lapasin et al., 2018, show a study where the gelation point is obtained through the Tung and Dynes method, which consists of evaluating the moduli and phase shift angle δ relation to time, as shown in **Fig. 2.17**.

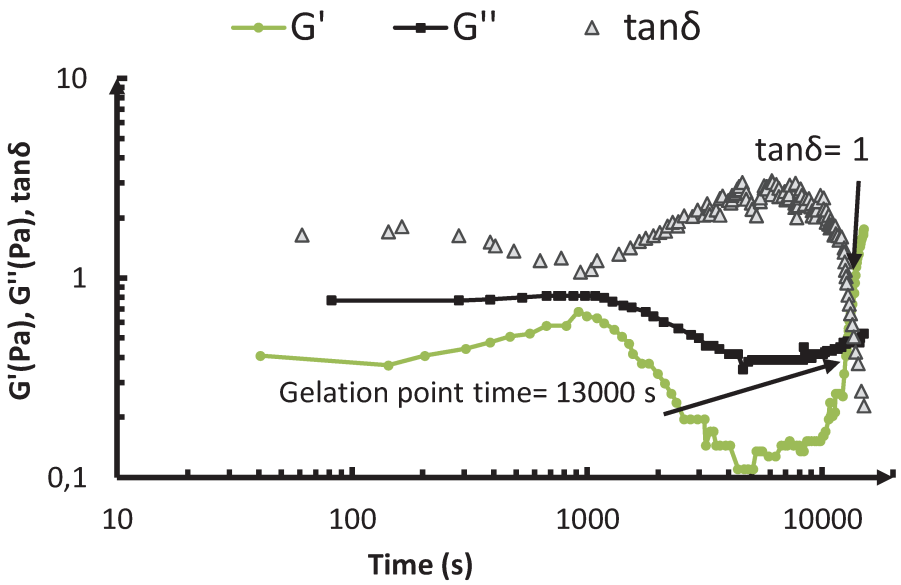

Fig. 2.17 G', G'' and tan δ vs reaction time (adapted from Romero-Zeron et al., 2008)

Marudova-Zsivanovits et al., 2007, evaluated the kinetic evolution of Xanthan gum solutions, including Cr^{3+}. They evaluated the elastic modulus against time by determining three interval ranges: the first one called the latent period, when the elastic module G' has practically the same value as xanthan gum–water solution without Cr^{3+} and the same xanthan gum concentration; the range II, characterized by a substantial increase of G' and a plateau; and the range III, where saturated values are observed. **Fig. 2.18** shows the results.

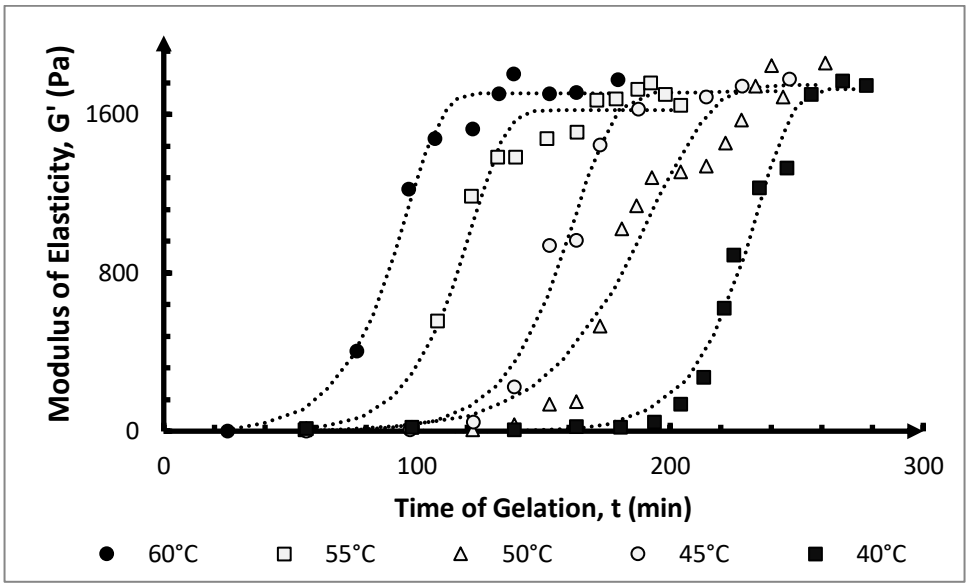

Fig. 2.18 Kinectic evaluation of Xanthan gum solutions with Cr^{3+} at different temperatures (adapted from Marudova-Zsivanovits et al., 2007)

In the linear viscoelastic range, both the G'(γ)- and G''(γ)-curves display constant plateau values. Linear-elastic behavior is found whenever Hooke's law is valid for the raw data in terms of **Eq. 2.8** or the rheological parameters as in **Eq. 2.9**, respectively. Linear-viscous behavior is found whenever Newton's law applies for **Eq. 2.10** or **Eq. 2.11**, respectively.

$$M_A / \phi_A = const \qquad \textbf{Eq. 2.8}$$

where M_A is the amplitude of the torque in the oscillatory test, mNm, and φ_A is the amplitude of the deflection angle, mrad.

$$\tau_A / \gamma_A = const\ (= G^*) \qquad \textbf{Eq. 2.9}$$

where τ_A is the shear stress amplitude in oscillatory tests, Pa, γ_A is strain amplitude, Pa, and G* is the complex shear modulus (Pa).

$$\tau_A / \dot{\gamma}_A = const\ (= \eta^*) \qquad \textbf{Eq. 2.10}$$

where τ_A is the shear stress amplitude, $\dot{\gamma}_A$ is shear rate amplitude, s^{-1}, and η* represents the complex viscosity, Pa·s.

The Cox-Merz relationship shows the following relationship for unbound polymers when held in the linear viscoelastic range:

$$|\eta^*| = \eta_0 \qquad \textbf{Eq. 2.11}$$

where |η*| represents the complex viscosity, which is measured via oscillatory tests (Pa·s), and η_0 the zero-shear viscosity, which is determined via rotational tests (Pa·s).

For a gel or a solid case, G' > G", the elastic behavior is predominant over the viscous one as in **Fig. 2.19**, where the material exhibits somewhat characteristic stiffness in gels, pastes, among others. But certain types of dispersions, foods, and other materials show low viscosity flow behavior at high shear rates. Still, the elastic modulus exceeds the viscous one (G' > G'') in the linear viscoelasticity range, LVE. In this case, they indicate gel-like consistency in the low-shear rate range, i. e, $\dot{y} \leq 1s^{-1}$ or $\dot{y} \leq 0.01s^{-1}$ for practical uses. Nevertheless, a weak gel structure can still impart a certain consistency and stability to these kinds of gels (Mezger, 2014).

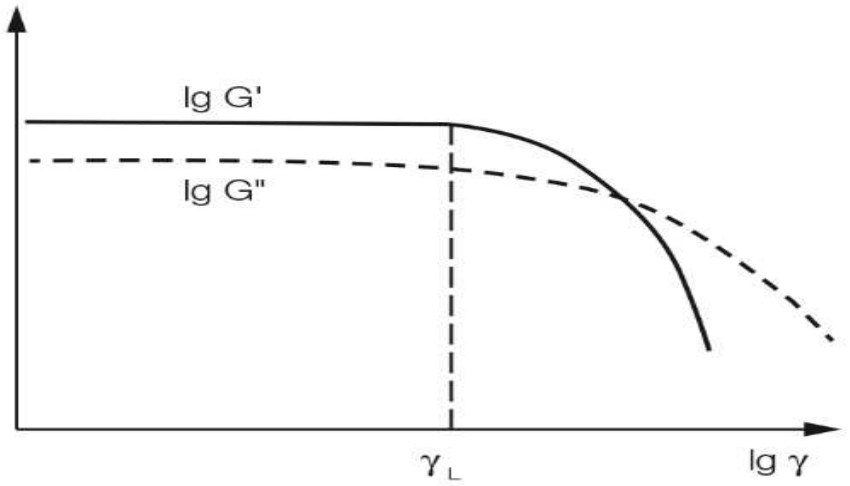

Fig. 2.19 Example of a strain amplitude test for a gel in the LVE range (adapted from Mezger, 2014)

In a liquid case, the viscous behavior dominates the elastic one (see **Fig. 2.20**). It is even possible to see this behavior in highly viscous materials with intertwined chains of molecules despite not having a consistent chemical network or physical network.. At rest, suspensions or emulsions are usually not stable since flow can occur at apparent rest. (Mezger, 2014).

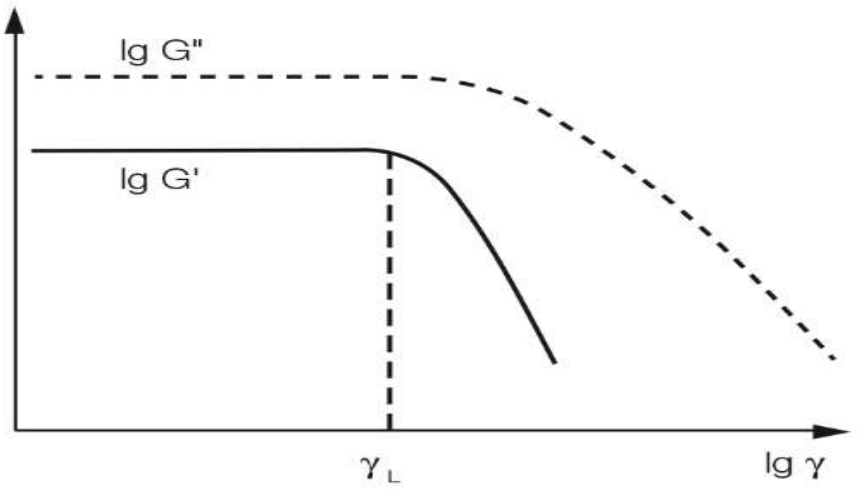

Fig. 2.20 Example of strain amplitude sweep test for a viscoelastic liquid in the LVE range (adapted from Mezger, 2014)

Weng et al., 2007, and Hvidt, 2013, applied a controlled shear stress test to find the Linear viscoelasticity range in the gels studied by each work. This measuring range (LVE) is considered the limiting value of the shear stress, or briefly, as the yield point τ_y. The tolerated deviation range has to be defined previously by the user; 10% is commonly used. Additionally, to determine the flow stress value, it is needed to pay attention to the pre-condition of G' > G'', therefore, the occurrence of a gel-like character or solid-state in the LVE range. Then, when reaching the crossover point G' = G'', the gel-like character with G' > G'' changes to the liquid state, showing G'' > G'. This point is called the flow point, τf, and the area between τy and τf is called the performance zone where the sample still has the characteristics of a gel with G'> G'', despite, the reversible-elastic deformation range has been already exceeded as shown in **Fig. 2.21** (Mezger, 2014).

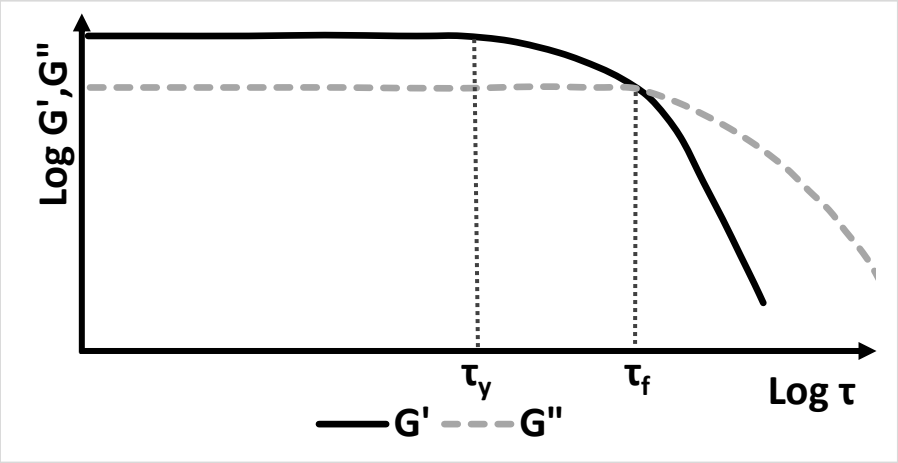

Fig. 2.21 Amplitude sweep, presented with shear stress τ plotted on the x-axis(adapted from Mezger, 2014)

Frequency sweep tests are performed at different frequencies, where the amplitude is kept at a constant value (and measuring temperature). Sometimes, the term dynamic oscillation is used as a synonym for variable frequency. The frequency represents the inverse of time; therefore, the short-term behavior is predicted at high-frequency values and the long-term behavior at low frequencies (Mezger, 2014).

Cross-linked polymers show the attachment of macromolecules through bonds that can be chemical or physical, restricting the movement of the molecules to each other through the length of these bonds. High maximum deformation values are obtained in a network showing some degree of cross-linking, delimited by the LVE range. Highly cross-linked polymers can be deformed only in a minimal range before irreversible deformation or, in some cases, destroyed, as shown in **Fig. 2.22** (Mezger, 2014).

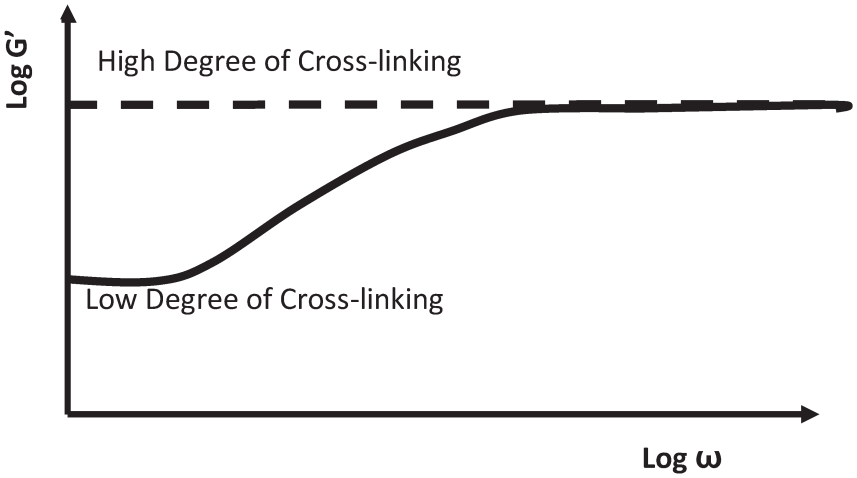

Fig. 2.22 Comparison of cross-linked polymers in principle, using G'-curves of frequency sweeps (adapted from Mezger, 2014)

Measurements of the gel modulus are used to determine the fraction of elastically effective network chains. From the rubber elasticity theory, the value of the plateau modulus G'_p, obtained by the mechanical oscillation measurements, is directly related to the number of elastically effective chains per unit volume (Kulicke et al., 1989).

Taking entanglements as localized points that are considered as fixed points like cross-links where the kinetic theory of rubber elasticity is applied. The plateau modulus, G'p, is an instantaneous modulus characterized by a single point in the modulus-time (modulus-frequency) curve that is represented by **Eq. 2.12**(Lomellini, 1992):

$$G'_P = (G')_{tan\delta \rightarrow minimum} \qquad \textbf{Eq. 2.12}$$

where the plateau modulus is determined by storage modulus value at the minimum point of tan δ.

2.5. NMR Basic Principles

Nuclear magnetic resonance (NMR) is one of the broad phenomena associated with electromagnetic radiation and matter. There are tests similar to this type of interaction, with the difference in the frequencies ranges used, such as X-rays from with an approximate frequency of 10^{18} Hz, the domestic microwave operation at frequencies of 10^9 Hz, induction through radiofrequency at the order of 10^6 Hz (Mishra et al., 2017).

The energy levels of NMR are associated with different nuclear magnetic moment orientations of an atom in an applied magnetic field. As we shall see, the spacings between these energy states correspond to radiation in the radiofrequency ranges. Thus transitions between the levels will be induced by an applied radiofrequency magnetic field (Cowan, 1997).

2.5.1. Relaxometry

Low resolution nuclear magnetic resonance relaxometry (LRNMR) helps to study and identify molecular species and complex materials. This technique is commonly used to determine and characterize solid-liquid and oil-water proportions in materials as diverse as oleaginous rocks, emulsions, among others. Relaxometry experiments consist of the application of an external static magnetic field B_0 to a sample containing NMR active nuclei. The net effect is a measurable magnetization parallel to B_0, due to the nuclear spin. This magnetization vector is perturbed through a sequence of pulses, which dephase the magnetization vector, and the magnetization relaxes back to its original state, hence the name relaxometry (Edelman, 2010).

2.5.2. Spin-echo Detection

The dephasing caused by the inhomogeneity of the static magnetic field B_0 is reversible. After an initial pulse of 90°, the proton magnetization vectors in the transverse planes can be re-phased when a 180° amplitude of the oscillating field pulse, B_1, is applied. When the phase angle of the transverse magnetization vector is equal to α. The application of a 180° pulse B_1 will change the phase angle to -α, reversing the transverse magnetization vectors phase order, slowing the vectors ahead of the faster ones. Later, when the fast vectors exceed the slower ones, they will cause the phase change, generating a signal that will be detected in the receiving coil. That signal is known as a spin-echo, and it occurs when the phase shift time is equal to the spin-echo peak at 2τ, defined as inter-echo spacing, TE. This procedure is illustrated in **Fig. 2.23** (Coates et al., 1999).

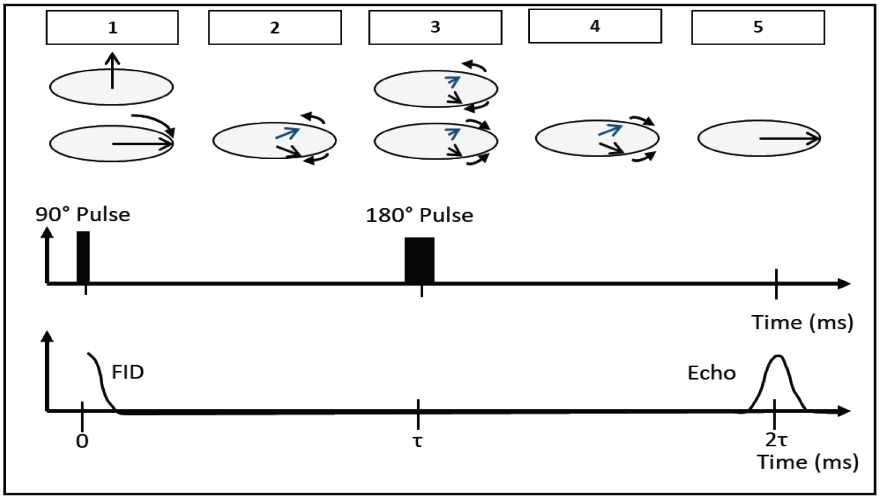

Fig. 2.23 Spin-echo generation (adapted from Coates et al., 1999)

2.5.3. Measurement of T_2

T_2 is the time constant associated with the intrinsic decay of transverse magnetization, irrespective of the inhomogeneity of the magnetic field. Measurements such as the height of the echo give a single data point. Therefore, it is necessary to capture many data points by repeating

the 90° -t- 180° -t- echo sequence with different delay intervals t to establish the value of T_2 (Cowan, 1997).

The repeated application of 180° pulses can phase the component magnetization and generate a series of spin echoes, as is showed in **Fig. 2.24**. A spin echo is formed midway between each pair of 180° pulses, generating the spacing time between echoes that was previously defined as TE. The CPMG sequence, named after its developers Carr, Purcell, Meiboom, and Gill, refers to the joint sequences of the 90° and 180° pulses, which omits the lag caused by the B_0 field inhomogeneity. However, the lag resulting from molecular interactions and diffusion is irreversible, causing the CPMG sequence decomposition. As shown in **Fig. 2.25**, an NMR logging tool measures the amplitude of the spin-echoes in the CPMG sequence to monitor the transverse magnetization decay and thus the irreversible dephasing (Coates et al., 1999).

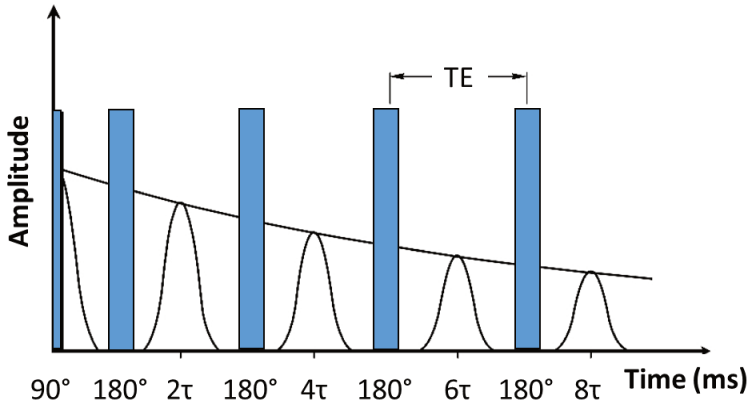

Fig. 2.24 Generation of a spin-echo train (adapted from Coates et al., 1999)

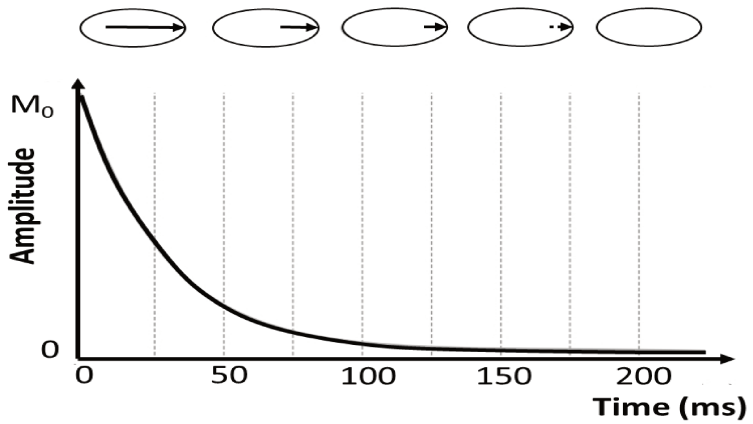

Fig. 2.25. The amplitudes of the decaying spin echoes (adapted from Coates et al., 1999)

Different authors have monitored the gelation through nuclear magnetic resonance relaxometry, obtaining effective results such as in the works presented by Gonera and Cornillon, 2002; Hansen and Lund, 1995 and Zhang et al., 2002. On the other hand, Romero-

Zeron et al., 2008, evaluated the use of low-field NMR as a non-intrusive technique to monitor gelation rates and characterize gel strength. That is based on the evolution of the transverse relaxation time (T_2), at the same time, analyzed a common problem in gels called syneresis.

Syneresis is the process first identified in colloidal solutions whereby the spontaneous gel contraction results from liquid expulsion (GeoffTanner, 2003). In 1928, Kunitz analyzed gelatin gel syneresis and realized two important factors affecting this phenomenon: osmotic pressure and polymeric gel matrix elasticity. Osmotic pressure is the standard thermodynamic quantity used to evaluate the driving force of the transfer of water from one phase to another. Due to not being destructive techniques, the methods used in NMR are used for a possible correlation between free or slightly bound water with potential syneresis (Mizrahi, 2010).

Continuing with the study presented by Romero-Zeron et al., 2008, they developed two graphs from the NMR test. **Fig. 2.26** shows the gels evolution and the syneresis effect appearance in one of them. **Fig. 2.27** illustrates the normalized amplitude and reaction time as a function of relaxation time, allowing us to observe the changes that the gel spectrum endures with the time.

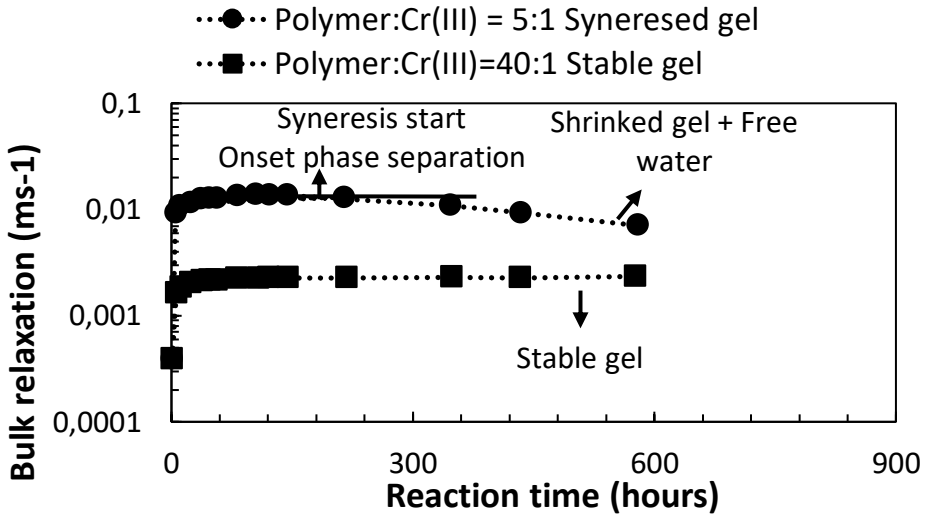

Fig. 2.26 Relaxation rate vs. time (adapted from Romero-Zeron et al., 2008)

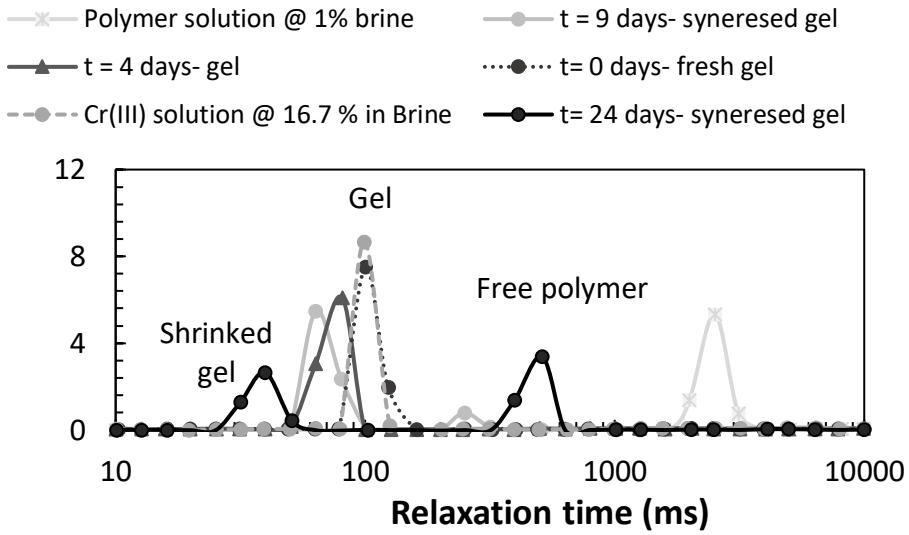

Fig. 2.27 Amplitude index vs. relaxation time (adapted from Romero-Zeron et al., 2008)

2.6. Bottle Testing Method

According to Sydansk and Smith, 1988, it is possible to provide a semiquantitative measurement of gelation rate and gel strength by bottle testing. It consists of inverting a bottle containing the gel and observing its behavior in a short time. Depending on how quickly the fluid flows and how much one can assign a strength code. By performing several tests with the system at a constant temperature, it is possible to observe the parameters as a function of time. The gel-strength code developed and used to characterize the bottle- testing data is included in **Table 2.6**.

Table 2.6 Gel Strength Codes of Bottle Testing (Sydansk and Smith, 1988)

CODE:	
A	**No detectable gel formed:** The gel appears to have the same viscosity as the original polymer solution and no gel is visually detectable.
B	**Highly flowing gel:** The gel appears to be only slightly more viscous than the initial polymer solution.
C	**Flowing gel:** Most of the detectable gel flows to the bottle or ampule top upon inversion
D	**Moderately flowing gel:** A small portion (about 5 to 15%) of gel doesn't readily flow to the bottle or ampule top upon inversion.
E	**Barely flowing gel:** The gel can barely flow to the bottle or ampule to and/or a significant portion (>15%) of the gel doesn't flow upon inversion.
F	**Highly deformable nonflowing gel:** The gel does not flow from the bottle or ampule top upon inversion. The gel just flows reach short of the bottle or ampule top.

G	**Moderately deformable nonflowing gel:** The gel flows about half way down the bottle or ampule upon inversion.
H	**Slightly deformable nonflowing gel:** Only the gel surface slightly deforms upon inversion.
I	**Rigid gel:** There is no gel-surface deformation upon inversion; and the gel is stable and clear.
J	**Ringing rigid gel:** A tuning-fork-like mechanical vibration can be felt after tapping the bottle. This code isn't used during high-temperature ampule testing due to the use of a safety shield container.

Karimi et al., 2014, evaluated the hydrolyzed polyacrylamide (HPAM) and Cr (III) gel system based on the bottle testing method and concluded that the final strength code of the gel is a very significant parameter. Knowing the final strength code of a gel can help to understand the expected goal from the gel. The illustrative gel-strength code is shown in **Fig. 2.28.**

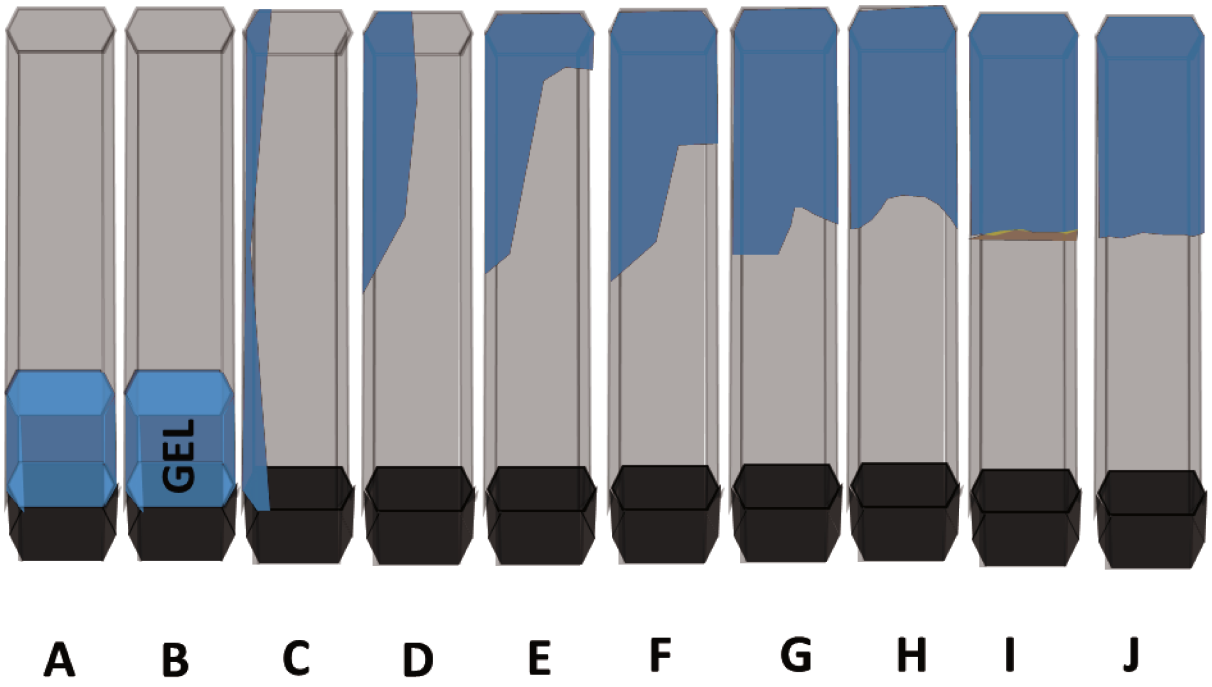

Fig. 2.28 Visualization of the Sydansk gel strength code table (adapted from Karimi et al., 2014)

2.7. Static Filtration Principles

The permeability alteration on the formation face is associated with the fluid filtration, which progresses to form an invaded zone due to the fine particles that the fluid can contain. That causes a deterioration in the formation and reduces its productivity, commonly known as formation damage. **Table 2.7** shows the most significant parameters observed in the well

filtration. From the number of shown mechanisms, it is clear that formation damage control is challenging as it can include more than one mechanism at a time (Peden et al., 1984).

Table 2.7 Parameters influencing borehole filtration (adapted from Peden et al., 1984)

Rock Properties	Wellbore Fluid Properties	Wellbore Hydraulic Conditions	Physical Environment of Wellbore
a) Tortuosity b) Relative Permeability to both in-situ and invading fluid c) Mean pore sizes d) porosity	a) Type of Fluid b) Base fluid properties (filtrate), particularly viscosity c) Chemical activity of constituent, e.g., surface activity d) Concentration of constituent particles e) Shape and size distribution of constituent particles f) Rheological properties of the fluid g) Type of cross-link	a) The annular velocity of mud flow b) The duration and sequence of the various methods of filtration in the borehole c) The shear stress/rate on the filter cake surface d) The mud circulation rate and nozzle discharge velocity	a) Temperature of fluid in the borehole b) Absolute pressure in the borehole c) Differential pressure between borehole and formation d) Inclination angle of the wellbore e) Frequency and severity of physical contact between the drill string and the filter cake on the borehole wall f) Drilling rate g) Rotary speed and type of bit

Static filtration occurs when fluid pumping is interrupted, creating a difference between the hydrostatic pressure in the wellbore and the reservoir pore pressure, and from that point, static filtration occurs. Static filtration rates are controlled by the continuous thickening of the mud cake (Calçada et al., 2011).

Spurt loss is the fluid loss per area before forming a filter cake and is very significant in naturally fractured reservoirs. It is directly proportional to reservoir permeability and is an essential part of the fracturing operation, and an efficient fluid-loss additive would not only coat the fracture face but also prevent excessive spurt loss from occurring (Speight, 2016).

Spurt-loss occurs in an initial brief period of rapid fluid loss and has been observed in laboratory experiments. Because of its brevity, it is commonly characterized as an apparent positive interception on plots of fluid-loss volume versus square root of time, as is shown in **Fig. 2.29** (Soliman, 1994).

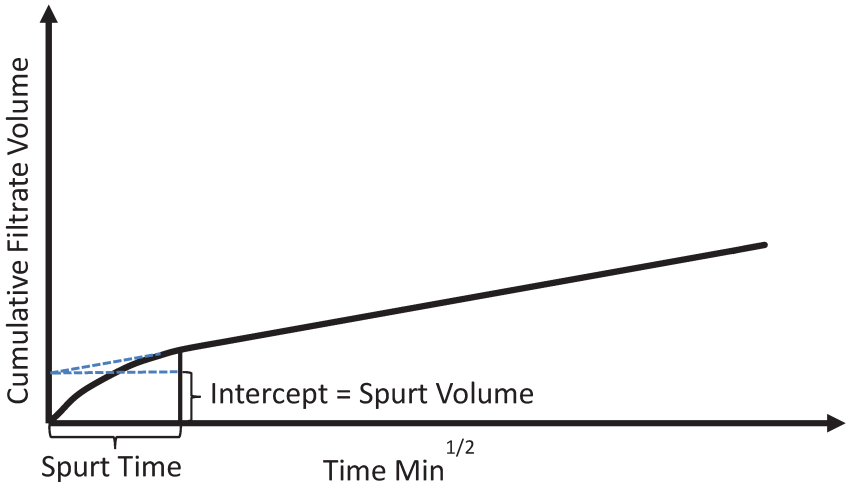

Fig. 2.29 Cumulative volume versus time (adapted from Soliman, 1994)

2.8. Design of Experiments

Design of Experiments (DOE) is defined as a systematic procedure carried out under controlled conditions to discover an unknown effect, test or establish a hypothesis, or illustrate a known effect. It involves determining the relationship between input factors affecting a process and the output of that process. It helps one to manage process inputs in order to optimize the output. They can be qualitative, like the type of catalyst, or quantitative, like the temperature. Sometimes, there are knowing factors affecting the responses in a given experiment, but which are difficult to control, or there is no interest (Barros Neto et al., 2010).

The correct approach to dealing with several factors is to conduct a factorial experiment. That is an experimental strategy in which factors are varied together, instead of one at a time. Fortunately, if there are four to five or more factors, it is usually unnecessary to run all possible combinations of factor levels. A fractional factorial experiment is a variation of the basic factorial design in which only a subset of the runs is used (Montgomery, 2017). **Fig. 2.30** shows an example between the number of experiments 2^k that could be reduced by a fractional factorial DOE to 2^{k-1}.

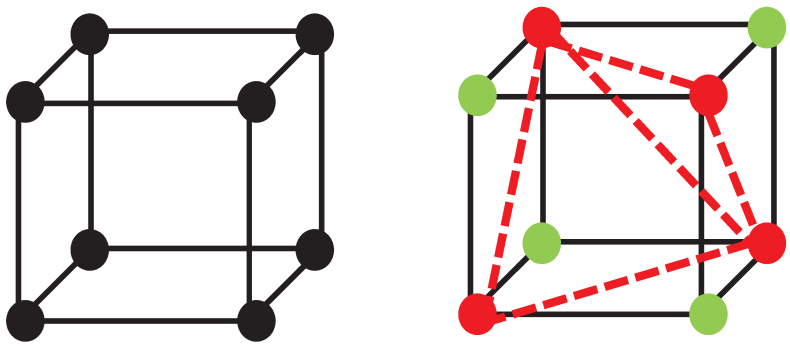

Fig. 2.30 Reducing a 3-factor full factorial design to a 'half fraction' design (adapted from Pallister et al., 2015)

2.8.1. Statistical Analysis

One of the most common problems for experimenters is determining the influence of one or more variables on another variable. In statistical language, the objective of the person carrying out the experiments is to discover the function of the factors on the answers, or at least to obtain a satisfactory approximation. One way to calculate the effects can be done by codifying the original variables where the real values of 2^k factors are replaced by factors $-1 \leq x_i \leq +1$. This methodology is widely applied because coded variables are very useful to determine the relative importance of factor effects (Montgomery, 2017). **Eq. 2.13** shows how to calculate and solve the coded values

$$coded\ value = \frac{real\ value - average\ of\ the\ values}{maximum\ value - minimum\ value} \quad \textbf{Eq. 2.13}$$

The statistical model used to describe the responses is related to the fit of a linear model to the planning points, where the matrix equation that describes the model is **Eq. 2.14.**

$$y = X\beta \quad \textbf{Eq. 2.14}$$

where $\hat{y}$ is a column vector with the answers, X is a matrix with each column corresponding to a factor or interaction, and each row is an experiment, and β is a column vector containing the model coefficients. For a factorial 2^2 case, the model would be developed as follows(Barros Neto et al., 2010):

$$y = \begin{bmatrix} \bar{y}_1 \\ \bar{y}_2 \\ \bar{y}_3 \\ \bar{y}_4 \end{bmatrix}; \boldsymbol{X} = [1 \quad x_1 \quad x_2 \quad x_{1,2}]\ ; \boldsymbol{\beta} = \begin{bmatrix} b_0 \\ b_1 \\ b_2 \\ b_{1,2} \end{bmatrix}$$

In order to calculate the intercept (b_0), it is necessary to add the column of 1's to the left of all columns, and the equation of the linear fit for a factorial DOE 2^2 would be as follows in **Eq. 2.15**.

$$y(x_1, x_2) = b_0 + b_1 x_1 + b_2 x_2 + b_{1,2} x_{1,2} + \varepsilon(x_1, x_2) \quad \textbf{Eq. 2.15}$$

where ε is the random error associated with answer $y(x_1, x_2)$. Furthermore, solving these equations implies finding β, which is done by the following matrix equation **Eq. 2.16**:

$$\beta = (X^T X)^{-1} X^T y \quad \textbf{Eq. 2.16}$$

where T indicates the transpose of X, and $(\cdot)^{-1}$indicates the inversion of a matrix.

2.8.2. Analysis of variance

The examination of residues is essential for us to assess the quality of fit of any model. First, the residues must be small because if a given model leaves many residues, it is probably a flawed model. The most used method to numerically evaluate a model fit quality is the Analysis of Variance (ANOVA). The standard error for the parameters is calculated using the covariance matrix, defined as in **Eq. 2.17** (Barros Neto et al., 2010).

$$Cov(\boldsymbol{\beta}) = \begin{bmatrix} V(b_0) & Cov(b_0, b_1) & Cov(b_0, b_2) \\ Cov(b_1, b_0) & V(b_1) & Cov(b_1, b_2) \\ Cov(b_2, b_0) & Cov(b_2, b_1) & V(b_2) \end{bmatrix} = (\boldsymbol{X}^T\boldsymbol{X})^{-1}\sigma^2 \qquad \textbf{Eq. 2.17}$$

where σ^2 is the experiment variance, V(b_1) is the variance of the parameter b_i and Cov (b_i, b_j) is the covariance between the parameters b_i and b_j. Using an estimate for σ^2, one can estimate the standard errors of the terms of b by the square root of the diagonal of the covariance matrix (since the standard deviation squared is the variance). The model quality analysis can be done through ANOVA. This methodology involves performing the decomposition of the variance of the model into components referring to the regression, the residue, and if there are replicates, the pure error, and the lack of adjustment (Barros Neto et al., 2010).

Table 2.8 Analysis of variance table (ANOVA) for a linear model used by the combined squares method (adapted from Barros Neto et al., 2010)

Variation Source	Sum of Squares (SS)	Degrees of Freedom	Mean Squares (MS)
Regression (*R*)	$SS_R = \sum_i^m \sum_j^{n_i} (\hat{y}_i - \bar{y})^2$	$p-1$	$MS_R = \frac{SS_R}{p-1}$
Residual (*r*)	$SS_r = \sum_i^m \sum_j^{n_i} (y_{ij} - \hat{y}_i)^2$	$n-p$	$MS_r = \frac{SS_r}{n-p}$
Pure error (Pe)	$SS_{Pe} = \sum_i^m \sum_j^{n_i} (y_{ij} - \bar{y}_i)^2$	$n-m$	$MS_{pe} = \frac{SS_{pe}}{n-m}$
Lack of Fit (LoF)	$SS_{LoF} = \sum_i^m \sum_j^{n_i} (\hat{y}_i - \bar{y}_i)^2$	$m-p$	$MS_{LoF} = \frac{SS_{LoF}}{m-p}$
Total (*T*)	$SS_T \sum_i^m \sum_j^{n_i} (y_{ij} - \bar{y})^2$	$n-1$	

Parameters: n_i is the number of repetitions at level i; m is the number of distinct levels of the factor; $n = \sum n_i$ is the total number of observations; p is the number of parameters; $\hat{y}$ is the predicted value, $\bar{y}$ is the total average value, $\bar{y}_i$ is the average value of level i; y_{ij} is the j-th

repetition of the i-th level. The calculation of the mean square (MS) is done by dividing the quadratic sum by the number of degrees of freedom.

The quadratic regression and residual sums, when added together, are equivalent to the total sum of squares (SS) $SS_T = SS_R + SS_r$. The residual sum of squares can be divided into two, the lack of fit and the pure error, $SS_r = SS_{Pe} + SS_{LoF}$. The Mean squares MS_R, MS_r, MS_{Pe} and MS_{LoF} are obtained by dividing the sum of squares by the number of degrees of freedom. Several quality parameters can be extracted from **Table 2.8**. The best known is the explained variance coefficient, $R^2 = SS_R/SS_T$. In essence, the closer to 1, the greater the regression contribution, and the smaller the residual found. This value can be overestimated if the number of parameters is large, in which case the adjusted explained variance coefficient is used, $R'^2 = MS_R/MS_T$. If there are replicates, it is possible to estimate the maximum percentage explainable variation, $\%max = (SS_T - SS_{ep})/SS_T$. In this case, the proximity of R^2 to %max is evaluated. Exceptionally for performing a regression of a simple line, the linear correlation coefficient r is equal to the square root of R^2 (Barros Neto et al., 2010).

Besides, statistical tests can be carried out to assess the quality of the model and assess whether there is a lack of adjustment. Two F statistics can be calculated and compared with the F distribution. First, the need for terms other than b_0 is assessed:

$$\hat{F}_{p-1,n-p} = MS_R/MS_r \qquad \textbf{Eq. 2.18}$$

If $\hat{F}_{p-1,n-p}$ is greater than $F_{p-1,n-p}$ tabulated value, it is concluded that the existence of these terms is justified. Another test that can be done, if there are replicates, is:

$$\hat{F}_{n-m,m-p} = MS_{pe}/MS_{LoF} \qquad \textbf{Eq. 2.19}$$

In this case, signs of lack of fit are assessed. If this calculated value is greater than the tabulated value, this indication is achieved. Therefore, it is necessary to increase the number of parameters, interactions, or add a quadratic term, because there is a significant lack of fit.

An estimate of σ^2 is used to calculate the confidence interval of the parameters, MS_r when there are no replicates or if the ratio MS_{Pe} / MS_{LoF} is low. Otherwise, MS_{Pe} is used, especially if the observed noise is not random. The number of degrees of freedom of σ^2 is equal to the number of degrees of freedom of the adopted square mean (Barros Neto et al., 2010).

2.8.3. Response Surface Methodology

Response surface methodology, or RSM, is a useful collection of mathematical and statistical techniques for problem modeling and analysis in which several variables influence the

response of interest, and the objective is to optimize this response. The response surface is usually graphically represented to help visualize the shape of a response surface. The contours of the response surface are often plot. Each contour corresponds to a particular height of the response surface. In the RSM evaluations, the relationship between the response and the independent variables is mainly unknown. Therefore, the objective is to find an adequate approximation for the functional relationship between the responses and the set of independent variables. If an expected fit is not achieved when a linear function model was applied, higher-order fits should be used to correctly determine the responses model (see Eq. 2.15) (Montgomery, 2017).

3. MATERIALS AND METHODS

This chapter includes the applied methodologies, related materials, and equipment used to develop the characterization and evaluation of this work.

3.1. Fluids Components

Based on the explanation of cross-linked polymer gels in **2.3**, the components showed in **Table 3.1** were selected to develop the present work.

Table 3.1 Fluids composition

Component	Function
Carboxymethylcellulose	Gelant agent
Hydroxyethylcellulose	Gelant agent
Sodium Chloride	Densifying material
Chromium (III) Acetate Hydroxide	Cross-linker agent
Iron (III) Chloride Hexahydrate	Cross-linker agent
Zirconyl Chloride Octahydrate	Cross-linker agent
Acrylic Acid	Gelant agent
Sodium hydroxide	pH increaser
Ammonium persulfate	Polymerization initiator
Deionized Water	Fluid base

Carboxymethyl cellulose (CMC) with molar mass of 250,000 $g \cdot mol^{-1}$ and 700,000 $g \cdot mol^{-1}$, both with a degree of substitution 0.9, hydroxyethylcellulose (HEC) with a molar mass of 720,000 $g \cdot mol^{-1}$, acrylic acid (AA, purity = 99%), ammonium persulfate (APS, purity ≥ 98%), chromium (III) acetate hydroxide, iron (III) chloride hexahydrate, zirconyl chloride octahydrate and sodium chloride (purity ≥ 99%) were all supplied by Sigma-Aldrich. Sodium hydroxide PA (purity = 97%) was purchased from Êxodo Científica. The supplier informed the purity level of the chemicals, and no further purification procedures were applied.

3.2. Methodology

Based on the characteristics described for a lost circulation system in section **2.2**, the work was developed in phases, as shown in **Fig. 3.1**. Each phase will be described in greater detail in later sections.

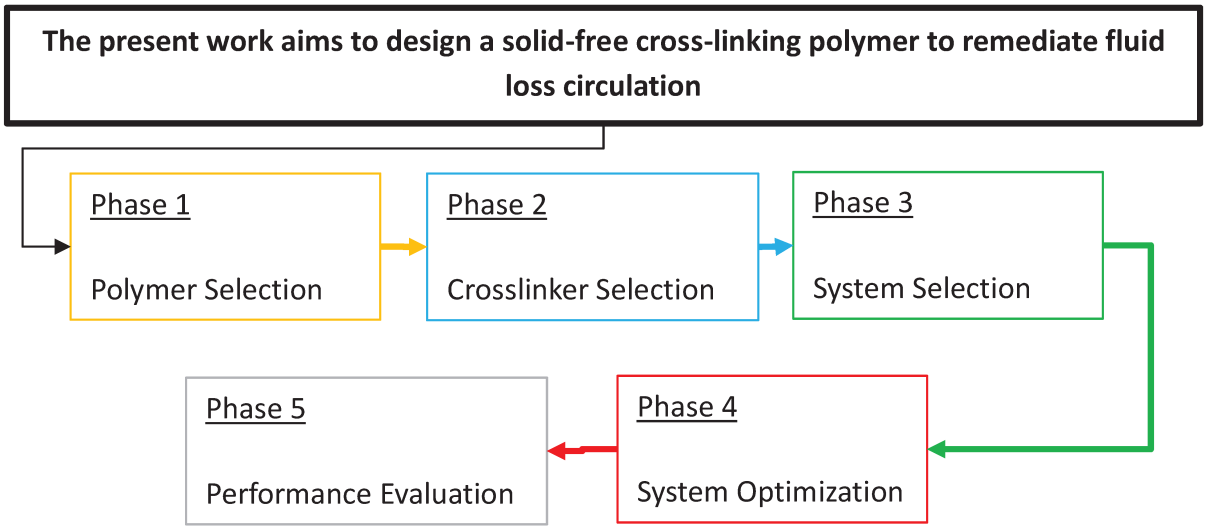

Fig. 3.1 Work-flow

3.2.1. Polymer Selection

The polymers used as gelling agents are defined. The polymer concentration regimes for each polymer type are obtained using flow curves. Then, the chosen polymer and its concentration are passed to the next stage, as shown in **Fig. 3.2**.

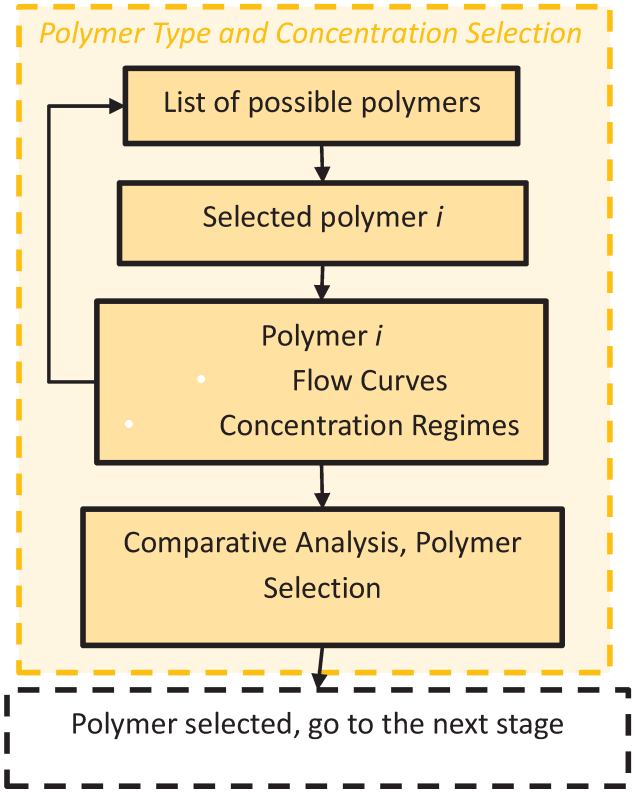

Fig. 3.2 Decision making for the polymer selection phase

The nominal molar mass of the hydroxyethyl-cellulose (HEC) and carboxymethyl-cellulose (CMC) used in the present work was 720,000 and 250,000 $g \cdot mol^{-1}$, degree of substitution 0.9, respectively. Each polymer concentration range was 600 ppm to 20,000 ppm for HEC and 600 ppm to 300,000 ppm for CMC. Both polymers were prepared by dissolving the polymer in a brine of 300,000 ppm of NaCl. The powder was gently sprinkled in the vortex created by a vigorous stirring of the deionized water, using a magnetic stirrer at ambient temperature. The solutions were left still for 48 hours to hydrate the polymers thoroughly.

The rheological characterization was carried out using a rheometer HAAKE MARS III equipped with a cone-and-plate geometry C35/2° Ti L (Radius Ri= 17,5 mm and ± delta Ri= 0,01 mm). A modular temperature controller MARS (TM-PE-P), controlled the temperature. Temperature stabilization was reached after approximately five minutes and corresponded to 25 °C ± 0.1 °C, 35 °C ± 0.1 °C, 45 °C ± 0.1 °C, 55 °C ± 0.1 °C, and 65 °C ± 0.1 °C, respectively for each case. The apparent viscosity as a function of shear rate was collected using a controlled rate (CR) mode in a share rate range from 0.001 s^{-1} to 10000 s^{-1}, with 30 seconds of acquisition for each of the 20 points forming the whole curve. The cell pressure corresponded to the atmospheric conditions. A TM-IN-H compartment cover was used to insulate the sample and prevent solvent evaporation in each case.

3.2.2. Cross-linker and System Selection

As shown in **Fig. 3.3**, once selected the polymer in the previous phase, its compatibility with the cross-linker agents was evaluated. Depending on the analysis, two formulations were carried out.

Initially, a brine was prepared by adding 240,000 ppm of NaCl to deionized water and stirring until complete dissolution of the salt. The polymer powder was added to the brine by sprinkling it onto the vortex created by a vigorous magnetic stirring at ambient temperature.

The first formulation was prepared by adding cross-linker agent powder directly to the polymeric brine solution. The proportion of 1:3 cross-linker ion and polymer carboxylate groups (COO-) was used considering the polymer average molar mass and its substitution degree. Then, these components were mixed thoroughly using a magnetic stirrer at ambient temperature.

The preparation of the second formulation was based on the formulation developed by Hussain et al. (2018), adapted to the objective and scope of this work. The procedure consisted of three steps. First, 770,000 ppm of the stock polymeric solution was mixed with 153,000 ppm of acrylic acid and 77,000 ppm of sodium hydroxide. The latter was used to neutralize the acid completely. Secondly, a solution composed of 870,000 ppm of deionized water, 124,000 ppm of ammonium persulfate, and 7,100 ppm of cross-linker agent was prepared.

Finally, the two fluids prepared in the first and second steps were thoroughly mixed. The fluid mass proportion used was 76.4% and 23.6%, respectively. Once both fluids were mixed, the polymerization and cross-linking reactions start, as described previously, leading to a translucent hydrogel. Immediately after mixed, the fluid was placed in the evaluation equipment/device (Rheometer, NMR, Sydansk bottle test) to start the measurements as soon as possible, minimizing the time between preparation and analyses.

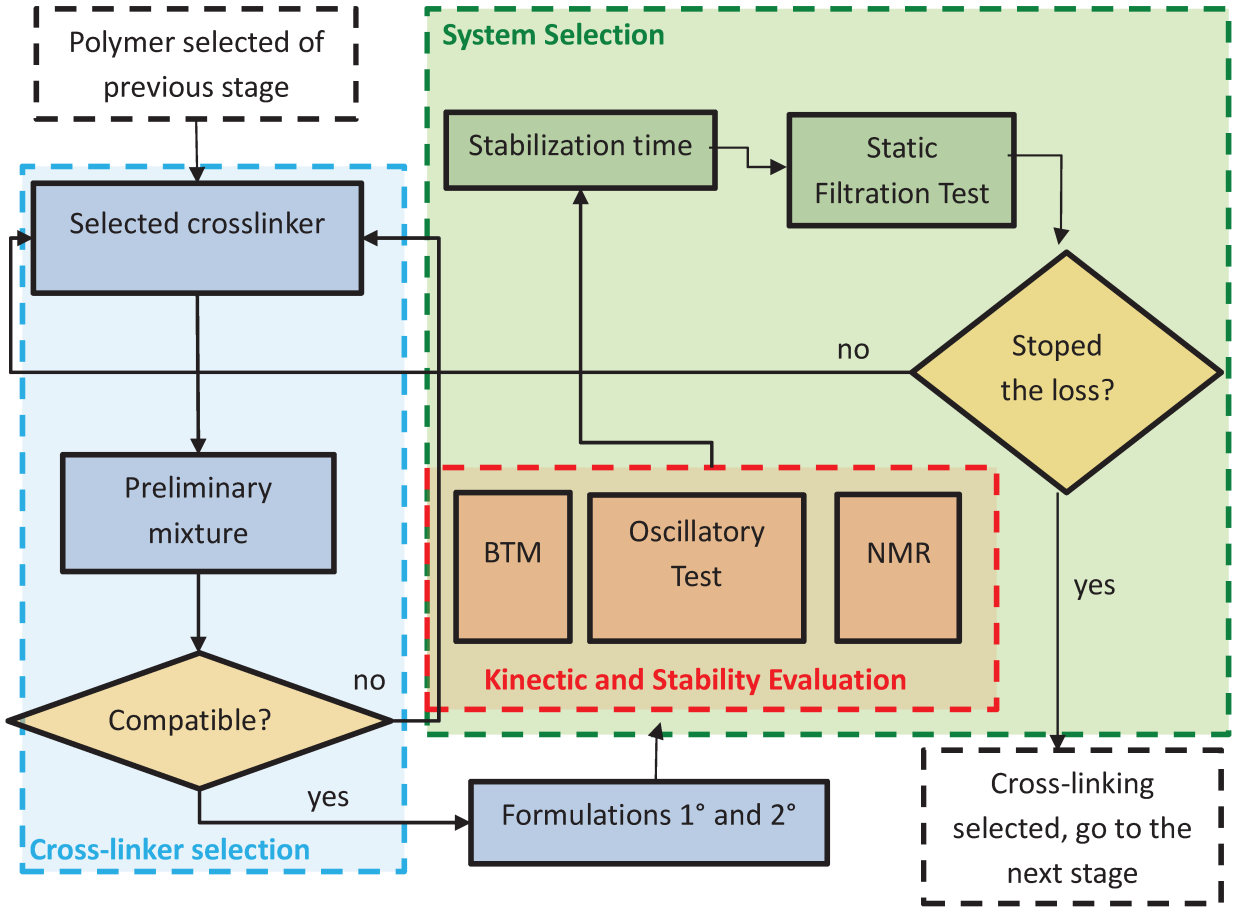

Fig. 3.3 Decision making for cross-linker and system selection phase

3.2.2.1. Fluid Formulations Characterization

The fluid density was measured with an Anton Paar DMA - 4100 density meter, **Fig. 3.4**, whose measuring principle is the oscillating U-tube method. The fluid sample is introduced into a U-shaped borosilicate glass tube, and therefore, the tube is excited to vibrate at a characteristic frequency. The characteristic frequency changes depending on the density of the sample. Finally, the fluid density value is determined through a precise determination of the characteristic frequency and a mathematical conversion with a 0.0001 g/cm³ of resolution. The tests were developed at 40° C and atmospheric pressure. The pH measurements were made by using a Ms Tecnopon mPA210 pHmeter at room temperature, **Fig. 3.5**.

Fig. 3.4 Anton Paar DMA - 4100 Densitymeter

Fig. 3.5 Ms Tecnopon mPA210 pHmeter

3.2.2.2. Gel Evaluation by Bottle Testing Method

This qualitative testing was used because of its helpfulness and easiness of evaluating the kinetic of both systems. In this case, several containers of 25 ml with 5 ml were filled with gel solution, placed in a hot water bath at 40°C and monitored every minute by taking a photo after each inversion of the container to allow the gel behavior analyzes over time and to classify it according to the scale established in **Table 2.6**.

3.2.2.3. Rheological Evaluation

The rheological characterization was carried out in a HAAKE MARS III rheometer using a parallel-plate geometry P60 Ti L. Oscillatory stress of 1 Pa was applied at 1 Hz for an extended period (17 hours) to determine the evolution of G' and G''. A modular temperature controller MARS (TM-PE-P) kept the temperature constant at 40.0 °C. The pressure of the system was ambient. A TM-IN-H compartment cover was used to insulate the sample and prevent solvent evaporation during the measurements.

3.2.2.4. NMR Evaluation

Relaxation data were measured at 40°C using a BRUKER Minispec MQ-Series 7.5 Relaxometer (**Fig. 3.6**) at a frequency of 7.5MHz. The CPMG parameters were set at follows: scan number =16, with phase shifting, recycle delay = 5 s, gain = 58 dB, pulse separation = 0.4 ms, pulse number = 4000. Both hydrogel formulations were monitored every 5 minutes for 2 hours to obtain

the gelation time. After that, data acquisition frequency changed once every hour up to 48 h to evaluate the stability of the samples. The transverse relaxation time (T_2) was caused only by bulk relaxation since there is no effect from surface relaxation, and the relaxation caused by diffusion in a magnetic field is negligible. The T_2 was obtained by the monoexponential, and the distribution of T_2 values, relevant when studying syneresis, was obtained by applying a numerical inversion by the CONTIN method to the CPMG decay data, using the built-in software of the equipment.

Fig. 3.6 BRUKER Minispec MQ-Series 7.5

3.2.2.5. Static Filtration Test

A High Pressure-High Temperature (HPHT) Filter Press 175 ml produced by Fann (**Fig. 3.7**) was used to carry out the static filtration experimental work. This test was based on the recommended practices in (API PFM, 2001) and (API 13B-1, 2017). Even though a filtration cell is not the adequate equipment to evaluate a circulation loss fluid, this equipment was used to compare the proposed systems and as an indication to select the best one among them. The test temperature was 40°C to match the other experiments. A differential pressure of 100 psi was applied through a disk of 40 Darcies, measured by mercury injection capillary pressure technology, as reported in the disk specifications.

Fig. 3.7 Filter Press HPHT 175 ml Fann

3.2.3. System Optimization

After polymer cross-linking system selection, the steps described in **Fig. 3.8** were carried out. Then, the system was evaluated with the new conditions established for this stage. When necessary, the formulation was adapted to be compatible with those new conditions at 70°C and the requirements for designing experiments (DOE) implementations to optimize the formulation.

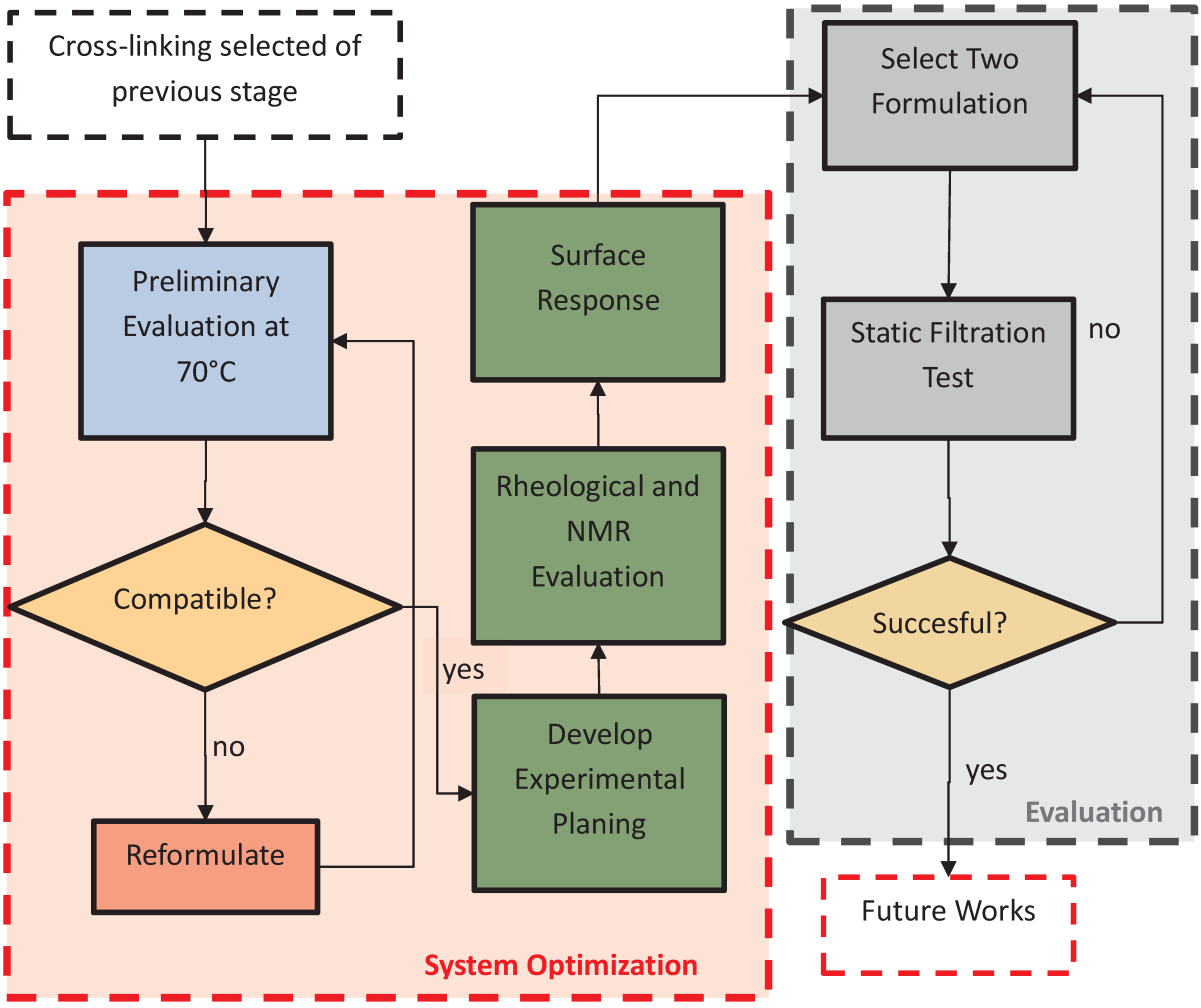

Fig. 3.8 Decision make for system optimization and performance evaluation phase

In order to achieve the most advantageous composition to fulfill the role of a loss control fluid, in this stage, a more in-depth analysis was made on the system composition and how the content of the component affects the system rheology, stability and gelation. That was done by using fractional factorial DOE to reduce the number of experiments. The experimental planning included five variables, with two levels and a triplicate at the central point, defined by **Eq. 3.1**, where NE represents the number of experiments, NL is the number of levels, NV is the number of variables, and NR is the number of replicates. The DOE study is based on a rheological and a NMR evaluation.

$$NE = \frac{NL^{NV}}{NL} + NR \qquad \textbf{Eq. 3.1}$$

The methodology applied to mount the fractional factorial DOE is explained through an example of 2^{4-1} = 8 experiments. First, planning 2^3 is built, which is expanded using a generative expression. This expression dictates how the factor **4** column will be obtained, and it is directly related to the resolution and confusion of the effects on the contrasts (contrast is the calculated effect for reduced DOE). **Table 3.2** is obtained using the generatrix $\boldsymbol{I = 1234}$, equivalent to $\boldsymbol{4 = 123}$.

Table 3.2 Fractional factorial DOE 2^{4-1} with generatrix expression $4 = 123$

n	1	2	3	4=123
1	−	−	−	−
2	+	−	−	+
3	−	+	−	+
4	+	+	−	−
5	−	−	+	+
6	+	−	+	−
7	−	+	+	−
8	+	+	+	+

It is possible to check if the new column was created correctly by counting the number of levels "+" and "-", which must be equal in all columns.

From the generatrix expression, it is possible to obtain the multiplications of columns that result in another column, based on two rules:

1. A column multiplied by itself results in the column identity I, which has only "+". After, $\boldsymbol{1 \cdot 1 = 2 \cdot 2 = I}$.
2. Multiplications are distributive and commutative, that is, $\boldsymbol{(12)3 = 1(23) = 123 = 321}$

The most common relationship is the expression that generates the fourth column. However, from $\boldsymbol{I = 1234}$**,** it is possible to reach $\boldsymbol{1 = 234}$, and this can be verified by multiplying the appropriate columns in **Table 3.2**. That means that the coefficients for calculating the effect of interaction **234** are equal to the coefficients of calculating **1**. That results in the confusion of these two effects in the calculated contrast of 1. If there are more generative expressions (less DOE), more effects will be confused in contrast. In this example, the main contrasts l_i are the confusion of the following effects:

$$\boldsymbol{l_1 = 1 + 234}$$

$$l_2 = \mathbf{2} + \mathbf{134}$$

$$l_3 = \mathbf{3} + \mathbf{124}$$

$$l_4 = \mathbf{4} + \mathbf{123}$$

3.2.3.1. Rheological Evaluation

The same equipment and geometry showed in item **3.2.2.3** were used to make the rheological evaluation for the DOE. Unlike the system selection stage, the thermal bath was used to regulate 70 °C at the plate geometry base. The rheometer was configured to perform three measurements to evaluate: the kinetics of the gel, the elastic module G' and the viscous module G''. For that, the following configuration in the rheometer were used: parallel-plate geometry P60 Ti L and oscillatory stress of 1 Pa, applied at 1 Hz for a time of 3 hours. As proposed by Mezger (2014), to evaluate the consistency at rest and long-term storage gel stability, a frequency sweep test was carried out with a range of 0,01 Hz to 100 Hz and oscillatory stress of 1 Pa. Finally, a controlled shear stress test was studied with a range of 0,1 Pa to 1000 Pa and a constant frequency of 1 Hz to estimate the yield stress and the gel flow point.

Additionally, a variation of the Hills equation presented by Turner et al. (2015) was used to determine the kinetic gelation constant. That was a consequence of the fit quality of the elastic modulus curves, G', see **Eq. 3.2,** where G'_{min} is the minimum removal asymptote, G'_{max} is the maximum value of elastic module (Pa), n is the Hill parameter (unitless) which reflects the steepness (sigmoidicity) of the curve, E is the asymmetry parameter (unitless) that provides significant flexibility in the initial rate and the curve shape, and k_{Hills5} is represented in **Eq. 3.3** , where $t_{0.5}$ is the half-life or time for 50 % occurrence of the maximum value of G'.

$$G' = G'_{min}\ \frac{(G'_{min} + G'_{max})}{\left(1 + \left(\frac{t}{k_{Hills5}}\right)^{-n}\right)^{E}} \qquad \textbf{Eq. 3.2}$$

$$t_{0.5} = k_{Hills5}\left(2^{\left(\frac{1}{E}\right)} - 1\right)^{\left(\frac{1}{-n}\right)} \qquad \textbf{Eq. 3.3}$$

3.2.3.2. NMR Evaluation

The same equipment described in item **3.2.2.4** was used again. The differences relayed on temperature that was 46 °C (recommended temperature in API PFM (2001)) and the CPMG parameters that changed for each experiment, the test time was 8 hours

3.2.3.3. Response Surface

Once the fractional factorial DOE has been assembled, the lack of fit analysis must be performed where the least-squares methodology was applied, using a linear fit. Once the adjustments had been made, the analysis of variance (ANOVA) described in item **2.8.2** was carried out. The matrix operations were solved using Excel functions, and F distribution was calculated for a certain degree of freedom, using the Excel function = INV.F(x, df1, df2) for a given level of significance.

After having developed the ANOVA, the response surface was modeled in the region under investigation employing the linear function of the factors described in **Eq. 2.15**. All response surface graphics were designed using OriginPro.V2016 software.

3.2.4. Performance Evaluation

An adapted static filtration test was set up to evaluate the selected formulations in a high permeability disk possible. First, the gel components were mixed and distributed between a container of 350 ml and the filtration press, then injected at a constant flow rate of ml/min using a Teledyne ISCO dual-pump air-valve 260D; the fluid was passed through a disk of 40 Darcies, collected by a beaker of 500 ml and measured in a by an Ohaus ARD110 balance. After some time, the gel had been formed, and no more fluid had been produced. At this point, the pump was set to apply constant pressure of 300 psi, the maximum safe pressure for this system, in order to evaluate if the gel could sustain this pressure, and finally, the mass data was acquired by Labview software. The schematic representation of the adapted static filtration test is shown in **Fig. 3.9**.

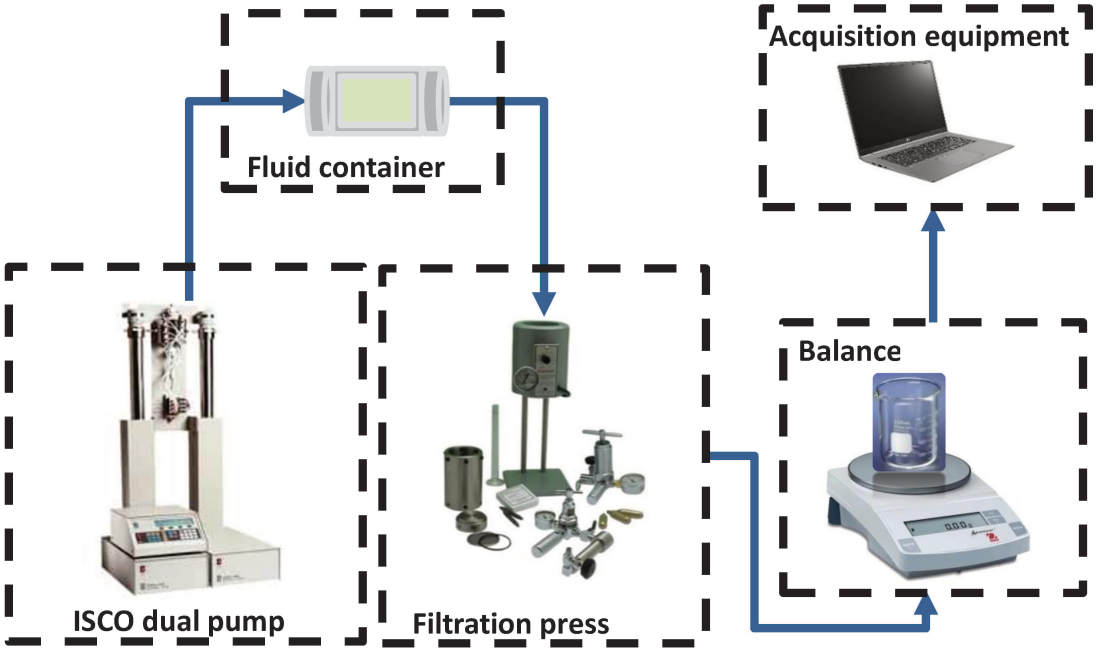

Fig. 3.9 Schematic design of the adapted static filtration test.

4. RESULTS AND DISCUSSION

This chapter describes the results obtained by applying the methodology shown in Chapter **3**.

4.1. Polymer Selection

In this stage, the procedure described in item **3.2.1** is applied. **Fig. 4.1** and **Fig. 4.2** present the apparent viscosity versus shear rate for different HEC and CMC concentrations, 720,000 and 250,000 $g \cdot mol^{-1}$, respectively. Continuous lines represent the best power-law fits. One can see that the apparent viscosity increases with increasing polymer concentrations. That behavior may arise from the combined effects of molecular chain resistance and the increased entanglement among the polymer molecules.

On the other hand, it is possible to note the decrease of the pseudoplastic behavior with the temperature increase for both polymers.

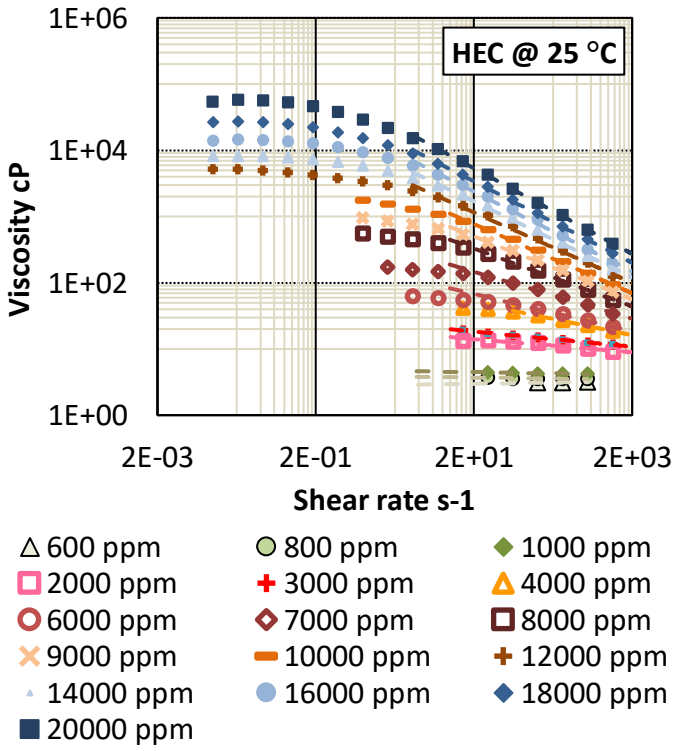

Fig. 4.1 Viscosity versus shear rate curves of HEC solutions at 25°C

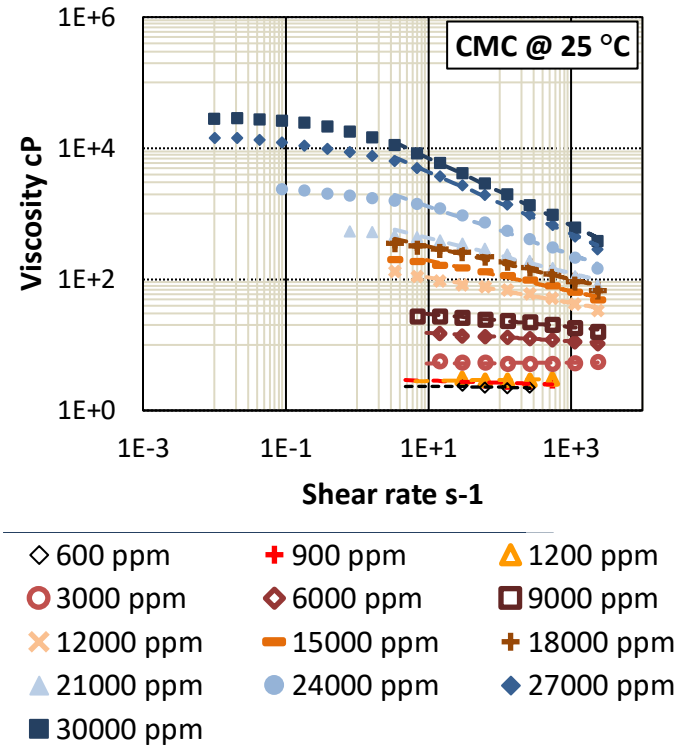

Fig. 4.2 Viscosity versus shear rate curves of CMC solutions at 25°C

Fig. 4.3 and **Fig. 4.4** show the concentration regimes and the correspondent transitions given by the slopes for both polymers, HEC, and CMC, respectively. The method used to calculate the transitions regimes consists of plotting the apparent viscosity versus polymer concentration at specific shear rates in logarithmic scales. The reference shear rate of 127 s^{-1} was chosen for this work because more points were measured at this shear rate.

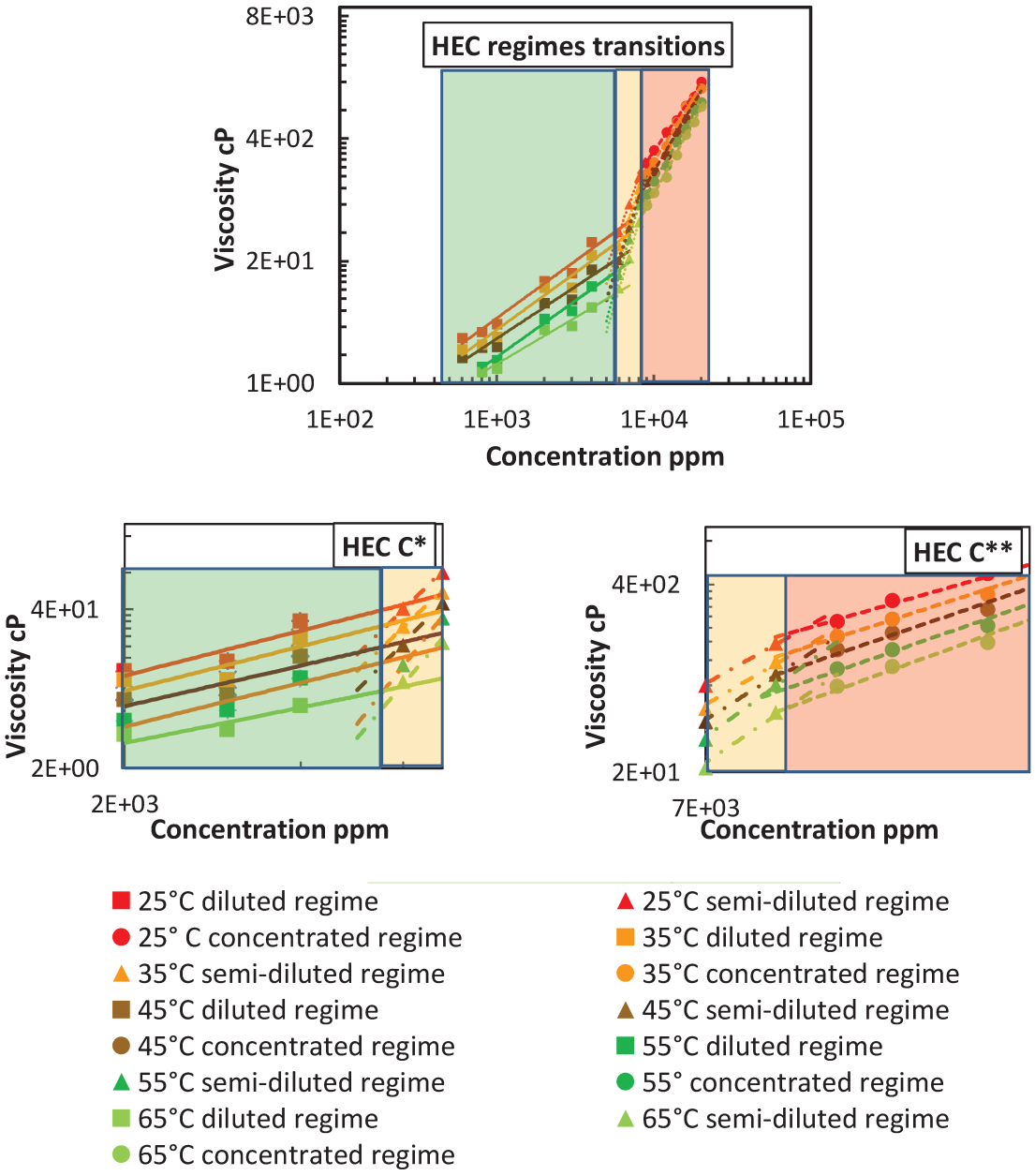

Fig. 4.3 Overlap concentration C* and C of HEC sample at a shear rate of 127 s^{-1} for different temperature**

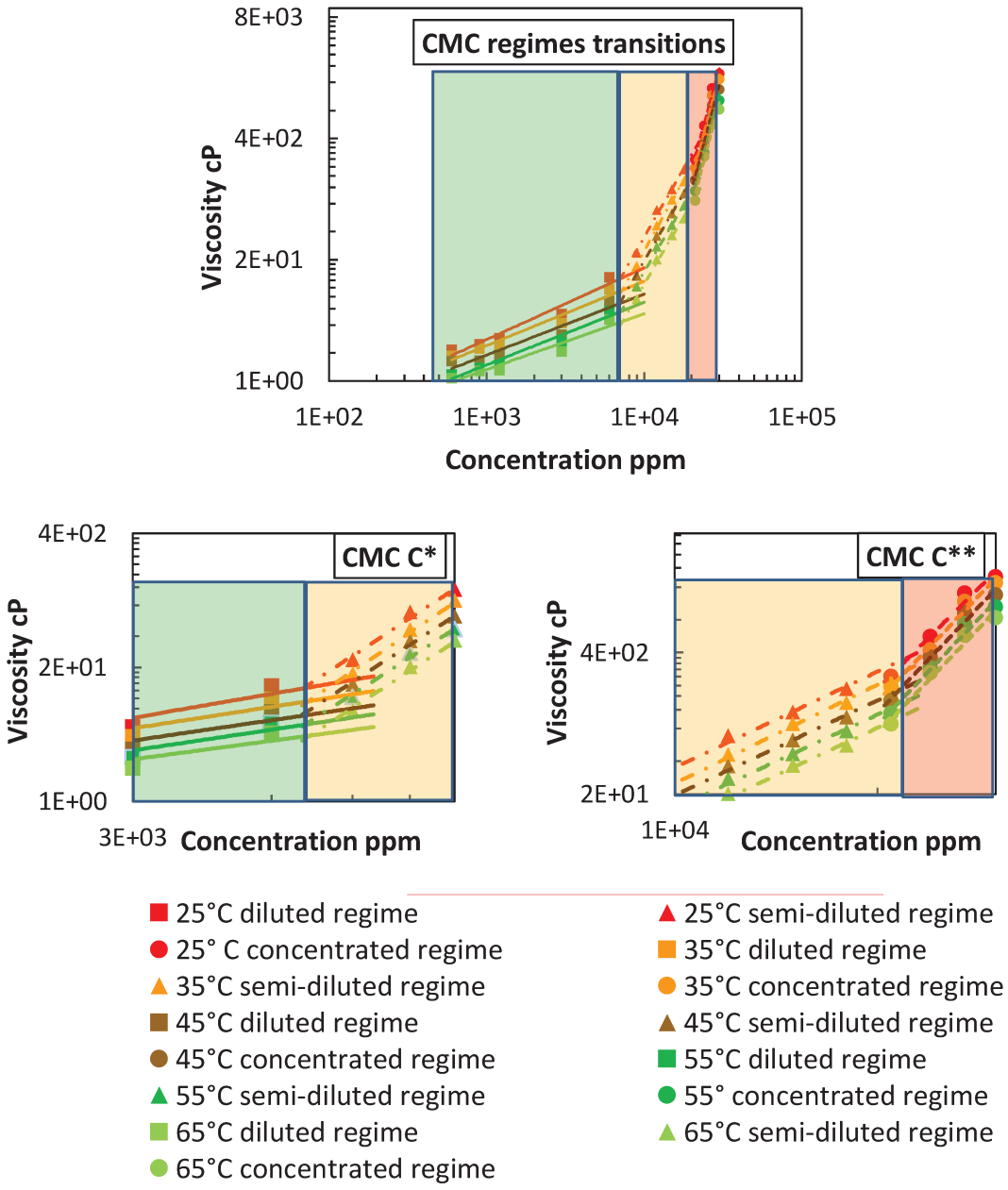

Fig. 4.4 Overlap concentration C* and C of CMC sample at a shear rate of 127 s^{-1} for different temperature**

Table 4.1 and **Table 4.2** show the obtained values of C* and C** for HEC and CMC, respectively, at each temperature.

Table 4.1 Values for C* and C of HEC at different temperatures**

Temperature	C*	C**
25°C	≈ 6000 ppm	≈ 9500 ppm
35°C	≈ 6000 ppm	≈ 9000 ppm
45°C	≈ 6000 ppm	≈ 8500 ppm
55°C	≈ 6000 ppm	≈ 8000 ppm
65°C	≈ 6000 ppm	≈ 7800 ppm

As one can see in both tables that the transition from the diluted regime to the semi-diluted one was not affected by the temperature increase, showing almost the same value for all temperature levels. On the other hand, the transition between semi-diluted to concentrated regimes seems to have been affected by the temperature, decreasing as temperature increased.

Table 4.2 Values for C* and C of CMC at different temperatures**

Temperature	C*	C**
25°C	≈ 7000 ppm	≈ 22500 ppm
35°C	≈ 7000 ppm	≈ 22000 ppm
45°C	≈ 7000 ppm	≈ 21700 ppm
55°C	≈ 7000 ppm	≈ 21500 ppm
65°C	≈ 7000 ppm	≈ 21000 ppm

The results for HEC and CMC were similar. In summary, C* was not affected by the temperature level in the transition of diluted to the semi-diluted regime. However, a small effect was observed in C** values obtained for the transition between semi-diluted to the concentrated regime, where it can be said that this effect is because the increase in temperature facilitates the movement of the polymer chains in concentrated solutions. Therefore it translates into a reduction in viscosity, generating lower values of c**.

One of the reasons for the significant difference in viscosity at the same concentration of both polymers is the molar mass difference. Nevertheless, it is possible to note that the semi-diluted regime is more significant in CMC than the HEC in this case. According to Ouaer and Gareche (2018) and Nguyen et al. (1996), it is crucial to define this regime since viscosity is a direct measure of a fluid's resistance to flow; concentrated solutions show high viscosity because of the extra resistance present among the chains containing more molecules. For this reason, CMC was chosen as the base polymer to go through the next phases. That decision was based on the flexibility offered by CMC semi-diluted regime. The concentration chosen was 12,500 ppm, which is on approximately half of this regime for CMC.

4.2. Cross-linker and System Selection

Once the polymer was selected, its compatibility was evaluated to form a cross-linking system by adding metal ions. It was decided to decrease its concentration to 240,000 ppm to avoid solubility problems due to the high concentration of NaCl in the previous phase. First, a quick compatibility evaluation was performed using the bottle test method at room temperature; the mixture between CMC and Zirconyl Chloride Octahydrate did not have a gel formation. Then the mixture CMC and Iron (III) Chloride Hexahydrate was evaluated, where initially, a gel evolution could be observed on the Sydansk scale, but 5 minutes after a rigid gel had formed, it began to degrade. Therefore, and finally, the mixture between CMC and Chromium (III) Acetate Hydroxyde was carried out, where the latter did show the formation of a rigid and stable gel over time at room temperature conditions. Therefore Chromium (III) Acetate Hydroxyde was the cross-linker agent of choice for use in the next phases.

4.2.1. Preparation

According to the concentrations established to carry out the two formulations proposed in item **3.2.2**, and once the polymer and the base cross-linking agent were defined, the lost circulation systems were prepared. **Table 4.3** shows the density and pH measurements for the first and second formulation. **Table 4.4** presents the final composition obtained by mixing *a* and *b* fluids from the second formulation.

Table 4.3 Fluids properties at 40°C

Formulation	Density (g/cm^3)	pH
First	1.176	6.40
Second	1.125	5.14

Table 4.4 Concentration of components of the second system

Components	Concentration (ppm)	Concentration (w/w%)
Carboxymethyl cellulose	9596	0.96%
Sodium Chloride	183505	18.35%
Acrylic Acid	116984	11.70%
Sodium Hydroxide	58874	5.89%
Deionized Water	600214	60.02%
Ammonium Persulfate	29157	2.92%
Chromium (III) Hydroxide Acetate	1669	0.17%

4.2.2. Gel evaluation by bottle testing method

Applying the gel-strength codes defined by Sydansk (**Table 2.6**), it is possible to see both systems evolution at 40°C. **Fig. 4.5** shows the evolution of the first system until it reached a value of I on the Sydansk scale at 41 minutes. The gel continued to evolve and, after 200 minutes, reached a state of ringing gel (J). That was not included in the photo because it was not possible to differentiate this state from the previous one. In the same way, **Fig. 4.6** presents the process for the second system. It shows that a strong gel (I) formed at 24 minutes remained constant over time. **Fig. 4.7** shows the gels after two days at 40°C. The first system suffered a significant syneresis effect between 19 and 44 hours, unlike the second one, which remained unchanged for two days. Sydansk bottle test method helped evaluate the gelling evolution; however, their results are only indicative, and it becomes inaccurate and inconvenient for long time scales, requesting complementary analysis by other techniques.

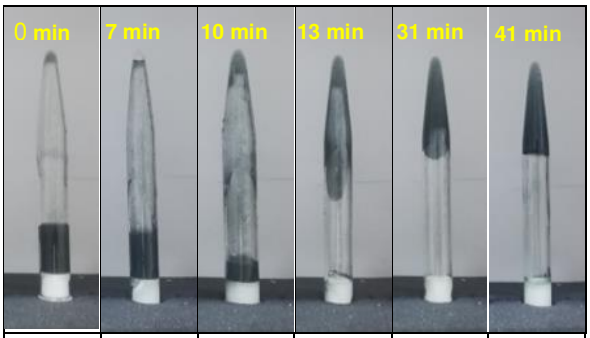

Fig. 4.5 Bottle test of the first system at 40°C

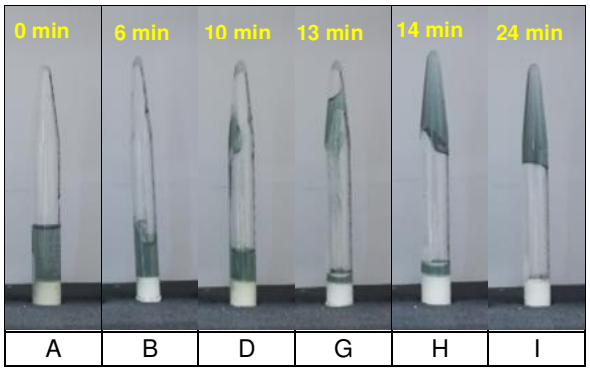

Fig. 4.6 Bottle test of the second system at 40°C

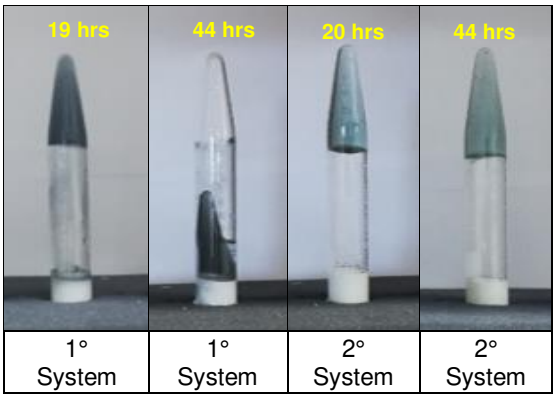

Fig. 4.7 Bottle test of both systems after 2 days at 40°C, showing the syneresis on the first system

4.2.3. Rheological evaluation of cross-linked system

The two formulated systems were submitted to oscillatory tests, and three zones of transition were identified in both formulations. **Fig. 4.8** shows the evolution of G' and G'' for the first system where the transition zones are marked as points A, B, and C. It should be noted that G'' was very noisy after 150 minutes. A moving average filter was applied to smooth out the data and help visualization. Point A, at 41 minutes, shows a transition in the slope of G' and an abrupt change in G''. Point B, at 230 minutes, shows a possible early stabilization of G', and point C shows another transition of G' at 570 minutes. From point B on, one can see that the viscous and elastic moduli are approximately parallel, a behavior characteristic of a gel**. Fig. 4.9** shows the oscillatory

rheological measurements of the second system. Again, three transitions are seen for the gel (Points A, B, and C). Point A, at 30 min, shows an abrupt change in both moduli, Point B, at 120 min, correlates with the first stabilization of the elastic modulus G', and Point C, at 350 min, characterizes other transition. A parallel behavior between the elastic and the viscous modulus evidenced the gel behavior. In this case, a faster and more stable gel formation of the second system is observed and compared to the first one.

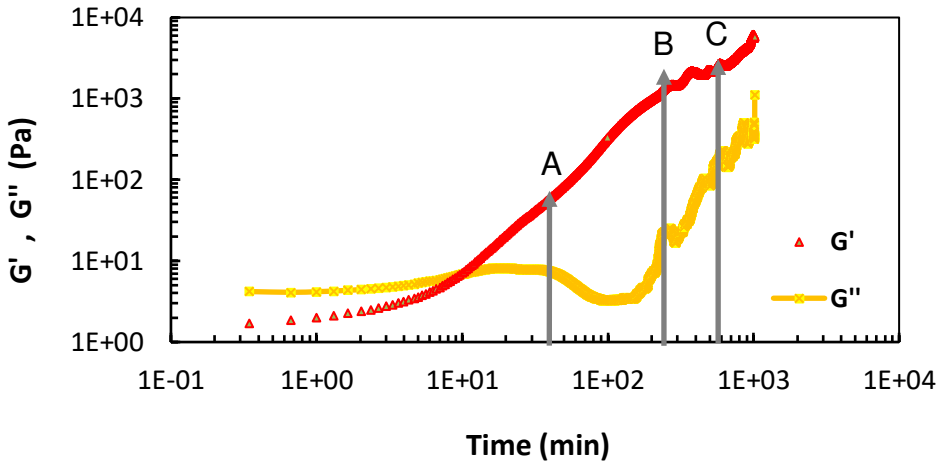

Fig. 4.8 Elastic (G') and viscous (G'') moduli vs time of the first system

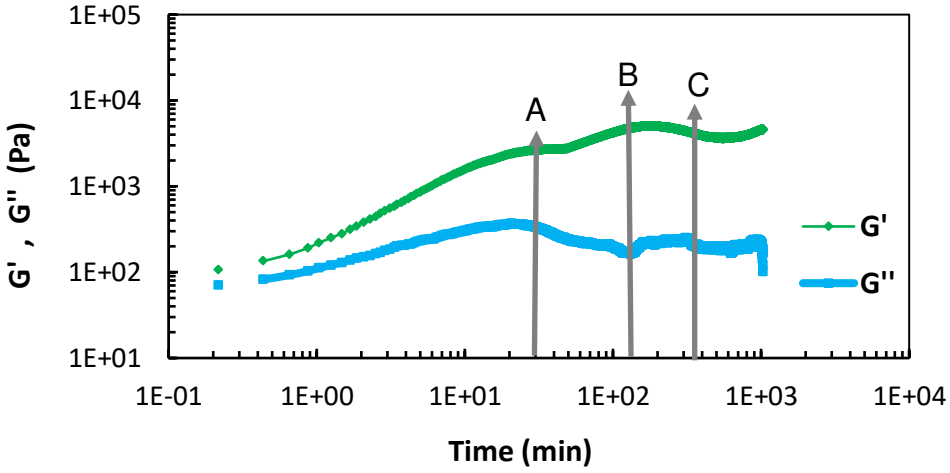

Fig. 4.9 Elastic (G') and viscous (G'') moduli vs time of second system

4.2.4. RMN evaluation of cross-linked system

Both systems were monitored using low-field NMR. The T2 measured values were inverted to obtain the relaxation rate, which is proportional to the gel strength. The results were plotted against time (see **Fig. 4.12).** One can see that the first system reached the gelation point at 41 minutes and stabilized at 570 minutes, while the second system reached the gel consistency and achieved faster stabilization, at 16 minutes and 30 minutes, respectively.

Additionally, the second system showed better stability over time. **Fig. 4.13** shows that after 1052 minutes, a second 1/T2 population appeared, with shorter 1/T2 values. That was accompanied by a visual shrinking of the gel and the appearance of a significant liquid layer. Both observed phenomena prove that the second 1/T2 population results from the syneresis on the first system. Additionally, since the gel is shrinking and becoming more concentrated, its 1/T2 value should increase, which was also observed. **Fig. 4.10** and **Fig. 4.11** show the T2 distributions for the first and second system. One can see that the T2 peak progressively displaces to the left in both systems, which indicates the formation of a rigid gel network because the signal shifts toward lower relaxation times. Besides that, it is possible to see the aforementioned additional peak in the right of **Fig. 4.10**, which represents syneresis of the first system.

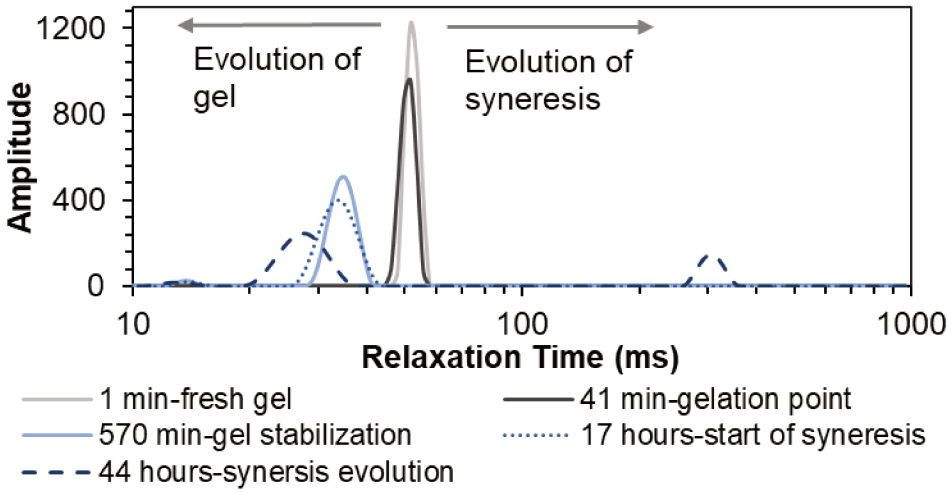

Fig. 4.10 Amplitude index vs relaxation time of the first system

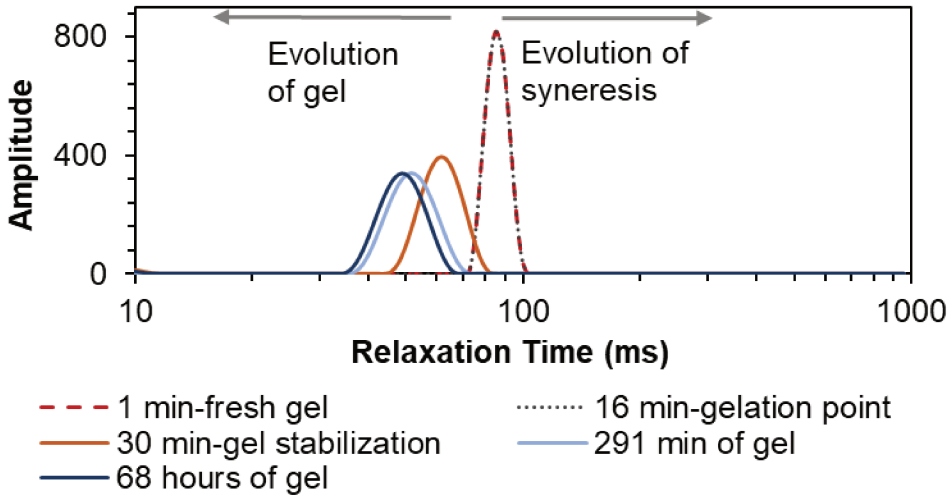

Fig. 4.11 Amplitude index vs relaxation time of the second system

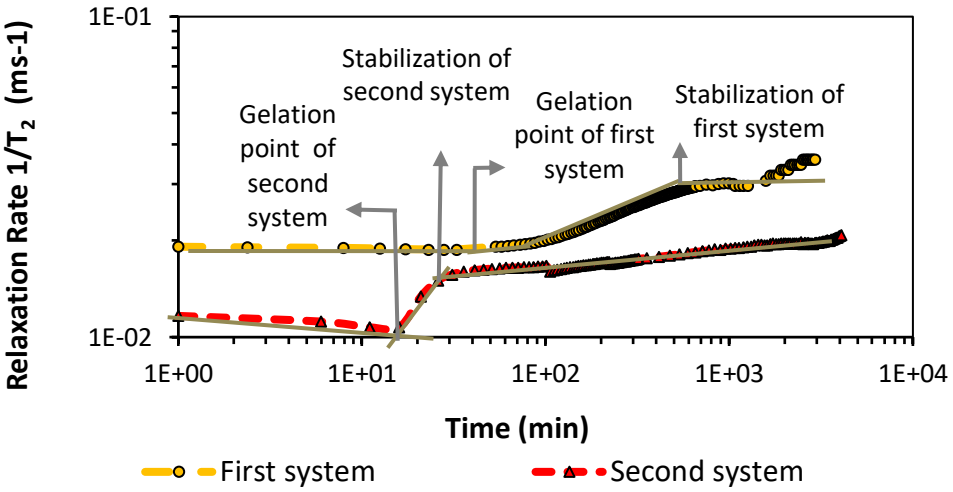

Fig. 4.12 Relaxation rate vs time of two hydrogel system

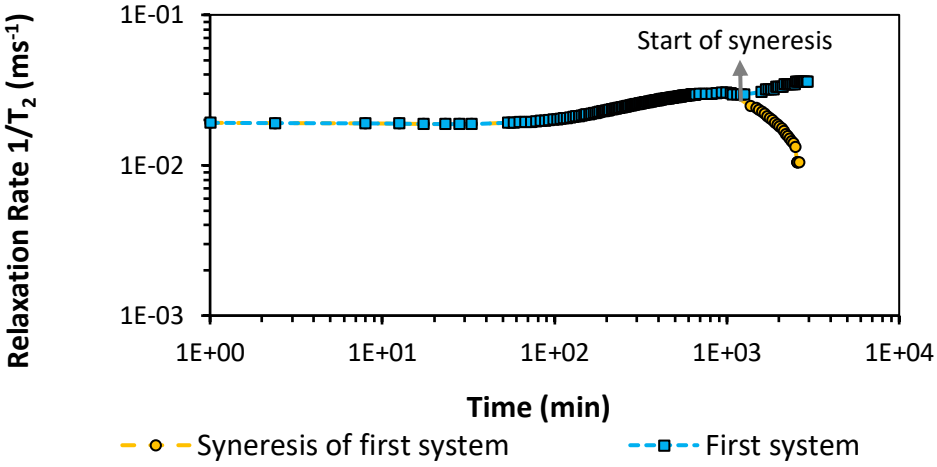

Fig. 4.13 Relaxation rate vs time of the first system showing the syneresis effect

Table 4.5 summarizes the results obtained through the different procedures used to characterize the fluids formulations and whose combined evaluation supported the Filtration Test planning. Sydansk's bottle test method helped us to evaluate the evolution of the gel by images. Although the results depended more heavily on the evaluator, it allowed to determine part of the transitions through the photos. Some changes were notorious such as when the fluid started to became a rigid gel. This first transition was captured by the oscillatory test (Point A) and the relaxometry analysis (Gel Point). On the other hand, the third or final transition, from a rigid gel (Stage I) to a ringing gel (Stage J), was difficult to differentiate visually on the bottle test. That transition was observed and correlated only for the first system through rheological and NMR analyses. For the second system, that transition could not be correlated using relaxometry because once the second system reached the rigid gel state, the movement of water molecules was inhibited, and then, the NMR test could not differentiate additional changes into the system.

On the other hand, the oscillatory measurements allowed us to determine three transition stages for both systems.

Table 4.5 Formulations Comparative Behavior

Method	Phase	First system	Second system
Bottle Test.	Stage I - Rigid Gel	41 min.	24 min.
	Stage J – Ringing-Rigid Gel	200 min.	Not reached.
Oscillatory Test.	Point A – Rigid Gel	41 min.	30 min.
	Point B – G' stabilization	230 min.	120 min.
	Point C – G" stabilization	570 min.	350 min.
NMR Test.	Gel point	41 min.	16 min.
	Stabilization point	570 min.	30 min.

4.2.5. Static Filtration Test

After the analysis of the fluids formulations, filtration tests were carried out for both systems. First, the cell was filled with the first formulation while in a liquid state. Five hundred and seventy minutes were waited for the hydrogel to evolve to a solid-like, then the filtration test started. **Fig. 4.14** shows the filtrated volume in green. In the same way, the cell was filled with the second formulation, but this time, the filtration was carried out after 30 minutes. These results are presented by the red and yellow lines in **Fig. 4.14**. This way, the fast gelation and the excellent efficiency of the second formulation to prevent circulation loss in a highly permeable disk were demonstrated. In addition, the filtration test results showed that the gel formed from the first system presented a considerable loss volume and could not mitigate the leak. On the contrary, the second system showed efficiency in stopping the loss, observing only a loss volume of approximately 2 ml.

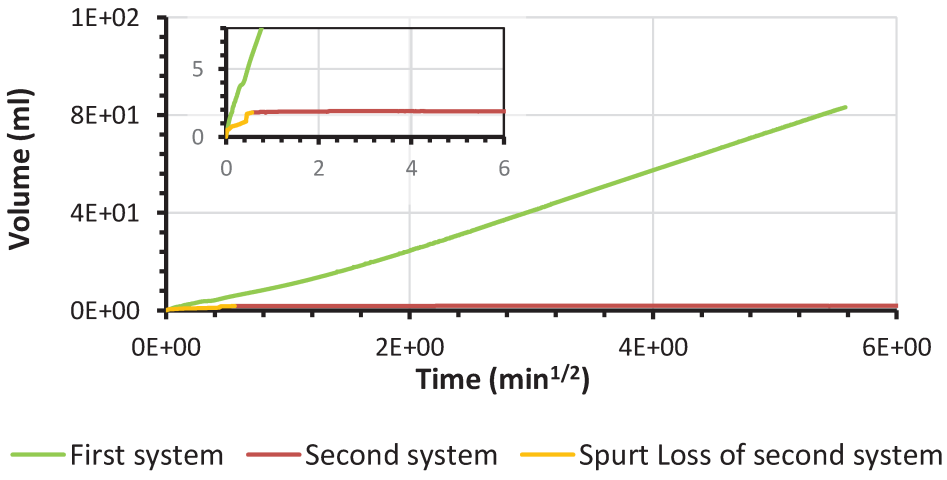

Fig. 4.14 Filtration test of both systems at a temperature of 40°C

4.3. System Optimization

At this stage, a new source of the CMC gelling agent was used because the provision of the previous one was not enough to complete the investigation process. The CMC molar mass changed from 250,000 $g \cdot mol^{-1}$ to 700,000 $g \cdot mol^{-1}$. Because of that change, the rotational rheological study was repeated to find the polymer concentration of 700,000 $g \cdot mol^{-1}$, equivalent to that of the previous polymer with a lower molar mass 250,000 $g \cdot mol^{-1}$. That was done by finding the same viscosity value for both CMC to reduce in some way the effects of the molar mass change. The preparation was described in Item **4.2.1,** and test conditions are presented in section **3.2.3**.

Once the selection stage was completed, it was possible to verify that the rebuilt system was very similar to the original one. Therefore, the optimization step for this system was then performed. Applying the concepts of **Eq. 3.1**, the number of levels = 2, variables = 5, and central points = 3 were define to determine the number of experiments = 19. **Table 4.6** defines the codes used for each of the analyzed variables and their respective values. Although the temperature is an essential factor in cross-linked polymer gels, its value was set at 70°C due to limitations of equipment temperature changes.

Table 4.7 shows the fractional factorial DOE with 19 experiments and how the variables and their contrast changes according to each experiment.

Table 4.7 was designed based on the matrix equation showed in **Eq. 2.14** and **Table 3.2**.

Table 4.6 Variable code for experimental planning

N°	VARIABLE	-1	0	+1.
1	pH	5	7	9
2	CMC	2000 ppm	4138 ppm	6275 ppm
3	AA	50000 ppm	101500 ppm	153000 ppm
4	APS	1000 ppm	1500 ppm	2000 ppm
5	Cr3+	3500 ppm	5300 ppm	7100 ppm

Table 4.7 Coded fractional factorial DOE, I=12345

	0	1	2	3	4	5	1-2	1-3	1-4	1-5	2-3	2-4	2-5	3-4	3-5	4-5
Exp 1	1	-1	-1	-1	-1	1	1	1	1	-1	1	1	-1	1	-1	-1
Exp 2	1	1	-1	-1	-1	-1	-1	-1	-1	-1	1	1	1	1	1	1
Exp 3	1	-1	1	-1	-1	-1	-1	1	1	1	-1	-1	-1	1	1	1
Exp 4	1	1	1	-1	-1	1	1	-1	-1	1	-1	-1	1	1	-1	-1
Exp 5	1	-1	-1	1	-1	-1	1	-1	1	1	-1	1	1	-1	-1	1
Exp 6	1	1	-1	1	-1	1	-1	1	-1	1	-1	1	-1	-1	1	-1
Exp 7	1	-1	1	1	-1	1	-1	-1	1	-1	1	-1	1	-1	1	-1
Exp 8	1	1	1	1	-1	-1	1	1	-1	-1	1	-1	-1	-1	-1	1
Exp 9	1	-1	-1	-1	1	-1	1	1	-1	1	1	-1	1	-1	1	-1
Exp 10	1	1	-1	-1	1	1	-1	-1	1	1	1	-1	-1	-1	-1	1
Exp 11	1	-1	1	-1	1	1	-1	1	-1	-1	-1	1	1	-1	-1	1
Exp 12	1	1	1	-1	1	-1	1	-1	1	-1	-1	1	-1	-1	1	-1
Exp 13	1	-1	-1	1	1	1	1	-1	-1	-1	-1	-1	-1	1	1	1
Exp 14	1	1	-1	1	1	-1	-1	1	1	-1	-1	-1	1	1	-1	-1
Exp 15	1	-1	1	1	1	-1	-1	-1	-1	1	1	1	-1	1	-1	-1
Exp 16	1	1	1	1	1	1	1	1	1	1	1	1	1	1	1	1
Exp 17	1	0	0	0	0	0	0	0	0	0	0	0	0	0	0	0
Exp 17	1	0	0	0	0	0	0	0	0	0	0	0	0	0	0	0
Exp 17	1	0	0	0	0	0	0	0	0	0	0	0	0	0	0	0

Initially, six parameters were defined to be analyzed by DOE and response surfaces. Those measurements, obtained by rheological analysis, were: the plateau modulus, G'p, the constant Khills, stability. The yield point value could not be obtained because the gel values were higher than the equipment limits.

The remaining measurements were obtained through the NMR, where the gelation onset time, Tg, was evaluated, and finally, the formation of syneresis in the gels was analyzed. The latter was not be included in the response surface as it was an analytic value. Plateau Modulus G'_p.

4.3.1. Plateau Modulus G'_p

The plateau modulus, G'_p, was obtained by taking the mean value of the elastic modulus G' values measured in the frequency test. That was done because those values stayed constant during the test. Once the results were obtained, the vector with model coefficients of each contrast by calculating the square root of the covariance matrix diagonal represented by **Eq. 2.16**. Consequently, the standard error was estimated for each of the contrasts by calculating the square root of the diagonal of the covariance matrix represented by **Eq. 2.17**. The experiment variance was calculated by applying the excel function VAR.S to the average of the replicates of Experiment 17, which resulted in 125009.39. The calculation of the standard errors allowed us to

identify six non-representative contrasts (1-3;2-3;2-4;2-5;3-4;4-5). Therefore, the vector with model coefficients was recalculated, excluding these six contrasts, to obtain a better result forecast by increasing the difference between the freedom degrees. All mentioned results are summarized in **.8**.

Table 4.8 Results forecasts and effects of modulus plateau G'_p

	G'p measured	G'p expected
Exp 1	983.03	453.28
Exp 2	25.45	-552.39
Exp 3	6772.51	6661.89
Exp 4	1878.01	1853.84
Exp 5	150.72	33.73
Exp 6	20.97	-47.92
Exp 7	7355.91	7166.36
Exp 8	1710.29	1434.29
Exp 9	529.77	568.17
Exp 10	329.18	226.88
Exp 11	6917.81	6627.12
Exp 12	3079.61	2782.77
Exp 13	1411.20	1072.64
Exp 14	5.20	-192.67
Exp 15	6563.63	6207.58
Exp 16	3637.14	3287.24
Exp 17	694.13	2348.93
Exp 17	1184.48	2348.93
Exp 17	1380.55	2348.93

Contrasts	Model coefficients	Standard error (+/-)	Verification
0	2348.93	81.11	✓
1	-1249.92	88.39	✓
2	2153.71	88.39	✓
3	21.23	88.39	✗
4	223.54	88.39	✓
5	231.00	88.39	✓
1-2	-913.18	88.39	✓
1-3	-13.56	88.39	✗
1-4	203.51	88.39	✓
1-5	-100.41	88.39	✓
2-3	56.15	88.39	✗
2-4	86.64	88.39	✗
2-5	-23.15	88.39	✗
3-4	73.87	88.39	✗
3-5	268.42	88.39	✓
4-5	33.64	88.39	✗

Once the representative contrasts were defined, the variance analysis, ANOVA, was carried out, using the least-squares method for the proposed linear model based on **Table 2.8**. In that table, there are ten parameters, nineteen observations numbers, and seventeen repetitions numbers for the plateau module results analysis. The indicators showed at the bottom of **Table 4.9** proved that data fitted well due to the coefficient of determination, R2=0.95, which was close to the maximum coefficient of determination, R2 max. However, the data did not fulfill the condition established by **Eq. 2.19**, this being a requirement of good fit, since the Distribution $F=19.35 > MS_{Lof} / MS_{Pe}= 5.46$.

Table 4.9. Analysis of variance (ANOVA) for modulus plateau, G'_p

Variation source	Sum of Squares (SS)	Degrees of Freedom	Mean Squares (MS)
Regression (*R*)	116030800	9	12892311
Residual (*r*)	6377484	9	708609
Pure error (Pe)	250019	2	125009
Lack of Fit (LoF)	4782040	7	683149
Total (*T*)	122408284.1	18	
R^2	R^2_{max}	MS_{Lof} / MS_{Pe}	Distribution F
0.95	1.00	5.46	19.35

Additionally, through **Fig. 4.15** and **Fig. 4.16**, a good fit could be observed by comparing the expected values with the measured ones, which should fall in a straight line with a unitary slope.

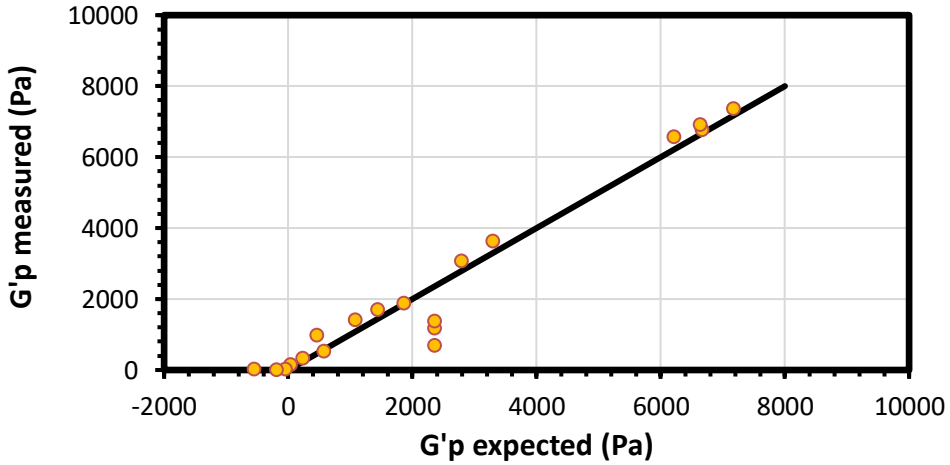

Fig. 4.15 Result obtained vs expected modulus plateau, G'_p

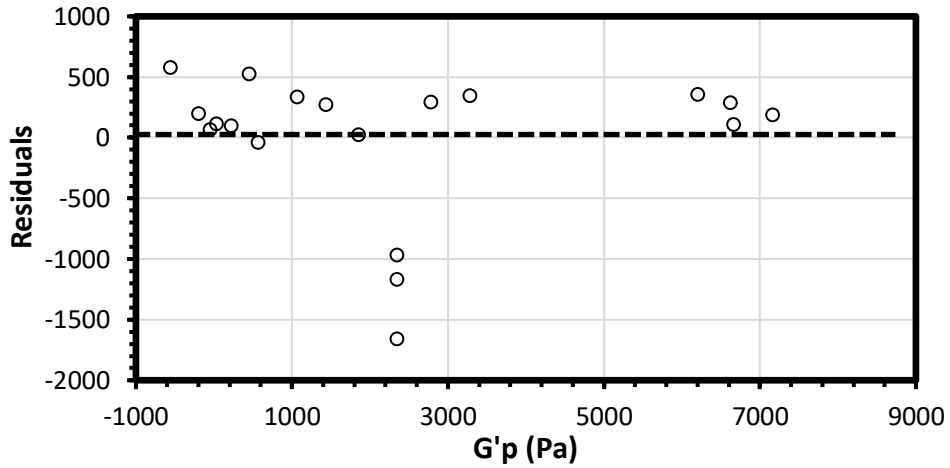

Fig. 4.16 Residues left by a linear model for the modulus plateau, G'_p

Through the model coefficient, β, it was possible to determine the most influential contrasts to raise the response surfaces. Therefore, when decoding the variables represented by **Eq. 2.13**, the variables with less representativeness were fixed at given values defined by the effect they would have depending on their coefficient vector values. In the modulus plateau case, G'_p, the contrasts that had great representativeness were the pH and acrylic acid concentration, AA. Therefore, in this case, the answer was raised only with the variables observed in **Fig. 4.17** and **Fig. 4.18**. The latter represents the response surface contours that help to a better reading of the response.

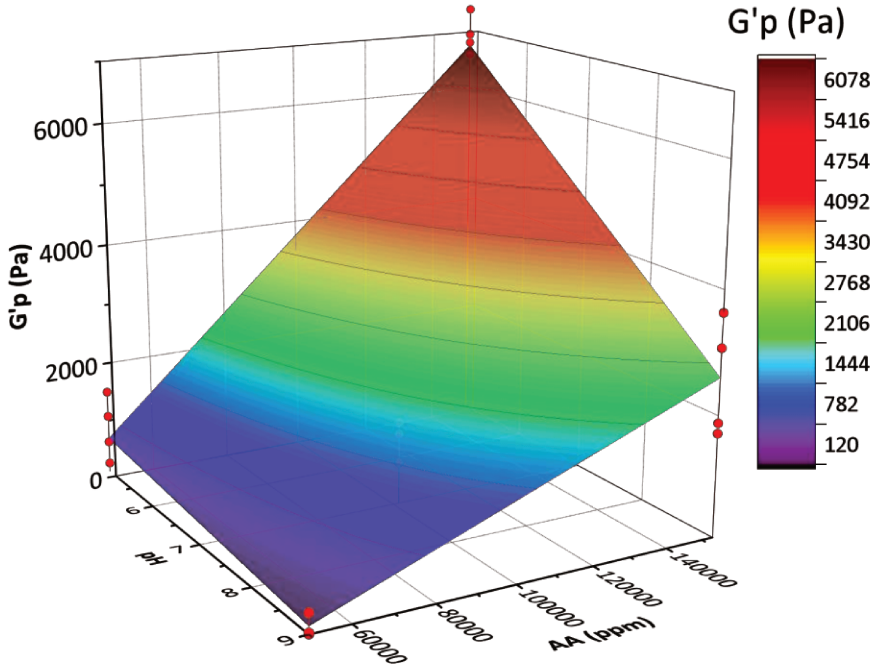

Fig. 4.17 Response surface, which relates the modulus plateau, G'_p, with the pH and acrylic acid concentration, AA

Fig. 4.17 shows that high values of modulus plateau, G'p, represented by the red color, are related to low pH values and high acrylic acid concentrations (AA). Otherwise, low values of modulus plateau, G'p, represented by the color purple, require high pH and low AA concentrations. **Fig. 4.18** translates all of that into contour graphics.

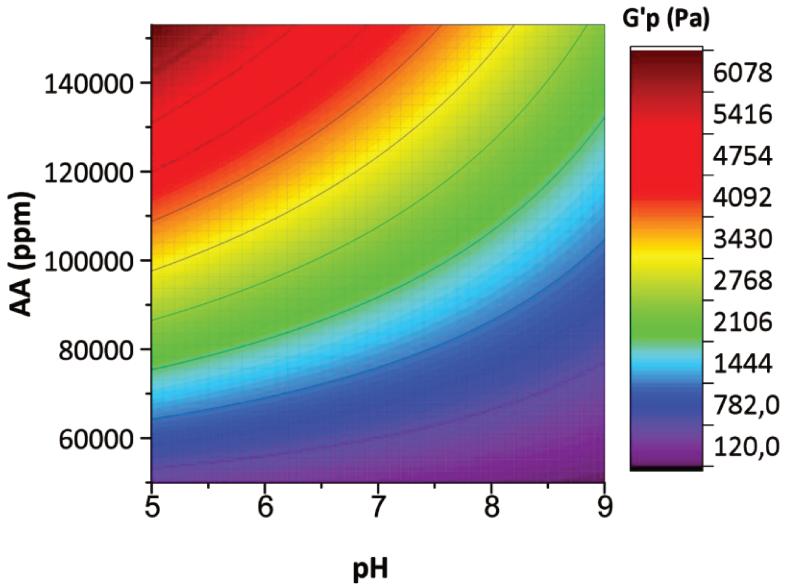

Fig. 4.18 Contour graphic representing Fig. 4.17

4.3.2. Constant khills

The constant Khills, calculated through **Eq. 3.2,** adjusted the equation representing the elastic modulus graphs, G', vs. time. NLFit function of the Originpro software was used for that. The experiment variance was calculated following the methodology presented in item **2.8.2**, and applying the excel VAR.S formula to the Experiment 17 replicates average, resulting in 11.48. The standard error calculation allowed us to identify four non-representative contrasts. Therefore, the vector with model coefficients were recalculated, excluding these four contrasts (1-3:1-4;2-4;3-5), allowing us to obtain a better result forecast by increasing the difference between freedom degrees. **Table 4.10** summarizes all the mentioned results.

Table 4.10 Results forecasts and the effects on constant khills

	khills measured	khills expected
Exp 1	27.89	27.84
Exp 2	7.10	7.00
Exp 3	7.40	6.88
Exp 4	6.15	5.37
Exp 5	6.83	8.09
Exp 6	6.12	4.70
Exp 7	15.88	16.68
Exp 8	6.72	4.62
Exp 9	20.82	18.84
Exp 10	11.10	11.79
Exp 11	21.17	19.64
Exp 12	9.87	11.24
Exp 13	28.86	28.19
Exp 14	11.64	11.02
Exp 15	15.23	15.02
Exp 16	9.79	9.85
Exp 17	7.99	12.92
Exp 17	10.32	12.92
Exp 17	14.67	12.92

Contrasts	Model Coefficients	Standard error (+/-)	Verification
0	12.92	0.78	✓
1	-4.73	0.85	✓
2	-1.76	0.85	✓
3	-0.65	0.85	✗
4	2.77	0.85	✓
5	2.58	0.85	✓
1-2	1.33	0.85	✓
1-3	0.66	0.85	✗
1-4	-0.74	0.85	✗
1-5	-2.86	0.85	✓
2-3	1.03	0.85	✓
2-4	-0.28	0.85	✗
2-5	-0.86	0.85	✓
3-4	0.97	0.85	✓
3-5	-0.06	0.85	✗
4-5	-0.91	0.85	✓

After the definition of the representative contrast, the variance analysis, ANOVA, was carried out, using the least-squares method for the proposed linear model based on **Table 2.8**. That table includes twelve parameters, nineteen observation numbers, and seventeen repetitions numbers for the constant khills results analysis. The indicators showed at the bottom of **Table 4.11** proved that there was no fitting lack once the coefficient of determination, R^2=0.94, was close to the maximum coefficient of determination, R^2_{max}, and not fulfill the condition established by **Eq. 2.19**, this being a requirement of a good fit, because of the Distribution F=19.30 > MS_{Lof} / MS_{Pe}= 0.20.

Table 4.11 Analysis of variance (ANOVA) for constant khills

Variation source	Sum of Squares (SS)	Degrees of Freedom	Mean Squares (MS)
Regression (*R*)	877	11	14503850
Residual (*r*)	36	7	637748
Pure error (Pe)	11	5	125009
Lack of Fit (LoF)	23	2	597755
Total (*T*)	913	18	
R^2	R^2_{max}	MS_{Lof} / MS_{Pe}	Distribution F
0.94	0.97	0.20	19.30

Fig. 4.19 and **Fig. 4.20** show that the fit residuals were small, corroborating a good fit for the linear model of this test.

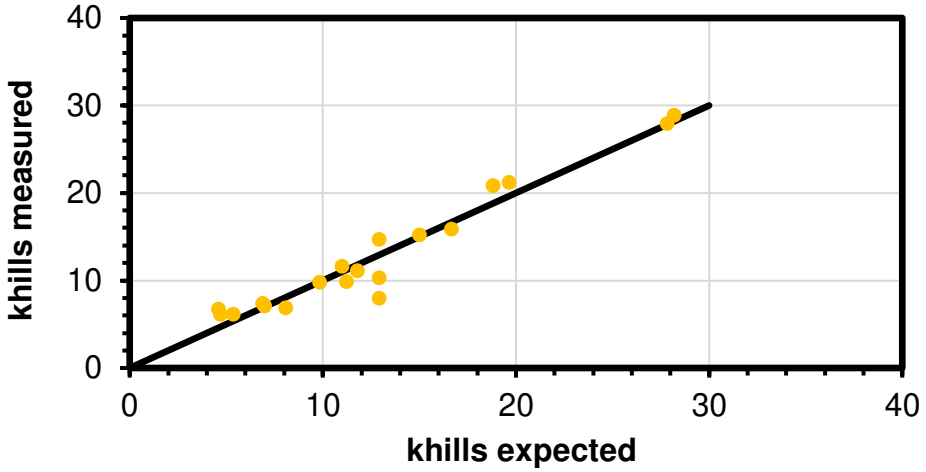

Fig. 4.19 Result obtained vs expected of constant khills

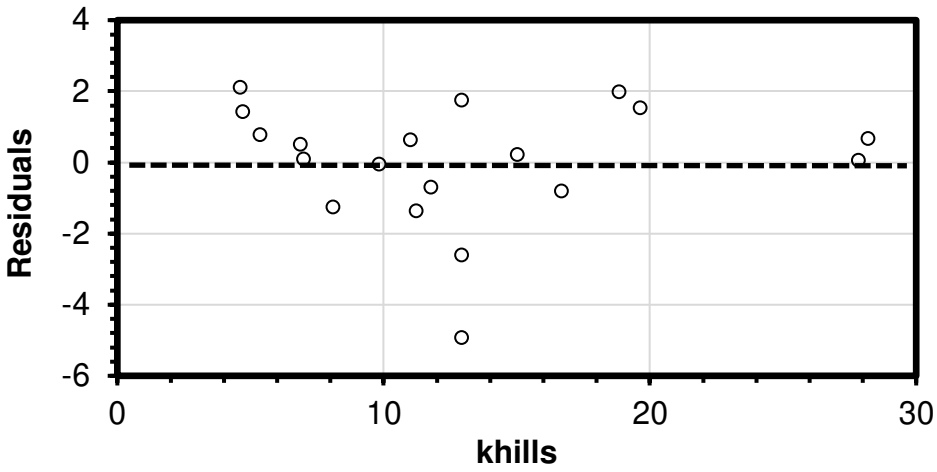

Fig. 4.20 Residues left by a linear model for the constant khills

In the constant khills analysis case, the contrasts with great representativeness were the pH, the acrylic acid concentration, AA, and the carboxymethyl cellulose concentration, CMC. The high values obtained from the constant khills refer to a slower kinetic. Otherwise, the values were low. **Fig. 4.21** and **Fig. 4.22** show us that to obtain high values of the constant khills, represented by the color red, it is required low pH values and low acrylic acid concentrations. The graph can also indicate that by increasing the pH values, the polymerization is being accelerated since the amount of charges is increasing, resulting in lower values of the constant khills.

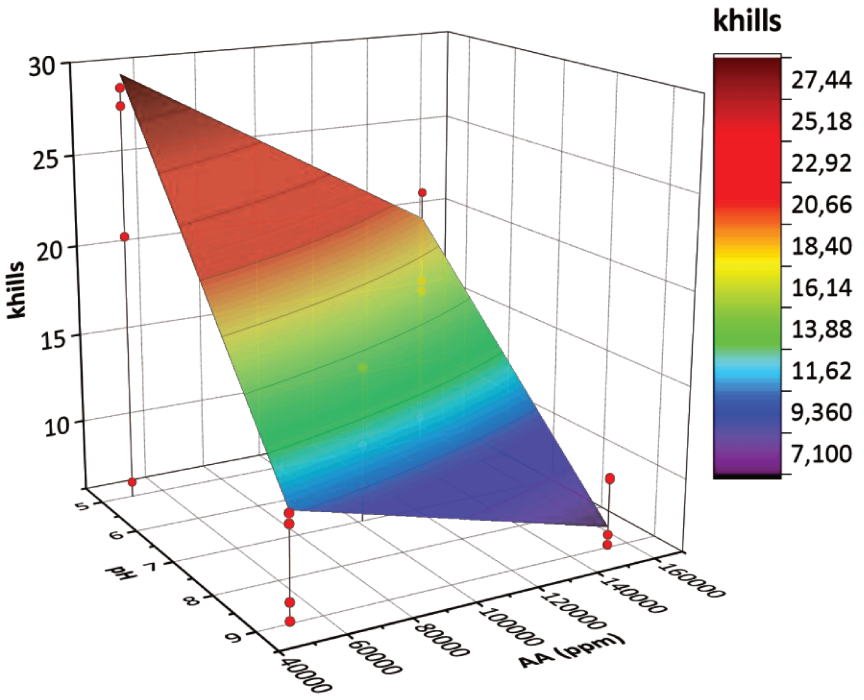

Fig. 4.21 Response surface, which relates the constant khills, with the pH and acrylic acid concentration, AA

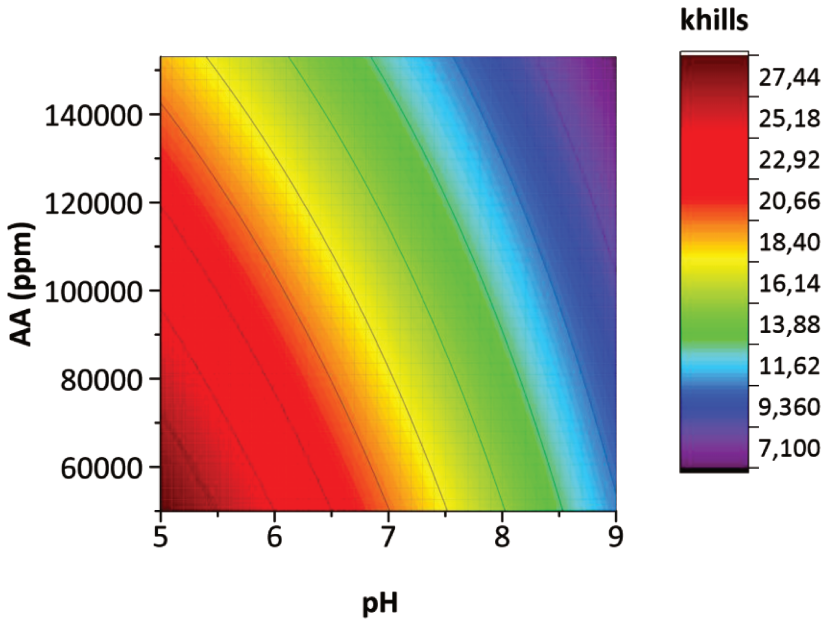

Fig. 4.22 Contour graphic representing Fig. 4.21

Fig. 4.23 and **Fig. 4.24** show the interaction between the pH and the CMC concentration. As mentioned above, low pH values are necessary to obtain high values of the constant khills. Additionally, one can see that as CMC concentration increases, constant khills values also increases slightly.

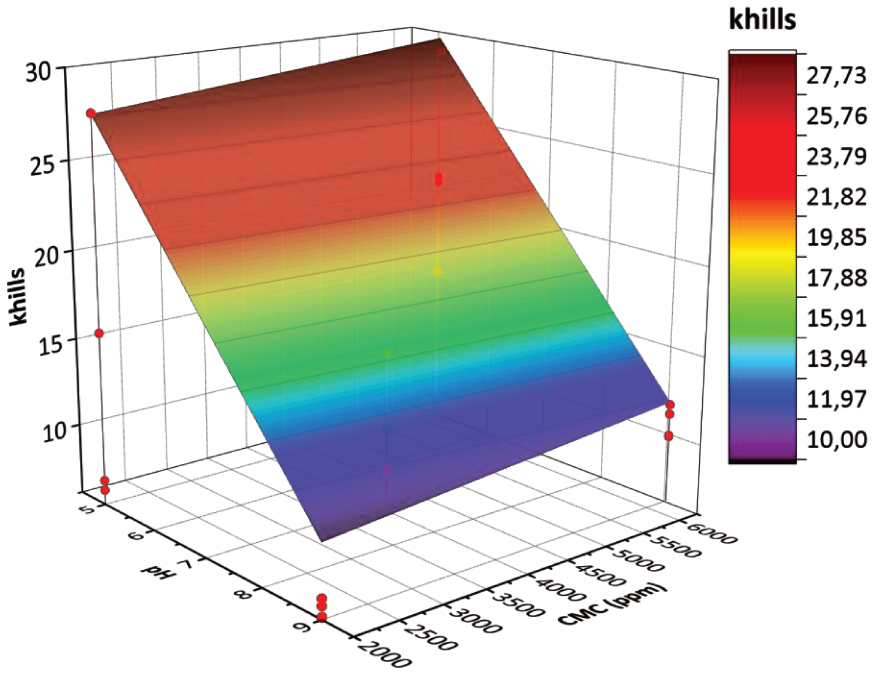

Fig. 4.23 Response surface, which relates the constant khills, with the pH and carboxymethyl cellulose concentration, CMC

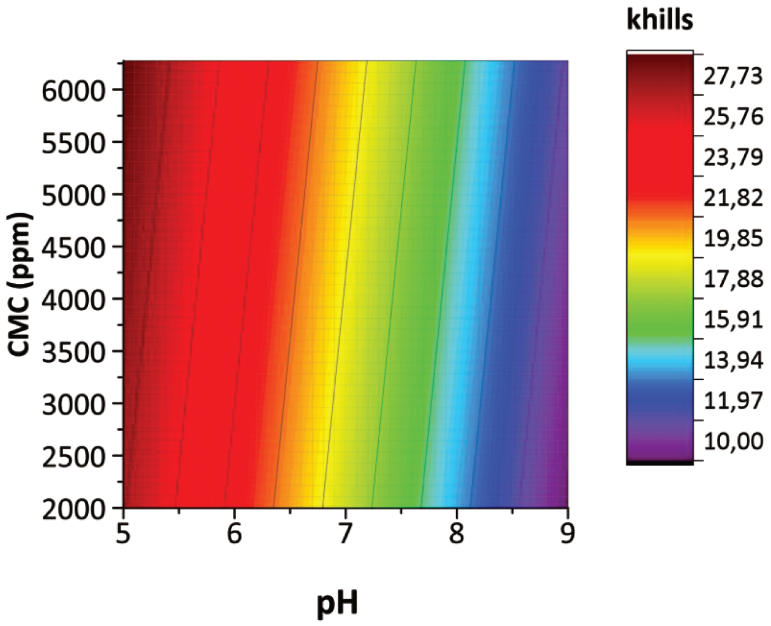

Fig. 4.24 Contour graphic representing Fig. 4.23

Fig. 4.25 and **Fig. 4.26** show the relationship between AA and CMC concentrations with the constant khills values.

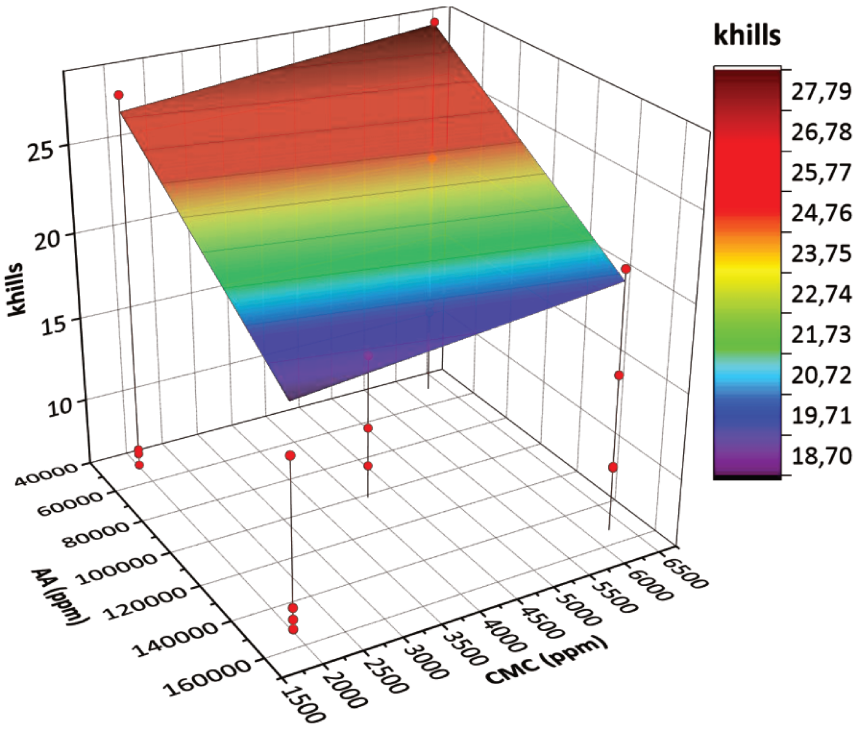

Fig. 4.25 Response surface, which relates the constant khills, with acrylic acid concentration, AA, and carboxymethyl celllulose concentration, CMC

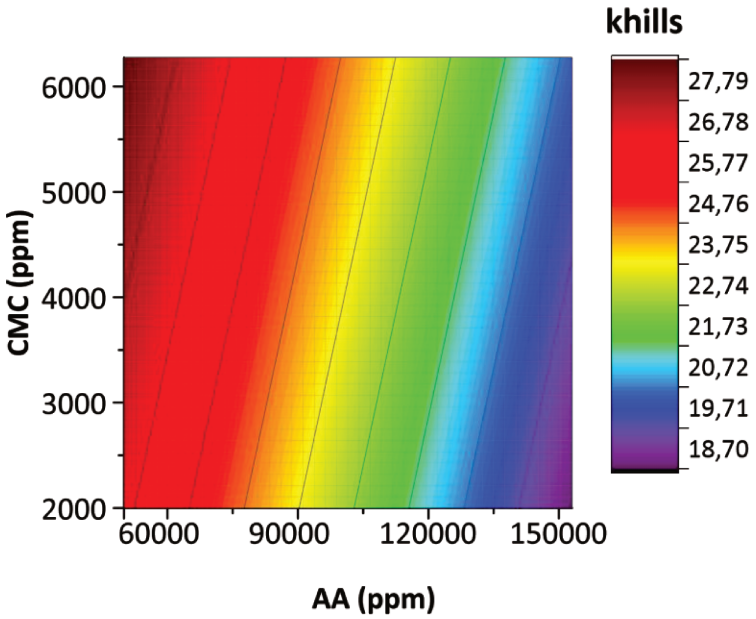

Fig. 4.26 Contour graphic representing Fig. 4.25

4.3.3. Stability of G'

The stability of elastic modulus, G', was determined by the proportion between G'max value, calculated by **Eq. 3.2**, and the value calculated for G'p. Following the methodology (see

item **2.8.2**), the variance of experiment was calculated by applying the excel formula VAR.S to the average of Experiment 17 replicates, resulting in 0.0057. The standard errors calculation allowed the identification of three non-representative contrasts (1-3;2-3;4-5). Therefore, the vector with model coefficients was recalculated, excluding these three contrasts to obtain a better result forecast by increasing the difference between the freedom degrees. **Table 4.12** summarized all the mentioned results.

Table 4.12 Results forecasts and effects of stability of G'

	G' stability measured	G' stability expected
Exp 1	0.99	0.96
Exp 2	0.19	0.15
Exp 3	1.29	1.27
Exp 4	0.75	0.76
Exp 5	0.44	0.44
Exp 6	0.10	0.09
Exp 7	0.89	0.87
Exp 8	0.44	0.39
Exp 9	0.99	0.95
Exp 10	0.55	0.52
Exp 11	0.98	0.97
Exp 12	0.72	0.73
Exp 13	0.96	0.96
Exp 14	0.07	0.07
Exp 15	0.89	0.87
Exp 16	0.64	0.59
Exp 17	0.58	0.66
Exp 17	0.48	0.66
Exp 17	0.63	0.66

Contrasts	Model coefficients	Standard error (+/-)	Verification
0	0.662	0.017	✓
1	-0.249	0.019	✓
2	0.144	0.019	✓
3	-0.126	0.019	✓
4	0.046	0.019	✓
5	0.053	0.019	✓
1-2	0.060	0.019	✓
1-3	0.008	0.019	✗
1-4	0.019	0.019	✓
1-5	0.025	0.019	✓
2-3	0.017	0.019	✗
2-4	-0.061	0.019	✓
2-5	-0.062	0.019	✓
3-4	0.042	0.019	✓
3-5	0.040	0.019	✓
4-5	0.005	0.019	✗

Once the representative contrasts were defined, the variance analysis, ANOVA, was carried out, using the least-squares method for the proposed linear model based on **Table 2.8**. The result analysis for the constant khills included thirteen parameters, nineteen observation numbers, and seventeen repetitions numbers. The indicators at the bottom of **Table** 4.13 proved no fitting lack once the coefficient of determination, R2=0.97, was close to the maximum coefficient of determination, R2 max. However, the established condition by **Eq. 2.19** was not fulfill, this being a requirement of good fit, since the Distribution F=19.25 > MS_{Lof} / MS_{Pe}= 1.22.

Table 4.13 Analysis of variance (ANOVA) for stability of G'

Variation source	Sum of Squares (SS)	Degrees of Freedom	Mean Squares (MS)
Regression (*R*)	1.91	12	14503850
Residual (*r*)	0.05	6	637748
Pure error (Pe)	0.03	4	125009
Lack of Fit (LoF)	0.01	2	597755
Total (*T*)	1.96	18	
R^2	R^2_{max}	MS_{Lof} / MS_{Pe}	Distribution F
0.97	0.99	1.22	19.25

Like the previous results, **Fig. 4.27** and **Fig. 4.28** show a good data fit, with small variation in part of the replicates, which were the points in the middle of the graphs.

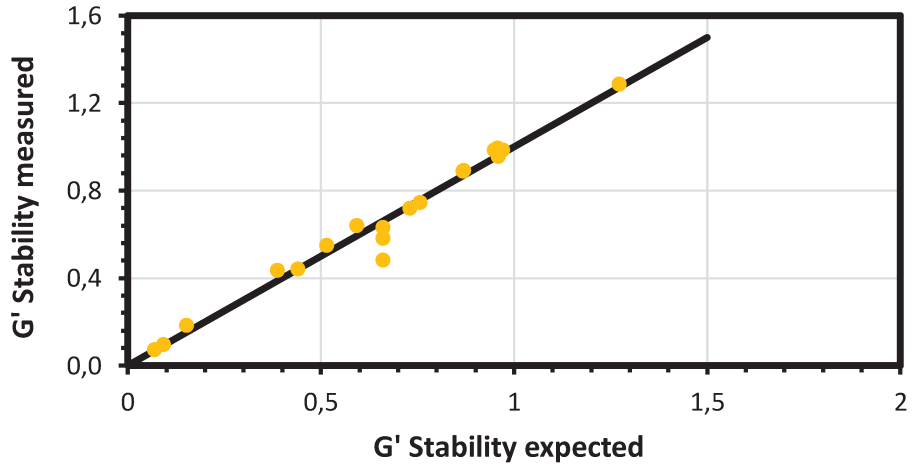

Fig. 4.27 Result obtained vs expected for stability of G'

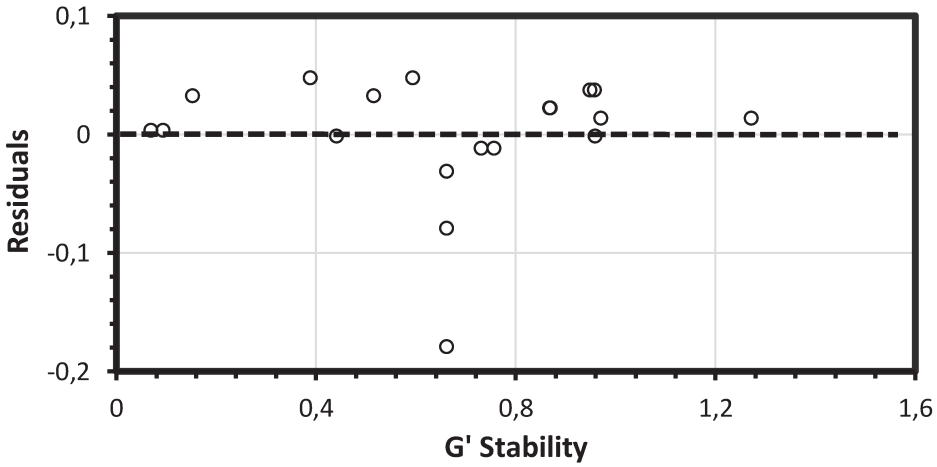

Fig. 4.28 Residues left by a linear model for stability of G'

The contrasts with great representativeness on G' stability, were the pH, the acrylic acid concentration, AA, and the ammonium persulfate concentration, APS. Values close to 1,

represented by the color red, show that there was not a very large variation in the elastic modulus values, G', during the different tests. On the contrary, values very less than 1 showed a drop in the G' values, interpreting that like a gel degradation in the course of the tests.

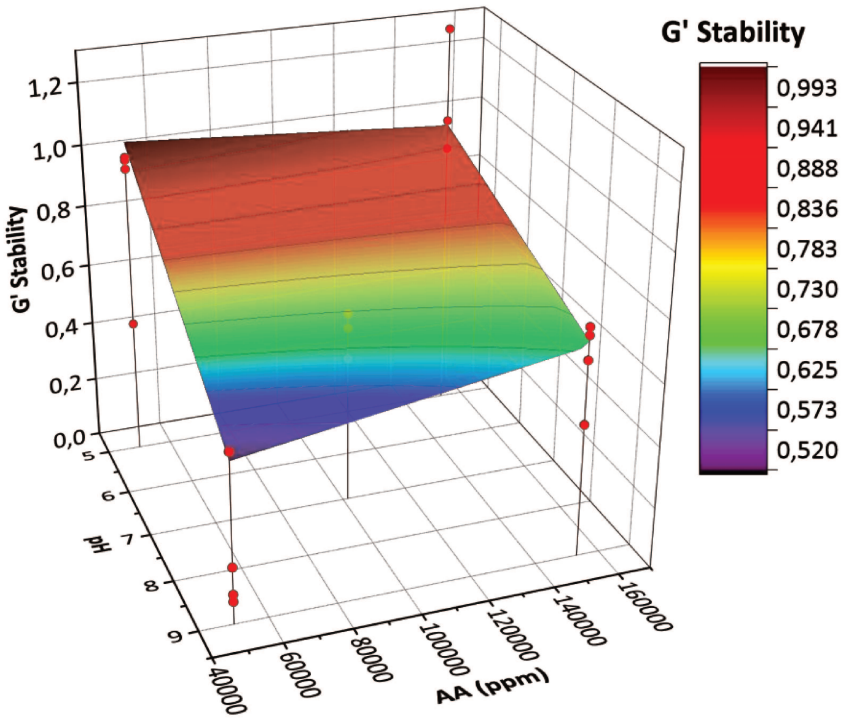

Fig. 4.29 Response surface, which relates the stability of G', with the pH and acrilyc acid, AA

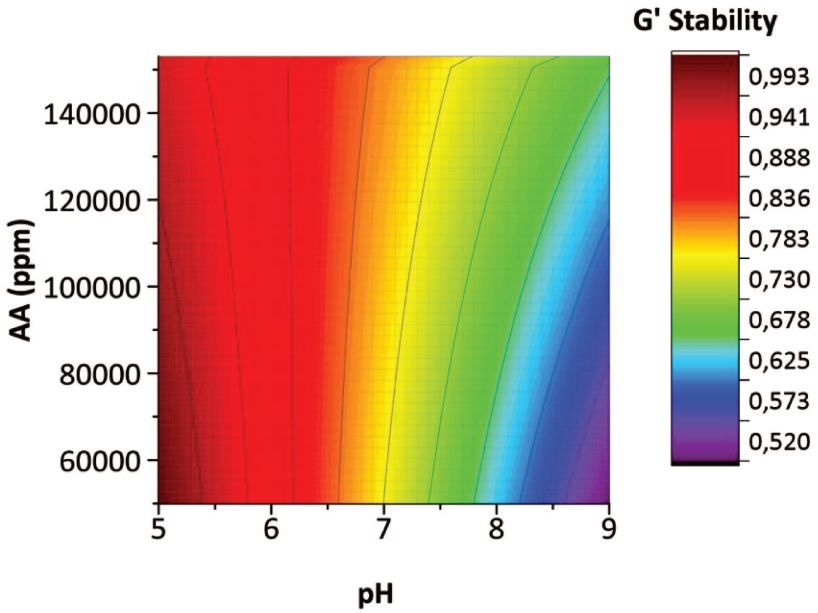

Fig. 4.30 Contour graphic representing Fig. 4.29

Fig. 4.29 and **Fig. 4.30** show the relationship among G 'stability, the pH and the AA concentration. On the other hand, **Fig. 4.31** and **Fig. 4.32** show G 'stability result as an effect of the pH and the APS concentration.

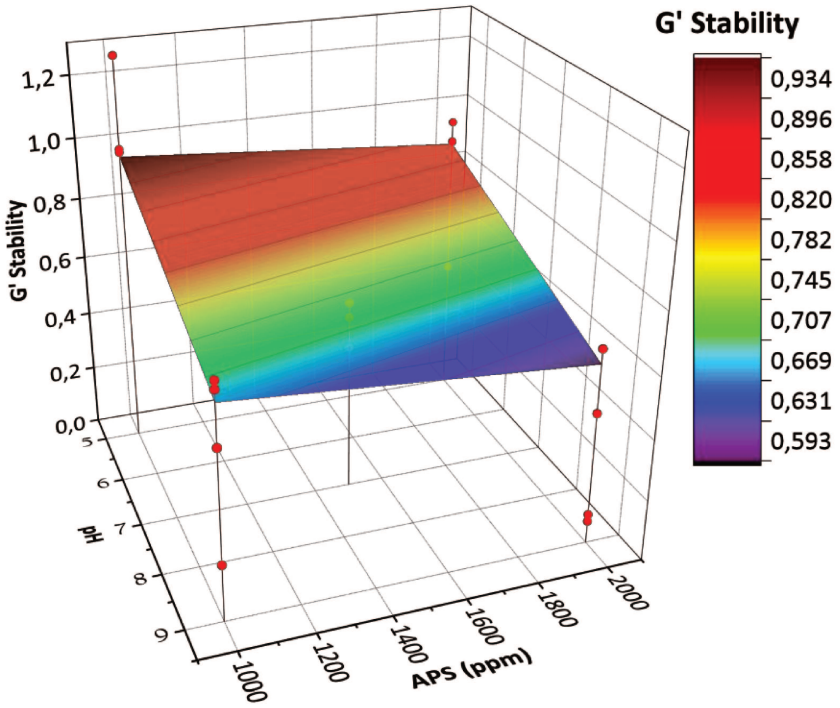

Fig. 4.31 Response surface, which relates the stability of G', with the pH and ammonium persulfate concentration, APS

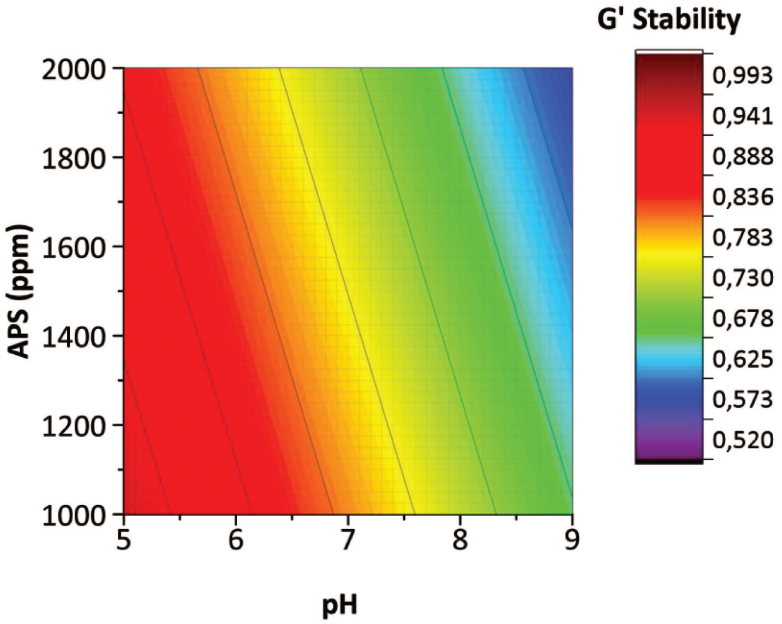

Fig. 4.32 Contour graphic representing Fig. 4.31

Through **Fig. 4.33** and **Fig. 4.34**, one can see that when working with low AA and APS concentrations, it is possible to improve the values of elastic modulus, G '.

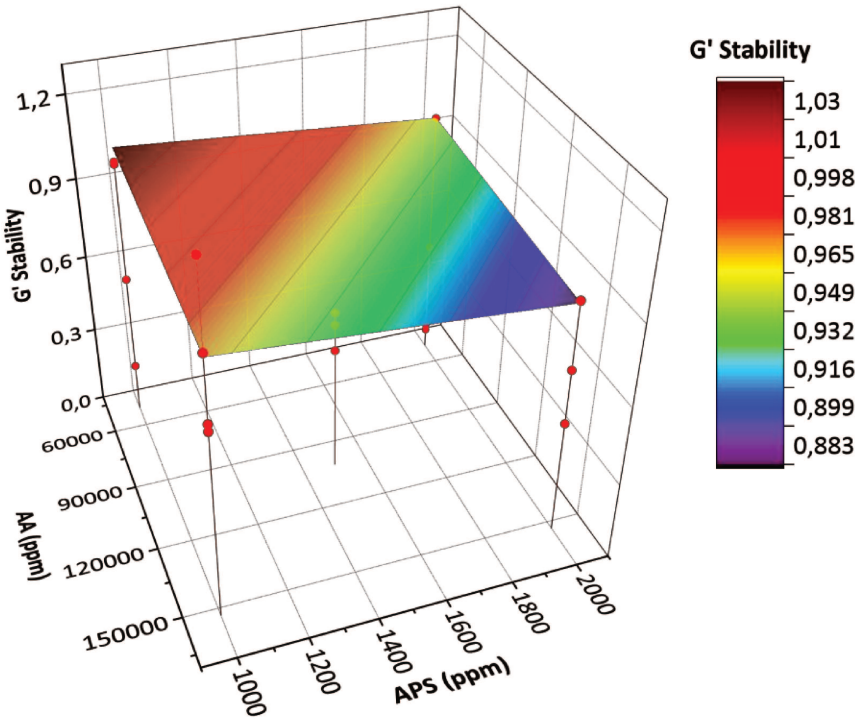

Fig. 4.33 Response surface, which relates the stability of G', with acrilyc acid concentration, AA, and ammonium persulfate concentration, APS

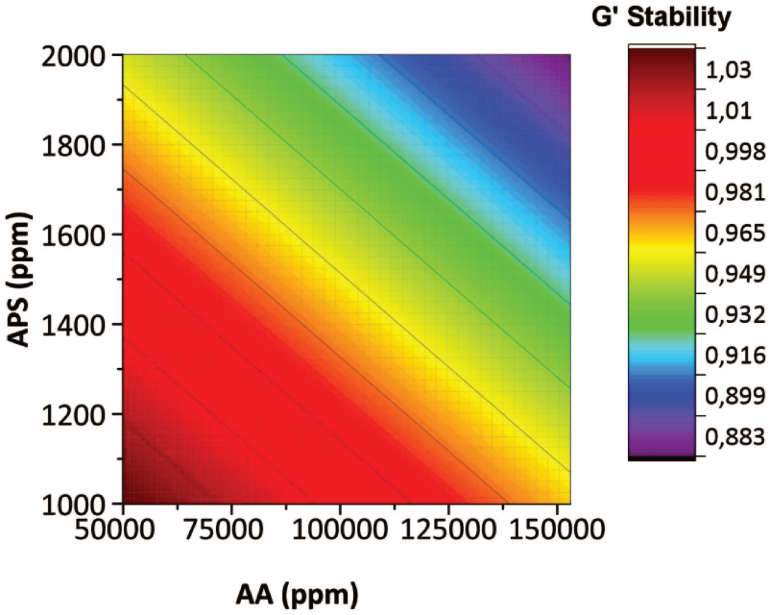

Fig. 4.34 Contour graphic representing Fig. 4.33

4.3.4. NMR measurements

The first result obtained by the NMR measurements at 46 °C was the gelation onset time, Tg. That result was determined through the relaxation time graphs applying the methodology described in Item **4.2.4**. Following the methodology described in item **2.8.2**, the variance of the experiment was calculated by applying the excel formula VAR.S to the average of Experiment 17 replicates, resulting in 11.41. The calculation of the standard errors allowed the identification of three non-representative contrasts (1-5;2-3;2-5). Therefore, the vector with model coefficients was recalculated, excluding these three contrasts to obtain a better result forecast by increasing the difference between the freedom degrees. **Table 4.14** summarizes all the mentioned results.

Table 4.14 Results forecasts and effects of stability of Tg

	Tg NMR measured	Tg NMR expected
Exp 1	23.70	23.54
Exp 2	10.97	11.81
Exp 3	30.43	29.22
Exp 4	11.25	11.04
Exp 5	13.05	12.84
Exp 6	8.20	6.98
Exp 7	19.77	20.61
Exp 8	4.27	4.11
Exp 9	18.90	18.38
Exp 10	5.30	3.77
Exp 11	21.60	22.76
Exp 12	14.68	14.84
Exp 13	15.80	15.95
Exp 14	10.87	12.02
Exp 15	28.75	27.22
Exp 16	16.72	16.19
Exp 17	15.55	15.71
Exp 17	17.60	15.71
Exp 17	11.00	15.71

Contrasts	Model coefficients	Standard error (+/-)	Verification
0	15.705	0.775	✓
1	-5.609	0.844	✓
2	2.543	0.844	✓
3	-1.214	0.844	✓
4	0.686	0.844	✗
5	-0.599	0.844	✗
1-2	-1.095	0.844	✓
1-3	0.945	0.844	✓
1-4	0.924	0.844	✓
1-5	0.684	0.844	✗
2-3	0.155	0.844	✗
2-4	1.318	0.844	✓
2-5	-0.501	0.844	✗
3-4	2.670	0.844	✓
3-5	1.043	0.844	✓
4-5	-1.124	0.844	✓

After the representative contrasts were defined, the variance analysis, ANOVA, was carried out, using the least-squares method for the proposed linear model. Based on **Table 2.8**, the constant khills result analysis included thirteen parameters, nineteen numbers of observations, and seventeen numbers of repetitions. The indicators showed at the bottom of **Table 4.15** proved that there was no fitting lack, once the coefficient of determination, R2=0.96, was close to the maximum one, R2 max. On the other hand, the condition established by **Eq. 2.19** was not fulfilled, this being a requirement of good fit, since the Distribution F=19.25 > MS_{Lof} / MS_{Pe}= 0.06.

Table 4.15 Analysis of variance (ANOVA) for Tg

Variation source	Sum of Squares (SS)	Degrees of Freedom	Mean Squares (MS)
Regression (*R*)	870.28	12	14503850
Residual (*r*)	38.20	6	637748
Pure error (Pe)	2.93	4	125009
Lack of Fit (LoF)	22.82	2	597755
Total (*T*)	908.48	18	
R^2	R^2 max	MS lof / MS Pe	Distribution F
0.96	0.97	0.06	19.25

Fig. 4.35 and **Fig. 4.36** confirmed a good fit for the linear model again by applying the least-squares method.

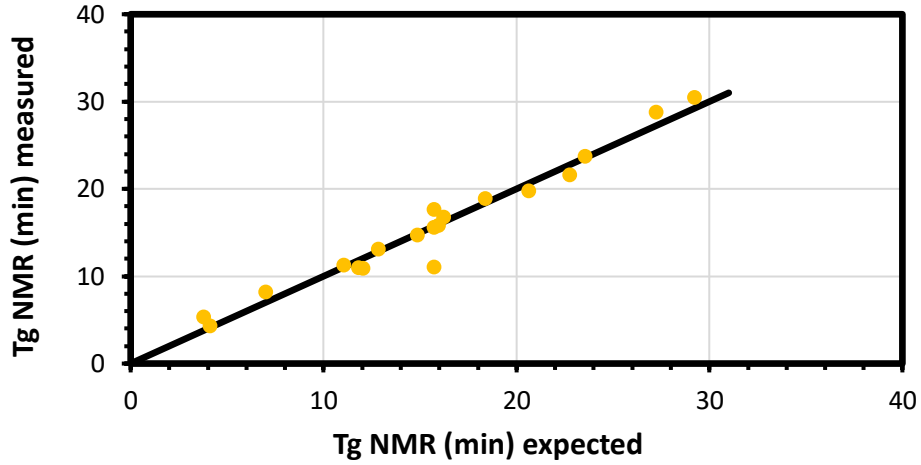

Fig. 4.35 Result obtained vs expected for Tg

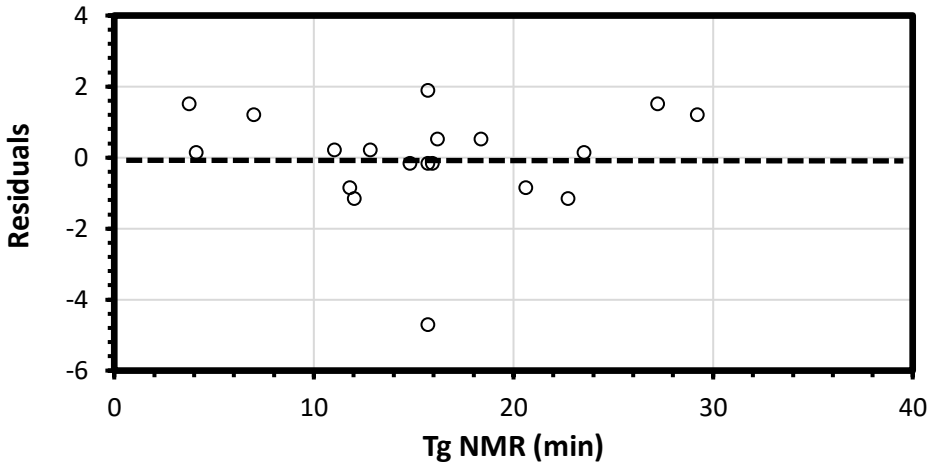

Fig. 4.36 Residues left by a linear model for stability of Tg

The contrasts with great representativeness for onset gelation time, Tg, were the pH, acrylic acid concentration, AA, and ammonium persulfate concentration, APS. **Fig. 4.37** and **Fig.**

4.38 show us that to obtain slower kinetics, represented by the color red, it is necessary to work with low pH values and high AA concentrations.

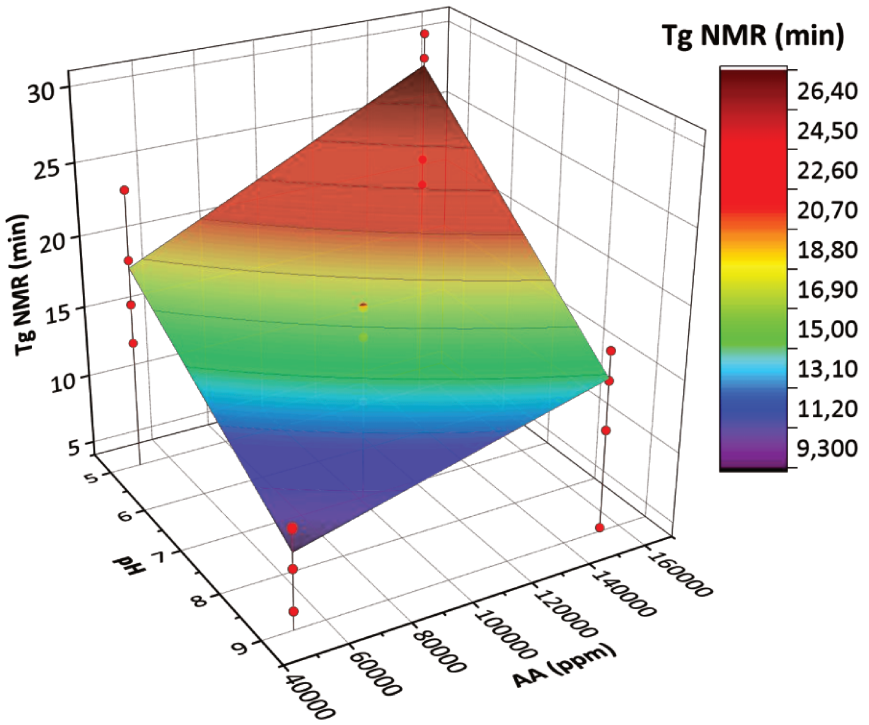

Fig. 4.37 Response surface, which relates the Tg, with the pH and acrylic acid concentration, AA

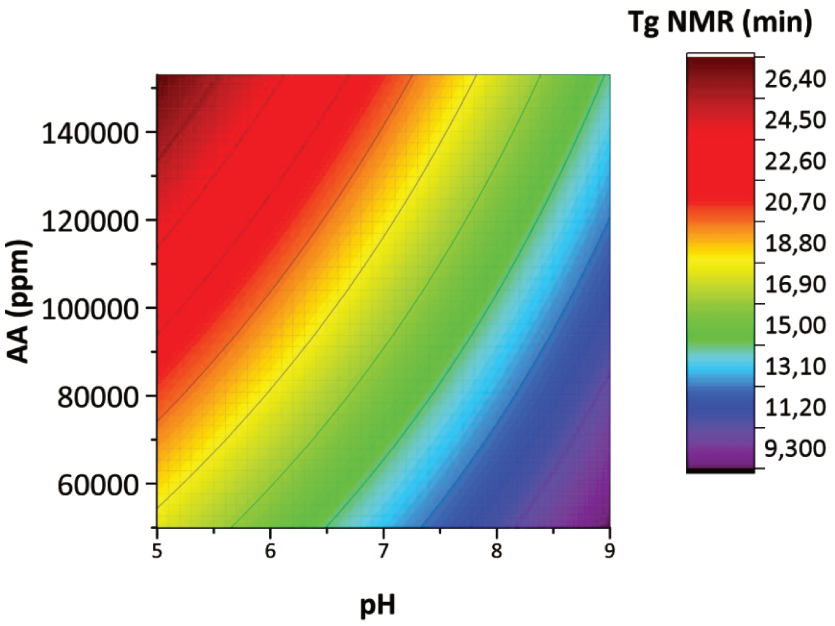

Fig. 4.38 Contour graphic representing Fig. 4.37

Fig. 4.39 and **Fig. 4.40** show us that due to the significant effect that pH has on Tg values, the effect of APS is diminished.

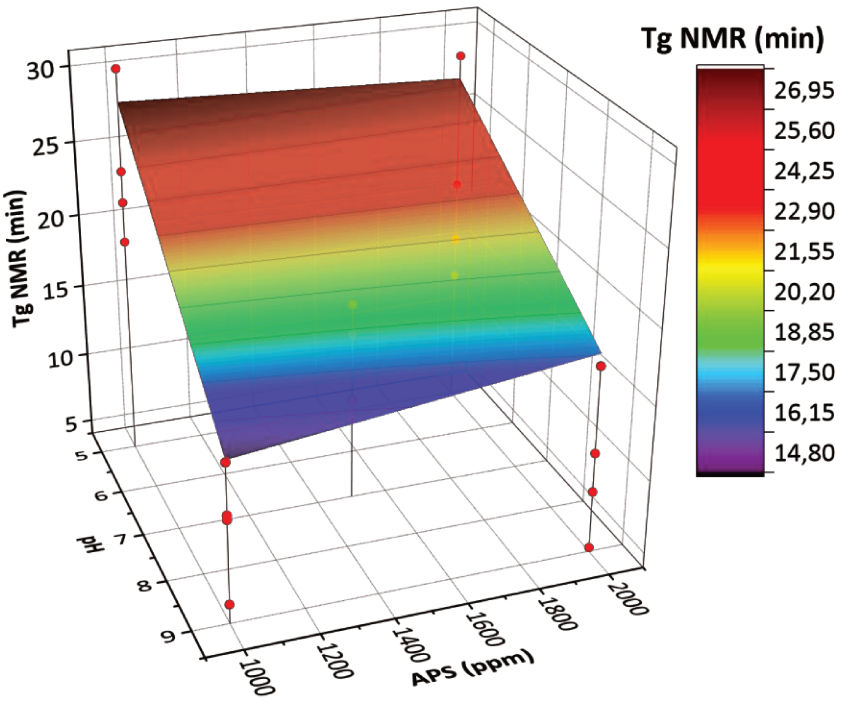

Fig. 4.39 Response surface, which relates the Tg, with the pH and ammonium persulfate concentration, APS

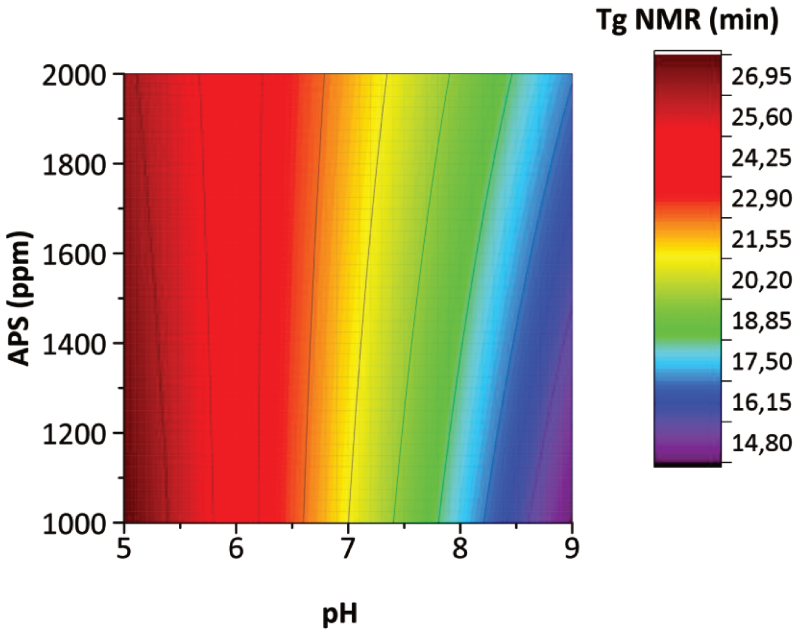

Fig. 4.40 Contour graphic representing Fig. 4.39

Fig. 4.41 and **Fig. 4.42** show us that to obtain slower onset gelation times, Tg, it is necessary to have low levels of APS concentration and high AA values.

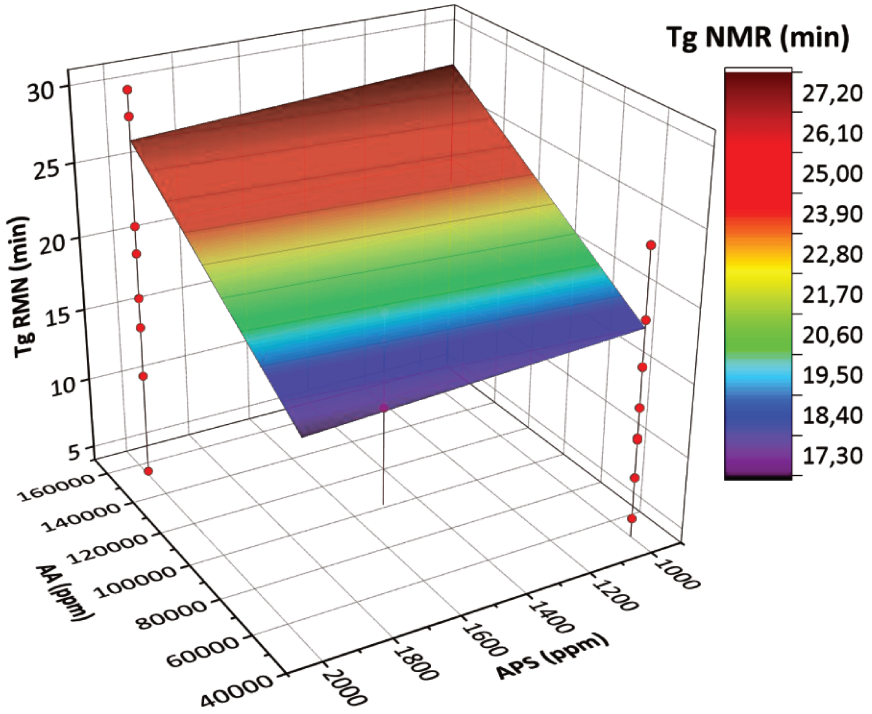

Fig. 4.41 Response surface, which relates the Tg, with acrilyc acid concentration, AA, and ammonium persulfate concentration, APS

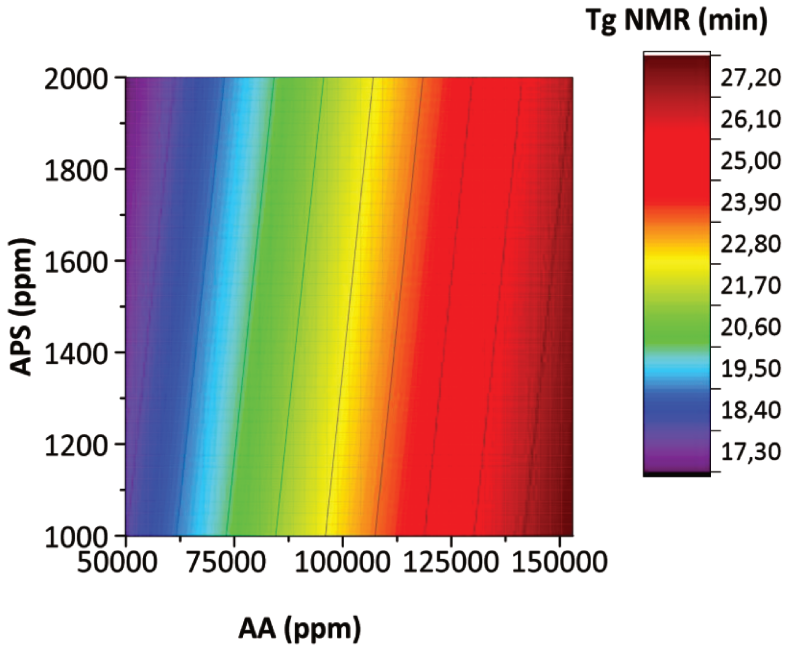

Fig. 4.42 Contour graphic representing Fig. 4.41

Finally, **Table 4.16** shows the effect of syneresis on the experiment results, where the check sign represents the presence of syneresis. The tests were evaluated as described in Item **4.2.4**, where at first glance, it is possible to say that the even experiments that represent the high pH values were those affected by syneresis.

Table 4.16 summary of the experiments that had the presence of the syneresis effect

exp 1	exp 2	exp 3	exp 4	exp 5	exp 6	exp 7	exp 8	exp 9	exp 10
✗	✓	✗	✓	✗	✓	✗	✓	✗	✓
exp 11	exp 12	exp 13	exp 14	exp 15	exp 16	exp 17	exp 17	exp 17	
✗	✓	✗	✓	✗	✓	✗	✗	✗	

Table 4.17 summarize the results, facilitating the experiments selection for the next step as established in **Fig. 3.8**.

Table 4.17 Summary of the design of experiments and their respective results

	0	1	2	3	4	5	1-2	1-3	1-4	1-5	2-3	2-4	2-5	3-4	3-5	4-5	G'p (Pa)	Khills	Stability G'	Tg
Exp 1	1	-1	-1	-1	-1	1	1	1	1	-1	1	1	-1	1	-1	-1	983.03	27.89	0.99	23.70
Exp 2	1	1	-1	-1	-1	-1	-1	-1	-1	-1	1	1	1	1	1	1	25.45	7.10	0.19	10.97
Exp 3	1	-1	1	-1	-1	-1	-1	1	1	1	-1	-1	-1	1	1	1	6772.51	7.40	1.29	30.43
Exp 4	1	1	1	-1	-1	1	1	-1	-1	1	-1	-1	1	1	-1	-1	1878.01	6.15	0.75	11.25
Exp 5	1	-1	-1	1	-1	-1	1	-1	1	1	-1	1	1	-1	-1	1	150.72	6.83	0.44	13.05
Exp 6	1	1	-1	1	-1	1	-1	1	-1	1	-1	1	-1	-1	1	-1	20.97	6.12	0.10	8.20
Exp 7	1	-1	1	1	-1	1	-1	-1	1	-1	1	-1	1	-1	1	-1	7355.91	15.88	0.89	19.77
Exp 8	1	1	1	1	-1	-1	1	1	-1	-1	1	-1	-1	-1	-1	1	1710.29	6.72	0.44	4.27
Exp 9	1	-1	-1	-1	1	-1	1	1	-1	1	1	-1	1	-1	1	-1	529.77	20.82	0.99	18.90
Exp 10	1	1	-1	-1	1	1	-1	-1	1	1	1	-1	-1	-1	-1	1	329.18	11.10	0.55	5.30
Exp 11	1	-1	1	-1	1	1	-1	1	-1	-1	-1	1	1	-1	-1	1	6917.81	21.17	0.98	21.60
Exp 12	1	1	1	-1	1	-1	1	-1	1	-1	-1	1	-1	-1	1	-1	3079.61	9.87	0.72	14.68
Exp 13	1	-1	-1	1	1	1	1	-1	-1	-1	-1	-1	-1	1	1	1	1411.20	28.86	0.96	15.80
Exp 14	1	1	-1	1	1	-1	-1	1	1	-1	-1	-1	1	1	-1	-1	5.20	11.64	0.07	10.87
Exp 15	1	-1	1	1	1	-1	-1	-1	-1	1	1	1	-1	1	-1	-1	6563.63	15.23	0.89	28.75
Exp 16	1	1	1	1	1	1	1	1	1	1	1	1	1	1	1	1	3637.14	9.79	0.64	16.72
Exp 17	1	0	0	0	0	0	0	0	0	0	0	0	0	0	0	0	694.13	7.99	0.58	15.55
Exp 17	1	0	0	0	0	0	0	0	0	0	0	0	0	0	0	0	1184.48	10.32	0.48	17.60
Exp 17	1	0	0	0	0	0	0	0	0	0	0	0	0	0	0	0	1380.55	14.67	0.63	11.00

4.4. Performance Evaluation

Once the optimization was carried out, two experiments were chosen for the following evaluation step using the method described in item **3.2.4** and the information given in **Table 4.17**; they were experiments 11 and 1. Experiment 11 represented a high value of modulus plateau, good kinetics, and stability. On the other hand, experiment 1 showed a low value of the modulus plateau.

First, experiment 11 was evaluated. **Fig. 4.43**. In that figure, the light blue part represents the injection at a constant flow of 1 $ml \cdot min^{-1}$, the beginning of the red part can be interpreted as the start gelation inside the filter press, and where the pressure start to increase to maintain a constant flow of 1 $ml \cdot min^{-1}$ and the beginning of the yellow part represents the moment in which

the constant flow of 1 ml·min^{-1} was changed to a constant pressure of 300 psi. This last period also represents the gel state required to control loss in a 40 Darcies permeability disk.

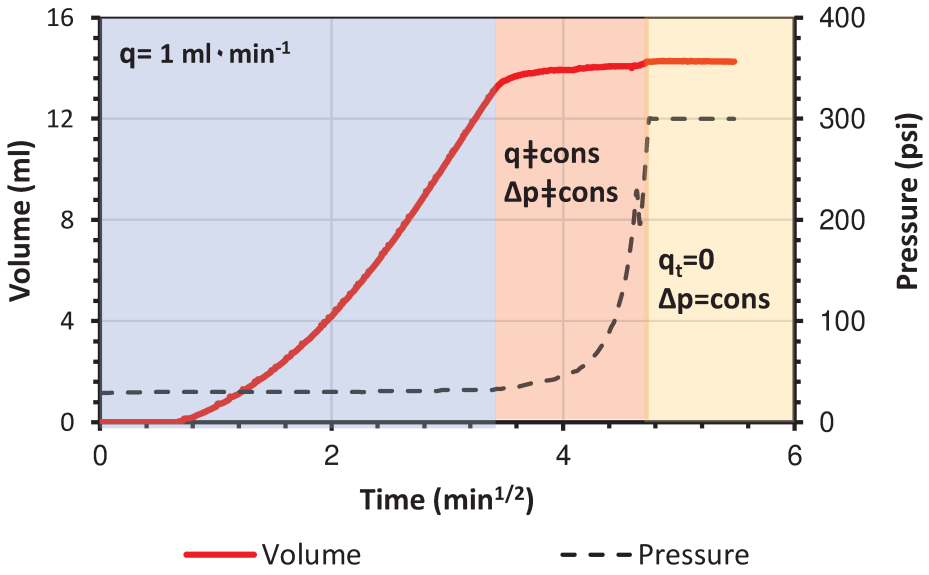

Fig. 4.43 Modified static filtration results for experiment 11

Fig. 4.44 shows the results of the Experiment 1. The procedures and the evaluation were carried out in the same way as Experiment 11. The initial behavior was similar to experiment 11 and is evidenced by the blue part, and the beginning of the red part. The red region represents the start of gelation inside the filtration press of Experiment 1. During this stage, the differential pressure increased and once it reached approximately 110 psi, the gel rupture was evidenced, demonstrating ineffectiveness to control the fluid loss.

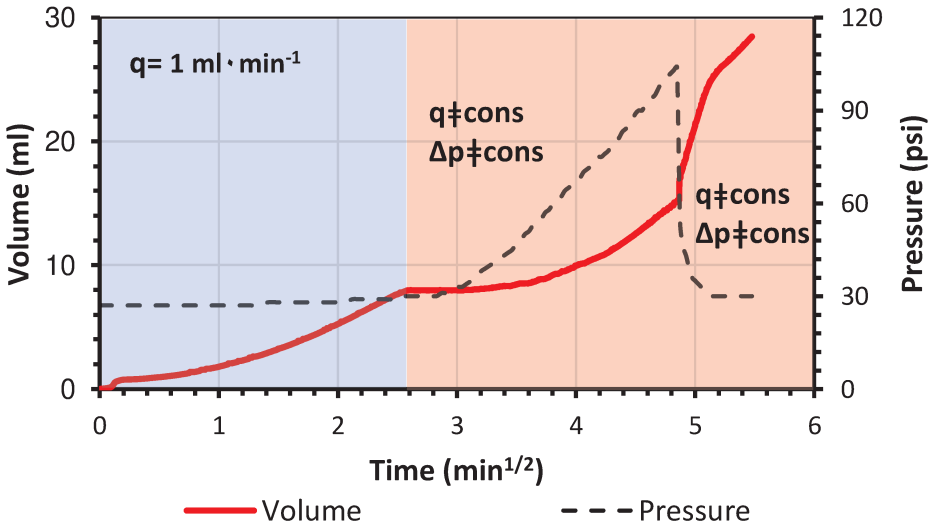

Fig. 4.44 Modified static filtration results for experiment 1

Because of the ineffectiveness of experiment 1 and the significant difference of modulus plateau values compared with that of experiment 11, the third experiment with an intermediate value of modulus plateau was performed. Despite not having good kinetic and stability response, experiment 12 was evaluated to observe the effectiveness of modulus plateau values in controlling fluid loss.

Fig. 4.45 shows the filtration results of experiment 12, where like in the previous tests, the blue part represents the injection at a at constant flow of 1 ml·min^{-1}. The beginning of the red part represents the start of gelation of experiment 12, and at which the pressure begins to increase until it reaches the beginning of the yellow part, representing the change for injection at a constant differential pressure of 300 psi.

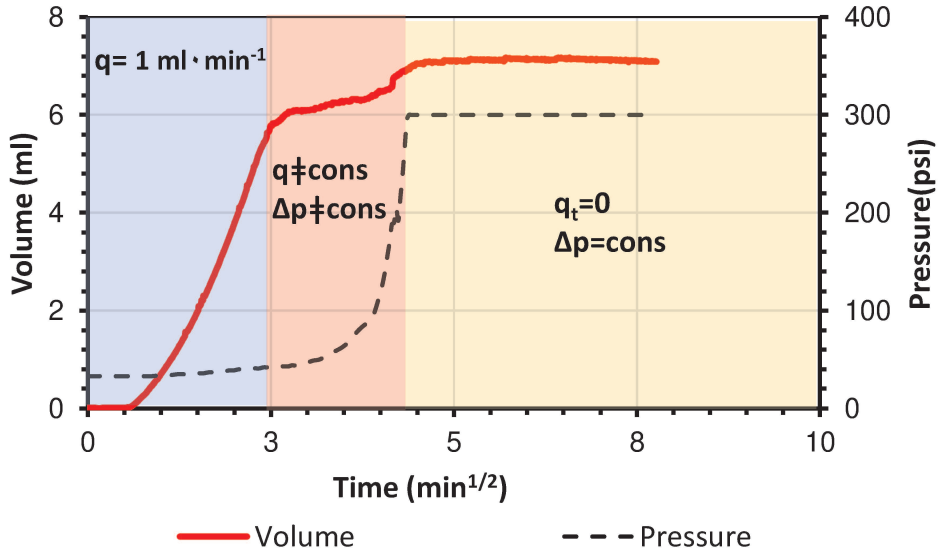

Fig. 4.45 Modified static filtration results for experiment 12

5. CONCLUSIONS AND RECOMMENDATIONS

This experimental study showed a workflow based on laboratory tests to design a water-based fluid to control circulation loss. A DOE was also implemented to optimize the composition of the fluid. The main findings and recommendations for future works are summarized here.

5.1. Conclusions

The polymer selection study stage helped to determine the polymer type and the correspondent optimal polymer concentrations range for building a treatment fluid to be applied during drilling and completion operations. Thus, carboxymethyl cellulose was selected due to its broad semi-dilute regimen.

The kinetics of gel systems were evaluated using three methodologies. The effectiveness of each method and concordance among them were evidenced, such as in the case of the rigid gel state determination. The methodologies also helped to identify the significant difference between the two proposed gel systems. A much more robust network of cross-linked chains was observed in the second system, which resulted in a more resistant gel with a more homogeneous behavior during the rheological and NMR tests. That was also demonstrated when the static filtration test was carried out. Although this test is not very representative for circulation loss evaluation, it helped us to evaluate the filtration capacity of the systems in high permeability disks, where the poor performance of the first system was evidenced. In contrast, the second system effectively controlled the loss in high permeability disks.

By applying a fractional factorial DOE, the number of experiments was significantly reduced, and a great fit among all results and a linear model was found by applying the least-squares method.

By analyzing the effects, pH was identified as the variable with the most significant effect on all the results. This result showed that when working with high pH values, weaker gels with less stability are generated. Besides, by accelerating the kinetics experiments and employing NMR tests, it was possible to observe the pH effect on the appearance of syneresis in the gels. The presented response surfaces can easily evidence that.

The increase in AA concentration allowed us to obtain gels with high values of modulus plateau, G'_p. However, the increase had a little negative effect on the stability and, in addition, faster kinetics at 70 °C. Otherwise, the NMR test evidenced that the AA concentration increase generated higher Tg values representing slower kinetics. That difference highlights the great importance of the temperature effect on the system composition.

Initially, a high APS concentration seemed effective for the treatment fluid system performance, but as temperature increased, its effect on gel degradation was observed.

Therefore, the APS concentration range was reduced to make the system compatible with 70 °C. Due to that, the AA concentration influence during the obtaining of results was relatively small. However, the stability reduction resulting from APS concentrations increase could still be seen, besides a slight kinetics acceleration.

Through response surfaces, it was also possible to see the CMC effect in the experiments. Despite not being as representative as other studied variables, slower kinetics could be observed.

The modified static filtration test allowed us to evaluate the modulus plateau response in the filter press, showing that high modulus values improved the filtration control in high permeability disks. The graphs resulting from the test also helped determine the gelation and the stabilization points within the filter press.

Despite not having carried out tests of lost circulation in fractures, the potential of the proposed system was evidenced throughout this work, showing both the resistance to pressure differential during the filtration tests, the kinetics that can be adjusted, and the gel stabilities that can be convenient during drilling and completion operations in reservoir areas. The self-degradation that APS has on the system can be convenient for the treatment operations in reservoir zones.

5.2. Recommendations

Some recommendations for future work are:

- Include the effect of temperature in the optimization of the system, due to the great importance it has on the cross-linking of polymers.
- Expand the range of APS concentration towards lower values used in the present work to determine its effects better.
- Carry out a study on the interest shear rates to show the effect it can have on the system.
- Include a study on retarders, accelerators, and corrosion inhibitors since they are components of great importance depending on the depths and conditions in which the system will be applied.
- Perform an evaluation of the NMR tests at the corresponding temperatures of the rheometer to homogenize the test conditions and to have more robust evidence of the techniques proposed in this work.
- Evaluate the proposed system in both static and dynamic lost circulation tests in order to increase its representativeness in real cases.

REFERENCES

Ahmad, A., 2001. Gels Handbook. Elsevier. https://doi.org/10.1016/B978-0-12-394690-4.X5073-7

Al-Hameedi, A.T.T., Dunn-Norman, S., Alkinani, H.H., Flori, R.E., Torgashov, E. V., Hilgedick, S.A., Almohammedawi, M.M., 2017. Preventing, Mitigating, or Stopping Lost Circulation in Dammam Formation, South Rumaila Field, Iraq; Requires Engineering Solutions, the Best Treatments Strategies, and Economic Evaluation Analysis, in: SPE/IATMI Asia Pacific Oil & Gas Conference and Exhibition. Society of Petroleum Engineers. https://doi.org/10.2118/186180-MS

Al-Muntasheri, G.A., Nasr-El-Din, H.A., Zitha, P.L.J., 2008. Gelation Kinetics and Performance Evaluation of an Organically Cross-linked Gel at High Temperature and Pressure. SPE J. 13, 337–345. https://doi.org/10.2118/104071-PA

API 13B-1, A.P.I., 2017. Recommended Practice for Field Testing Water-based Drilling Fluids, 5th ed. ed.

API PFM, A.P.I., 2001. MANUAL DE FLUIDOS DE PERFORACIÓN. Dallas, Texas.

Baroid Drilling Fluids, 2012. Baroid Fluids Handbook, 10th ed.

Barros Neto, B., Scarminio, I.S., Bruns, R.E., 2010. Como Fazer Experimentos: Pesquisa e Desenvolvimento na Ciência e na Indústria., 12th–2010th ed. Campinas, SP.

Beda, G., Carugo, C., 2001. Use of Mud Microloss Analysis While Drilling to Improve the Formation Evaluation in Fractured Reservoir, in: SPE Annual Technical Conference and Exhibition. Society of Petroleum Engineers, pp. 3687–3699. https://doi.org/10.2118/71737-MS

Benchabane, A., Bekkour, K., 2008. Rheological properties of carboxymethyl cellulose (CMC) solutions. Colloid Polym. Sci. 286, 1173–1180. https://doi.org/10.1007/s00396-008-1882-2

Bird, R.B., Stewart, W.E., Lightfoot, E.N., 1960. Transport Phenomena. John Wiley & Sons, Inc.

Blauch, M.E., Broussard, G.J., Sanclemente, L.W., Weaver, J.D., Pace, J.R., 1989. Fluid-Loss Control Using Crosslinkable HEC in High-Permeability Offshore Flexure Trend Completions, in: SPE Annual Technical Conference and Exhibition. Society of Petroleum Engineers. https://doi.org/10.2118/19752-MS

Bleackley, D., Strathman, M.S., 2011. Driving Project Efficiency and Cost Control in the Upstream Oil and Gas Industry. J. Pet. Technol. 63, 28–31. https://doi.org/10.2118/0111-0028-JPT

Bourgoyne, A.T.J., Millheim, K.K., Chenevert, M.E., Young, F.S.J., 1986. Applied Drilling Engineering. Richardson, Texas.

Bruton, J., Ivan, C., Heinz, T., 2001. Lost Circulation Control: Evolving Techniques and Strategies to Reduce Downhole Mud Losses, in: Proceedings of SPE/IADC Drilling Conference. Society of Petroleum Engineers, pp. 334–342. https://doi.org/10.2523/67735-MS

Brydson, T.J.A., 2017. Brydson's Plastics Materials, Brydson's Plastics Materials. Elsevier. https://doi.org/10.1016/C2014-0-02399-4

Caenn, R., Darley, H.C.H., Gray, G.R., 2011. Composition and Properties of Drilling and Completion

Fluids, in: Composition and Properties of Drilling and Completion Fluids. Elsevier, pp. i–ii. https://doi.org/10.1016/B978-0-12-383858-2.00026-3

Calçada, L.A., Scheid, C.M., de Araújo, C.A.O., Waldmann, A.T.A., Martins, A.L., 2011. Analysis of dynamic and static filtration and determination of mud cake parameters. Brazilian J. Pet. Gas 5, 159–170. https://doi.org/10.5419/bjpg2011-0016

Carreau, P.J., 1972. Rheological Equations from Molecular Network Theories. Trans. Soc. Rheol. 16, 99–127. https://doi.org/10.1122/1.549276

Castelain, C., Doublier, J.L., Lefebvre, J., 1987. A study of the viscosity of cellulose derivatives in aqueous solutions. Carbohydr. Polym. 7, 1–16. https://doi.org/10.1016/0144-8617(87)90037-3

Chang, F.F., Ali, S.A., Cromb, J., Bowman, M., Parlar, M., 1998. Development of a New Cross-linked-HEC Fluid Loss Control Pill for Highly-Overbalanced, High-Permeability and/or High Temperature Formations, in: SPE Formation Damage Control Conference. Society of Petroleum Engineers, pp. 215–227. https://doi.org/10.2118/39438-MS

Chang, H.L., Sui, X., Xiao, L., Guo, Z., Yao, Y., Yiao, Y., Chen, G., Song, K., Mack, J.C., 2006. Successful Field Pilot of In-Depth Colloidal Dispersion Gel (CDG) Technology in Daqing Oilfield. SPE Reserv. Eval. Eng. 9, 664–673. https://doi.org/10.2118/89460-PA

Chellappah, K., Majidi, R., Aston, M., Cook, J., 2018. A practical model for wellbore strengthening. Soc. Pet. Eng. - IADC/SPE Drill. Conf. Exhib. DC 2018 2018-March, 6–8. https://doi.org/10.2118/189589-ms

Chen, Y., Yu, M., Miska, S., Ozbayoglu, E., Zhou, S., Al-Khanferi, N., 2017. Fluid flow and heat transfer modeling in the event of lost circulation and its application in locating loss zones. J. Pet. Sci. Eng. 148, 1–9. https://doi.org/10.1016/j.petrol.2016.08.030

Coates, G.R., Xiao, L., Prammer, M.G., 1999. NMR logging. Halliburton Energy Services Publication.

Cole, R.C., Ali, S.A., Foley, K.A., 1995. A New Environmentally Safe Cross-linked Polymer for Fluid-Loss Control, in: SPE Production Operations Symposium. Society of Petroleum Engineers, pp. 743–753. https://doi.org/10.2118/29525-MS

Cook, J., Growcock, F., Guo, Q., Hodder, M., Van Oort, E., 2011. Stabilizing the wellbore to prevent lost circulation. Oilf. Rev. 23, 26–35.

Cowan, B., 1997. Nuclear Magnetic Resonance and Relaxation, Choice Reviews Online. Cambridge University Press. https://doi.org/10.1017/CBO9780511524226

David, R.M., Saputelli, L., Hafez, H., Narayanan, R., Colombani, P., Al Naqbi, T., 2017. Upstream Data Architecture and Data Governance Framework for Efficient Integrated Upstream Workflows and Operations, in: Abu Dhabi International Petroleum Exhibition & Conference. Society of Petroleum Engineers. https://doi.org/10.2118/188962-MS

DeGeare, J., 2003. Pipe Sticking, in: The Guide to Oilwell Fishing Operations. Elsevier, pp. 13–23. https://doi.org/10.1016/B978-0-12-420004-3.00005-8

Edelman, D.C., 2010. Branding in the Digital Age : You ' re Spending Your Money in All the Wrong Places Block That Metaphor Branding in the Digital Age : You ' re Spending Your Money in Al ... The Journey in Practice Launching a Pilot. Harv. Bus. Rev. 42, 1–6. https://doi.org/10.1002/cmr.a

Elkatatny, S., Ahmed, A., Abughaban, M., Patil, S., 2020. Deep Illustration for Loss of Circulation

While Drilling. Arab. J. Sci. Eng. 45, 483–499. https://doi.org/10.1007/s13369-019-04315-6

Ezeakacha, C.P., Salehi, S., Kiran, R., 2018. Lost circulation and filter cake evolution: Impact of dynamic wellbore conditions and wellbore strengthening implications. J. Pet. Sci. Eng. 171, 1326–1337. https://doi.org/10.1016/j.petrol.2018.08.063

Feng, Y., Gray, K.E., 2018. Lost Circulation and Wellbore Strengthening, Journal of Petroleum Science and Engineering, SpringerBriefs in Petroleum Geoscience & Engineering. Springer International Publishing, Cham. https://doi.org/10.1007/978-3-319-89435-5

Feng, Y., Gray, K.E., 2017. Review of fundamental studies on lost circulation and wellbore strengthening. J. Pet. Sci. Eng. 152, 511–522. https://doi.org/10.1016/j.petrol.2017.01.052

Feng, Y., Jones, J.F., Gray, K.E., 2016. A Review on Fracture-Initiation and -Propagation Pressures for Lost Circulation and Wellbore Strengthening. SPE Drill. Complet. 31, 134–144. https://doi.org/10.2118/181747-PA

Ferras, M., Galal, M., Power, D., 2002. Lost Circulation Solutions for Severe Sub-Salt Thief Zones, in: Technology Conference 'Drilling & Completion Fluids and Waste Management. American Association of Drilling Engineers, Houston, pp. 1–7.

Fink, J., 2015. Water-Based Chemicals and Technology for Drilling, Completion, and Workover Fluids. Elsevier. https://doi.org/10.1016/C2014-0-02960-7

Gamage, P., Deville, J.P., Sherman, J., 2014. Solids-Free Fluid-Loss Pill for High-Temperature Reservoirs. SPE Drill. Complet. 29, 125–130. https://doi.org/10.2118/164064-PA

GeoffTanner, P.W., 2003. Syneresis, in: Sedimentology. Springer Netherlands, Dordrecht, pp. 1186–1189. https://doi.org/10.1007/978-1-4020-3609-5_232

Ghalambor, A., Salehi, S., Shahri, M.P., Karimi, M., 2014. Integrated Workflow for Lost Circulation Prediction, in: SPE International Symposium and Exhibition on Formation Damage Control. Society of Petroleum Engineers, pp. 87–96. https://doi.org/10.2118/168123-MS

Gibson, J., Javora, P.H., Adkins, M., 2011. Pre-Cross-Linked Pills Provide Efficient and Consistent Fluid Loss Control, in: SPE European Formation Damage Conference. Society of Petroleum Engineers, pp. 7–10. https://doi.org/10.2118/144213-MS

Gonera, A., Cornillon, P., 2002. Gelatinization of Starch/Gum/Sugar Systems Studied by using DSC, NMR, and CSLM. Starch - Stärke 54, 508–516. https://doi.org/10.1002/1521-379X(200211)54:11<508::AID-STAR508>3.0.CO;2-K

Grillet, A.M., Wyatt., N.B., Gloe, L.M., 2012. Polymer Gel Rheology and Adhesion, in: Rheology. InTech. https://doi.org/10.5772/36975

Hansen, E.W., Lund, T., 1995. Gelation of xanthan in the presence of trivalent chromic ions monitored by proton NMR spin-lattice relaxation. A kinetic study. J. Phys. Chem. 99, 9811–9817. https://doi.org/10.1021/j100024a023

Hashmat, M.D., Sultan, A.S., Rahman, S., Hussain, S.M.S., 2016. Cross-linked Polymeric Gels as Loss Circulation Materials: An Experimental Study, in: SPE Kingdom of Saudi Arabia Annual Technical Symposium and Exhibition. Society of Petroleum Engineers. https://doi.org/10.2118/182740-MS

Hashmat, M.D., Sultan, A.S., Rahman, S., Hussain, S.M.S., Ali, S.A., 2017. Flowing Gels for Loss Circulation Prevention, in: SPE Kingdom of Saudi Arabia Annual Technical Symposium and Exhibition. Society of Petroleum Engineers, pp. 2151–2160.

https://doi.org/10.2118/188103-MS

Hassan, Z., 2018. Common Drilling well problems (Reasons, indications, mitigation and prevention). https://doi.org/10.13140/RG.2.2.19138.48327

Himes, R.E., Ali, S.A., Hardy, M.A., Holtmyer, M.D., Weaver, J.D., 1994. Reversible, Crosslinkable Polymer for Fluid-Loss Control, in: SPE Formation Damage Control Symposium. Society of Petroleum Engineers, pp. 323–324. https://doi.org/10.2118/27373-MS

Hussain, I., Sayed, S.M., Liu, S., Yao, F., Oderinde, O., Fu, G., 2018. Hydroxyethyl cellulose-based self-healing hydrogels with enhanced mechanical properties via metal-ligand bond interactions. Eur. Polym. J. 100, 219–227. https://doi.org/10.1016/j.eurpolymj.2018.01.002

Hvidt, S., 2013. Yield stress determination of a physical gel. Nord. Rheol. Soc. Annu. Trans. 21, 311–314.

Islam, M.R., Hossain, M.E., 2020. Introduction. Drilling Engineering, in: Drilling Engineering. Elsevier, pp. 1–16. https://doi.org/10.1016/B978-0-12-820193-0.00001-0

Jahn, F., Cook, M., Graham, M., 2008. Hydrocarbon Exploration and Production, Second. ed, Natural Resources Forum. Elsevier, Aberdeen, UK.

Jiang, G., Deng, Z., He, Y., Li, Z., Ni, X., 2019. Cross-linked polyacrylamide gel as loss circulation materials for combating lost circulation in high temperature well drilling operation. J. Pet. Sci. Eng. 181, 106250. https://doi.org/10.1016/j.petrol.2019.106250

Karimi, S., Esmaeilzadeh, F., Mowla, D., 2014. Identification and selection of a stable gel polymer to control or reduce water production in gas condensate fields. J. Nat. Gas Sci. Eng. 21, 940–950. https://doi.org/10.1016/j.jngse.2014.10.026

Kulicke, W.-M., Aggour, Y.A., Nottelmann, H., Elsabee, M.Z., 1989. Swelling and Rheological Studies of Some Starch Hydrogels. Starch - Stärke 41, 140–146. https://doi.org/10.1002/star.19890410405

Kumar, A., Savari, S., Whitfill, D., Jamison, D., 2011. Application of fiber laden pill for controlling lost circulation in natural fractures. AADE Natl. Tech. Conf. Exhib. Houston, Texas, USA 12–14.

Lapasin, R., Mercuri, D., Segatti, F., De Conti, G., Grassi, M., Abrami, M., 2018. Rheological study on cross-linking and gelation of amidated carboxymethylcellulose solutions. Chem. Biochem. Eng. Q. 32, 439–449. https://doi.org/10.15255/CABEQ.2018.1380

Lavrov, A., 2016. Lost Circulation. Elsevier, Trondheim. https://doi.org/10.1016/C2015-0-00926-1

Lecolier, E., Herzhaft, B., Rousseau, L., Neau, L., Quillien, B., Kieffer, J., 2005. Development of a Nanocomposite Gel for Lost Circulation Treatment, in: Proceedings of SPE European Formation Damage Conference. Society of Petroleum Engineers, pp. 327–335. https://doi.org/10.2523/94686-MS

Lomellini, P., 1992. Effect of chain length on the network modulus and entanglement. Polymer (Guildf). 33, 1255–1260. https://doi.org/10.1016/0032-3861(92)90771-N

Luzardo, J., Oliveira, E.P., Derks, P.W.J., Nascimento, R.V., Gramatges, a P., Valle, R., Pantano, I.G., Sbaglia, F., Inderberg, K., 2015. Alternative Lost Circulation Material for Depleted Reservoirs, in: OTC Brasil. Offshore Technology Conference, pp. 1–20. https://doi.org/10.4043/26188-MS

Machado, J.C. V, 2002. Reologia e Escoamento de Fluidos – Ênfase na Indústria de Petróleo. Interciência.

Magzoub, M.I., Salehi, S., Hussein, I.A., Nasser, M.S., 2020. Loss circulation in drilling and well construction: The significance of applications of cross-linked polymers in wellbore strengthening: A review. J. Pet. Sci. Eng. 185, 106653. https://doi.org/10.1016/j.petrol.2019.106653

Maitra, J., Shukla, V.K., 2014. Cross-linking in Hydrogels - A Review. Am. J. Polym. Sci. 4, 25–31. https://doi.org/10.5923/j.ajps.20140402.01

Marudova-Zsivanovits, M., Jilov, N., Gencheva, E., 2007. Rheological investigation of xanthan gum–chromium gelation and its relation to enhanced oil recovery. J. Appl. Polym. Sci. 103, 160–166. https://doi.org/10.1002/app.25025

Mezger, T.G., 2014. The Rheology Handbook for users of rotational and oscillatory rheometers, 4th Editio. ed, International Journal of Productivity and Performance Management. Hanover, Germany.

Mishra, R.K., Cherusseri, J., Bishnoi, A., Thomas, S., 2017. Nuclear Magnetic Resonance Spectroscopy, in: Spectroscopic Methods for Nanomaterials Characterization. Elsevier, pp. 369–415. https://doi.org/10.1016/B978-0-323-46140-5.00013-3

Mizrahi, S., 2010. Syneresis in food gels and its implications for food quality, Chemical Deterioration and Physical Instability of Food and Beverages. Woodhead Publishing Limited. https://doi.org/10.1533/9781845699260.2.324

Montgomery, D.C., 2017. Design and Analysis of Experiments, Ninth. ed, Mycological Research. Hoboken, NJ : John Wiley & Sons, Inc., Arizona.

Moradi-Araghi, A., 2000. A review of thermally stable gels for fluid diversion in petroleum production. J. Pet. Sci. Eng. 26, 1–10. https://doi.org/10.1016/S0920-4105(00)00015-2

Nguyen, P.D., Weaver, J.D., Cole, R.C., Schulze, C.R., 1996. Development and Field Application of a New Fluid-Loss Control Material, in: SPE Annual Technical Conference and Exhibition. Society of Petroleum Engineers, pp. 933–941. https://doi.org/10.2118/36676-MS

Oliveira, P.D., Michel, R.C., McBride, A.J.A., Moreira, A.S., Lomba, R.F.T., Vendruscolo, C.T., 2013. Concentration Regimes of Biopolymers Xanthan, Tara, and Clairana, Comparing Dynamic Light Scattering and Distribution of Relaxation Time. PLoS One 8, e62713. https://doi.org/10.1371/journal.pone.0062713

Osswald, T., Rudolph, N., 2002. Polymer Rheology Fundamentals and Applications. Hanser Publishers, Munich.

Ouaer, H., Gareche, M., 2018. The rheological behaviour of a water-soluble polymer (HEC) used in drilling fluids. J. Brazilian Soc. Mech. Sci. Eng. 40, 1–8. https://doi.org/10.1007/s40430-018-1301-7

Pallister, J., Hollis, S.J., Bennett, J., 2015. Identifying Compiler Options to Minimize Energy Consumption for Embedded Platforms. Comput. J. 58, 95–109. https://doi.org/10.1093/comjnl/bxt129

Patel, M.C., Singh, A., 2016. Near Wellbore Damage and Types of Skin Depending on Mechanism of. https://doi.org/doi.org/10.2118/179011-MS

Paulauskiene, T., 2018. Petroleum Extraction Engineering, in: Recent Insights in Petroleum

Science and Engineering. InTech. https://doi.org/10.5772/intechopen.70360

Peden, J.M., Arthur, K.G., Avalos, M., 1984. The Analysis of Filtration Under Dynamic and Static Conditions, in: SPE Formation Damage Control Symposium. Society of Petroleum Engineers, pp. 283–294. https://doi.org/10.2118/12503-MS

Reddy, N., Reddy, R., Jiang, Q., 2015. Cross-linking biopolymers for biomedical applications. Trends Biotechnol. 33, 362–369. https://doi.org/10.1016/j.tibtech.2015.03.008

Romero-Zeron, L.B., Hum, F.M., Kantzas, A., 2008a. Characterization of Cross-linked Gel Kinetics and Gel Strength by Use of NMR. SPE Reserv. Eval. Eng. 11, 439–453. https://doi.org/10.2118/86548-PA

Romero-Zeron, L.B., Hum, F.M., Kantzas, A., 2008b. Characterization of Cross-linked Gel Kinetics and Gel Strength by Use of NMR. SPE Reserv. Eval. Eng. 11, 439–453. https://doi.org/10.2118/86548-PA

Russell, G.M., Masai, H., Terao, J., 2019. Platinum-acetylide crosslinkers for facile preparation of phosphorescent commodity polymer networks with defect-free chromophores. Mater. Lett. 247, 182–184. https://doi.org/10.1016/j.matlet.2019.03.123

Soliman, M.Y., 1994. METHOD FOR DETERMINING FLUID-LOSS COEFFICIENT AND SPURT-LOSS. 737,615.

Songire, S., Uppuluri, R., 2014. Guidelines for Breaker Selection in High Viscosity HEC Based Gel Plugs, in: Abu Dhabi International Petroleum Exhibition and Conference. Society of Petroleum Engineers, pp. 161–169. https://doi.org/10.2118/171696-MS

Speight, J.G., 2016. Handbook of Hydraulic Fracturing, John Wiley and sons. John Wiley & Sons, Inc, Hoboken, NJ. https://doi.org/10.1002/9781119225102

Speight, J.G., 2015. Occurrence and Formation of Crude Oil and Natural Gas, in: Subsea and Deepwater Oil and Gas Science and Technology. Elsevier, pp. 1–43. https://doi.org/10.1016/B978-1-85617-558-6.00001-5

Sydansk, R.D., Smith, T.B., 1988. Field Testing of a New Conformance-Improvement-Treatment Chromium(III) Gel Technology, in: Proceedings of SPE Enhanced Oil Recovery Symposium. Society of Petroleum Engineers, pp. 699–707. https://doi.org/10.2523/17383-MS

Szopinski, D., Kulicke, W.-M., Luinstra, G.A., 2015. Structure–property relationships of carboxymethyl hydroxypropyl guar gum in water and a hyperentanglement parameter. Carbohydr. Polym. 119, 159–166. https://doi.org/10.1016/j.carbpol.2014.11.050

Turner, B.D., Henley, B.J., Sleap, S.B., Sloan, S.W., 2015. Kinetic model selection and the Hill model in geochemistry. Int. J. Environ. Sci. Technol. 12, 2545–2558. https://doi.org/10.1007/s13762-014-0662-4

Varaprasad, K., Raghavendra, G.M., Jayaramudu, T., Yallapu, M.M., Sadiku, R., 2017. A mini review on hydrogels classification and recent developments in miscellaneous applications. Mater. Sci. Eng. C 79, 958–971. https://doi.org/10.1016/j.msec.2017.05.096

Vollmer, D.P., Lejeune, B.E., 2005. Brine and Permeability Effects on Cross-linked Fluid-Loss Pill Filter-Cake Formation, in: SPE International Symposium on Oilfield Chemistry. Society of Petroleum Engineers. https://doi.org/10.2118/93319-MS

Weng, L., Chen, X., Chen, W., 2007. Rheological Characterization of in Situ Crosslinkable Hydrogels Formulated from Oxidized Dextran and N -Carboxyethyl Chitosan. Biomacromolecules 8,

1109–1115. https://doi.org/10.1021/bm0610065

ZHANG, Q., MATSUKAWA, S., WATANABE, T., 2002. Ability of gelation of carrageenans studied by NMR and rheological methods. Fish. Sci. 68, 1667–1668. https://doi.org/10.2331/fishsci.68.sup2_1667

ANNEX A DECISION-MAKING FLOW DURING LOSS CIRCULATION PROBLEM (MAGZOUB ET AL. 2020)